THE UNIVERSITY
of EDINBURGH

Generation of mouse models of neurodevelopmental disorders using the CRISPR/Cas9 system

Yoo Koung Ko

Centre for Clinical Brain Sciences

College of Medicine and Veterinary Medicine

University of Edinburgh

A thesis submitted for the degree of

Doctor of Philosophy

2018

Declaration

I declare that this thesis was composed by myself, that work described herein, is my own except unless indicated otherwise and has not been submitted for any other degree.

Yoo Koung Ko

July 2018

Acknowledgements

I would first like to express my gratitude to my primary supervisor Dr. Noboru Komiyama for his continuous guidance and mentoring, and my second supervisor Prof. Seth Grant for providing me with invaluable opportunities, and for his advice and encouragement. I would like to thank Prof. Catherina Becker for her support, and for being an inspiration to me. I would also like to thank Prof. Peter Kind for chairing my thesis committee.

I would like to thank all the members of the Grant lab, in particular Cathy McLaughlin for her continuous help and support throughout my PhD study. I would also like to thank Dr. Elaine Marshall, Ann Ross, David Kerrigan, Kathryn Elsegood and Rand Dahan for their assistance and advice.

A special thank you goes to Susan Muir and Cristiana Bercea for her love and support. I would like to thank Kate Allan and Dr. Oonee Koh for their advice and encouragement. Thanks also to Eunee Koh and Daehee Park for rooting for me. Finally, I am forever grateful to my parents, Jong Joo Ko and In Pil Lee for everything.

Abstract

The N-methyl-D-aspartate receptors (NMDARs) and its interacting proteins constitute large macro-molecular complexes (NMDAR complexes) at glutamate synapses. Recent human genomic studies discovered many mutations in the genes encoding the components of NMDAR complexes in various neurodevelopmental disorders. However, little is known about how mutations in these genes alter molecular and cellular pathways leading to pathological phenotypes. To answer the question, our lab has been systematically mutating synaptic genes in mice using conventional gene targeting methods. To further accelerate generation of mutants we adopted the CRISPR/Cas9 genome editing system in mouse embryonic stem (ES) cells.

SH3 and multiple ankyrin repeat domains 3 (SHANK3) is a crucial scaffolding protein of NMDAR complexes and is implicated in autism spectrum disorders, intellectual disability, and schizophrenia. A CRISPR/Cas9-induced knockout mutation of SHANK3 was successfully introduced in ES cells, and these cells were injected into mouse blastocysts and three chimaeras were born. These chimaeras were then crossed with wild-type mice and germline transmission was confirmed.

Having established a knockout mutation using the CRISPR/Cas9 system, we moved on to modify Synaptic GTPase-activating protein 1 (SYNGAP1), another component of NMDAR complexes. *De novo* mutations of SYNGAP1 have been found in intellectual disability, autism spectrum disorders, and schizophrenia. To introduce a defined mutation in the SYNGAP1 gene, we designed a CRISPR/Cas9-mediated point mutation, and ES cell lines with the precise mutation were obtained. These cell lines were further developed to create a novel animal colony.

Here we demonstrate CRISPR/Cas9 facilitates disruption of SHANK3, as well as the precise editing in SYNGAP1 in mouse ES cells with high efficiency. Furthermore, we report successful generation and characterisation of genome-engineered mice using CRISPR/Cas9-modified ES cells.

Lay summary

Recent human genomic studies have identified several hundred gene mutations which result in neurodevelopmental disorders, including intellectual disability and autism spectrum disorders. Many of these genes encode proteins which are located in brain synapses. However, little is known about how the mutations in these synaptic genes lead to cognitive and behavioural deficits observed in the disorders.

Genetically modified mice are a strong tool to investigate the functions of such genes implicated in human diseases. Therefore, our lab has been systematically mutating synaptic genes in mice using conventional gene targeting methods. However, generation of mutant mice using this methodology is time-consuming, expensive, and laborious. To accelerate generation of mutant mice, we adopted a recently developed gene editing technology known as the CRISPR/Cas9 system.

Here we report rapid generation of genome-engineered mice using the CRISPR/Cas9 system in mouse embryonic stem (ES) cells. The CRISPR/Cas9 system facilitated deletion in an autism-associated gene SHANK3, as well as a precise gene editing in an intellectual disability-related gene SYNGAP1 in mouse ES cells with high efficiency. Using the modified ES cells, we successfully generated novel mouse models of neurodevelopmental disorders. Analysing these mutant mice will elucidate the structural and functional roles of these synaptic genes, and further our understanding of neurodevelopmental disorders.

List of Figures

Figure 1.1 | NMDAR and its interacting proteins. 4
Figure 1.2 | Structure and intragenic promoters of SHANK3. 6
Figure 1.3 | SHANK3 interacting proteins in the PSD. 6
Figure 1.4 | Small GTPase signalling. 12
Figure 1.5 | Ras-ERK pathway in neurons. 13
Figure 1.6 | SYNGAP1 isoforms. 15
Figure 1.7 | CRISPR/Cas9-mediated immunity in prokaryotes. 21
Figure 1.8 | CRISPR/Cas9 genome editing. 23
Figure 1.9 | DNA repair mechanisms. 24
Figure 1.10 | Experimental procedures of zygote injection and ES cell transfection. 27
Figure 3.1 | Workflow of mutant mouse generation. 46
Figure 3.2 | CRISPR/Cas9-mediated gene editing in ES cells. 47
Figure 3.3 | Genomic structure and splice variants of SHANK3. 49
Figure 3.4 | Loci of the selected guide sequences. 52
Figure 3.5 | Target selection and sgRNA expression vector construction 53
Figure 3.6 | Schematic of T7 endonuclease I assay. 55
Figure 3.7 | Mutation detection on transfected ES cells. 56
Figure 3.8 | SHANK3 sequence alignment. 60
Figure 3.9 | Interpretation of chromatogram for sequence analysis. 61
Figure 3.10 | CRISPR/Cas9-mediated SHANK3 targeting in ES cells. 62
Figure 3.11 | PCR primer design. 66
Figure 3.12 | PCR genotyping. 67
Figure 3.13 | Off-target analysis of three targeted ES cells. 71
Figure 3.14 | PCR genotyping of F2 mice (C17). 75
Figure 3.15 | Western blot of SHANK3 KO mice. 77
Figure 3.16 | The observed isoforms of SHANK3. 78
Figure 4.1 | Active site of Ras GTPase-GAP complex. 81
Figure 4.2 | Design of the donor DNAs. 83
Figure 4.3 | The R470A cell lines genotyping using restriction digestion. 85
Figure 4.4 | CRISRP/Cas9-mediated SYNGAP1 mutations in ES cells. 86
Figure 4.5 | Sequence analyses of each genotype. 88
Figure 4.6 | Extended sequence alignment of the selected R470A cell lines. 90
Figure 4.7 | Use of mixed donor templates to introduce heterozygosity. 92
Figure 4.8 | Comparison between mixed and single donor experiments. 93
Figure 4.9 | Sequence analysis of a heterozygous HDR cell line. 94
Figure 4.10 | Germline transmission of the R470A mutation. 96
Figure 4.11 | Western blot of SynGAP1mutant mice. 96
Figure 5.1 | Molecular pathway involving SHANK3 and SYNGAP1. 105

List of Tables

Table 1.1 | Human SHANK3 mutations. 9
Table 1.2 | Characterisation of the SHANK3 mutant mice. 10
Table 1.3 | Characterisation of the SYNGAP mutant mice. 14
Table 1.4 | Human SYNGAP1 mutations. 17
Table 1.6 | Zygote injection and ES cell-mediated methods. 29
Table 2.1 | Oligonucleotide sequences for CRISPR mice generation. 35
Table 2.2 |Standard PCR cycling protocol. 39
Table 2.3 | List of off-target sites. 41
Table 2.4 | Primary antibodies. 44
Table 3.1 | SHANK3 guide sequences generated by sgRNA Designer. 51
Table 3.2 | Sequence validation of guide oligo insertion into pX330. 54
Table 3.3 | Estimated cleavage band size of each sgRNA. 56
Table 3.4 | Estimation of indel percentage. 57
Table 3.5 | DNA translation of G4-C17 cell line. 61
Table 3.6 | Result of CRISPR-SHANK3 transfection. 62
Table 3.7 | SHANK3 exon 5 peptide sequences of homozygous G1 cell lines. 63
Table 3.8 | SHANK3 exon 10 sequences of homozygous G4 and G5 cell lines. 63
Table 3.9 | Exon skip analysis. 64
Table 3.10 | Genotyping primers. 66
Table 3.11 | Off-target analysis of three targeted ES cells (C17, C23 & C24). 70
Table 3.12 | Blastocyst injection of the selected ES cell lines. 72
Table 3.13 | Genotyping primers. 75
Table 4.1 | Size determination of DNA restriction fragments. 85
Table 4.2 | Blastocyst injection of homozygous HDR cell lines. 95
Table 5.1 | Germline transmission rate of CRISPR/Cas9-modified ES cell lines. 98

List of Abbreviations

aa	amino acid
Amp	Ampicilin
AMPA	α-amino-3-hydroxy-5-methyl-4-isoxazolepropionic acid
ANK	Ankyrin repeat domain
ASD	Autism spectrum disorder
bp	Base-pair
CaMKII	Ca2+/calmodulin-dependent kinase II
Cas9	CRISPR-associated protein 9
CC domain	Coiled-coil domain
CRISPR	Custered regularly interspaced short palindromic repeats
crRNA	CRISPR RNA
CTD	C-terminal domain
dCas9	Catalytically dead Cas9
del	Deletion mutation
DOC	Deoxycholate
DSB	Double stranded break
EDTA	Ethylenediaminetetraacetic acid
EEG	Electroencephalography
ERK	Extracellular signal-regulated kinases
ES (cell)	Embryonic stem (cell)
FMRP	Fragile X mental retardation protein
GAP	GTPase-activating protein
GDP	Guanosine diphosphate
GEF	Guanine nucleotide exchange factor
GKAP	Guanylate kinase-associated protein
GMP	Guanosine monophosphate
GTP	Guanosine triphosphate
HDR	Homology-directed repair
HRP	Horseradish peroxidase
ID	Intellectual disability
Indel	Insertion or the deletion of bases in the DNA
ins	Insertion mutation
iPSC	Induced pluripotent stem cell
KO	Gene kockout
LB	Lysogeny broth
LTP	Long-term potentiation
MAGUK	Membrane-associated guanylate kinase
mEPSC	Miniature excitatory postsynaptic current
mGluR	Metabotropic glutamate receptor
NF1	Neurofibromin
NMDAR	N-methyl-D-Aspartate receptor
nt	Nucleotide
PAM	Protospacer adjacent motif
PBS	Phosphate-buffered saline

PBS-T	Phosphate-buffered saline with Tween
PCR	Polymerase change reaction
PH	Pleckstrin homology
PMSF	Phenylmethylsulfonyl fluoride
PRO	Proline-rich region
PSD	Postsynaptic density
PSD95	Postsynaptic density protein 95
RNAi	RNA interference
SAM	Sterile alpha motif
SAP102	Synapse-associated protein 102
sEPSC	Spontaneous excitatory current
sgRNA	Single-guide RNA
SH3	SRC homology 3
SHANK3	SH3 and multiple ankyrin repeat domains 3
SNV	Single nucleotide variation
SYNGAP1	Synaptic Ras GTPase-activating protein 1,
Ta	Annealing temperature
TALEN	Transcription activator-like effector nucleases
TDB	Tail digestion buffer
Tm	Melting temperature of a primer
tracrRNA	Trans-activating crRNA
WT	Wil-type
ZFN	Zinc-finger nuclease

Contents

Acknowledgements ..... **v**

Abstract ..... **vii**

Lay summary ..... **ix**

List of Figures ..... **xi**

List of Tables ..... **xii**

List of Abbreviations ..... **xiii**

Chapter 1 Introduction **1**

1.1 NMDAR complexes 2

1.2 SHANK3 5

1.3 SYNGAP1 11

1.4 CRISPR/Cas9 genome editing system 19

Chapter 2 Materials and Methods **31**

2.1 General procedures and materials 32

2.2 Cloning using CRISPR/Cas9 backbone plasmid 33

2.3 Design of DNA repair templates 34

2.4 Chemical transformation 36

2.5 Plasmid DNA preparation and sequencing 36

2.6 Sequence analysis 37

2.7 Embryonic stem cell culture 37

2.8 DNA extraction from mammalian tissues 38

2.9 PCR amplification 39

2.10 Restriction enzyme digestion 39

2.11 Agarose gel electrophoresis 40

2.12 T7 endonuclease assay 40

2.13 Off-target analysis 41

2.14 Mouse colony establishment 42

2.15 Forebrain brain extraction 42

2.16 Western blot 43

Chapter 3 Design and generation of SHANK3 knockout mice **45**

3.1 Consideration of target sites 48

3.2 Target selection 50

3.3 CRISPR vector construction 52
3.4 Functional testing of sgRNAs 54
3.5 ES cell line generation 58
3.6 Sequence analyses 59
3.7 Design of PCR primers for genotyping 65
3.8 Off-target analysis 69
3.9 Blastocyst injection and mouse generation 72
3.10 Review of PCR genotyping 74
3.11 Western blot validation 76
Chapter 4 SYNGAP1 GAP-deficient mouse model generation 79
4.1 Mutation rationale and design 80
4.2 ES cell line generation 84
4.3 Sequence analyses 87
4.4 Introduction of specific homozygous and heterozygous mutations 91
4.5 Mouse generation 95
Chapter 5 Conclusion 97
5.1 General methodological discussion 98
5.2 Applications of CRISPR-based technologies 99
5.3 SHANK3 knockout mouse model 101
5.4 SYNGAP1 GAP-deficient mouse model 103
5.5 A common pathway of SHANK3 and SYNGAP1 104
Bibliography 107

Chapter 1 Introduction

1.1 NMDAR complexes

The N-methyl-D-aspartate receptor (NMDAR) is a glutamate-gated ion channel at the excitatory synapses in the central nervous system. NMDAR is one of three subtypes of ionotropic glutamate receptors, the others being the α-amino-3-hydroxy-5-methyl-4-isoxazolepropionic acid (AMPA) receptor and the kainite receptor (Fan et al. 2014; Clements & Westbrook 1991; Furukawa et al. 2005). When activated by glutamate and glycine (or D-serine), NMDARs mediate the flow of sodium (Na^+) and calcium (Ca^{2+}) into the cell, and potassium ions (K^+) out of the cell (Furukawa et al., 2005). Each NMDAR is a heterotetramer composed of two obligatory GluN1 and two modulatory GluN2 (A-D) or GluN3 (A-B) subunits (Ulbrich & Isacoff 2008; Collingridge et al. 2009). GluN2 subunit contains the evolutionarily divergent C-terminal domain which differentially interacts with other synaptic proteins (Ryan et al. 2008). NMDARs are critically involved in a variety of cellular processes and activity-dependent brain functions such as cortical circuit refinement, synaptic plasticity and cognitive functions (Akashi et al. 2009; O'Connor et al. 2014; Fan et al. 2014).

The functional diversity of NMDARs may be ascribed to its organisation at the postsynaptic density (PSD) (Fan et al. 2014). NMDARs bind more than 70 synaptic proteins forming macromolecular signalling complexes (Naisbitt et al. 1999; Husi et al. 2000; Grant & O'Dell 2001; Frank et al. 2016; Fernández et al. 2009). The C-terminal domain of Glu2B, in particular, plays a key role in the formation of ~1.5 MDa NMDAR complexes (Frank et al. 2016). The assembly of NMDARs with different synaptic proteins provides a means to modulate the receptor properties and trafficking, and links the receptor activation to various intracellular signalling pathways (Fan et al. 2014).

Human genomic studies have identified several hundred mutations in the genes encoding the components of NMDAR complexes in various neurodevelopmental disorders including autism spectrum disorders (ASD) (Durand et al. 2011; Berryer et al. 2013; De Rubeis et al. 2014; Lee et al. 2015), intellectual disability

(Hamdan *et al.*, 2009; Hamdan *et al* 2011; Rauch *et al.*, 2012; Mignot *et al.*, 2016) and schizophrenia (Gauthier *et al.*, 2009; Purcell *et al.*, 2014). Therefore, investigating protein interactions in NMDAR complexes will not only give insight into molecular mechanisms of NMDAR signalling, but also how its dysfunction relates to the pathophysiology of the neurodevelopmental disorders.

We focus our attention on two NMDAR-interacting proteins, SHANK3 (SH3 and multiple ankyrin repeat domains 3) and SYNGAP1 (Synaptic GTPase-activating protein 1) (**Figure 1.1**). We decided to study SHANK3 and SYNGAP1 together because of the following common features. First, haploinsufficiency in SHANK3 and SYNGAP1 is linked to the same set of brain disorders, including ASD (Durand et al. 2011; Berryer et al. 2013; De Rubeis et al. 2014; Lee et al. 2015), intellectual disability (Prasad *et al*., 2001; Hamdan *et al.*, 2009; Hamdan *et al* 2011; Rauch *et al.*, 2012; Mignot *et al.*, 2016), schizophrenia (Purcell et al. 2014; Gauthier et al. 2009) and epilepsy (Leblond et al. 2014; Berryer et al. 2013). Secondly, loss-of-function mouse models of these proteins have overlapping phenotypes such as seizures, spatial memory deficits and increased stereotyped behaviours (Peça et al. 2011; Kozol et al. 2015; Komiyama et al. 2002; Clement et al. 2012). Thirdly, both proteins are enriched at the PSD, and physically interact with each other through common binding partners such as the membrane-associated guanylate kinases (MAGUKs) (Naisbitt et al. 1999; Sakai et al. 2011) (**Figure 1.1**). Lastly, the C-terminal domain of GluN2B subunit plays a crucial role in these interactions (Kim et al. 2005). Considering these commonalities, we hypothesised these proteins form a multiprotein complex at the PSD and are involved in a common molecular pathway conferring the convergent clinical phenotypes. To test our hypothesis, we aimed to create novel mouse models carrying mutations in SHANK3 or SYNGAP1 using a recently developed genome engineering technology, the CRISPR/Cas9 system in mouse embryonic stem (ES) cells.

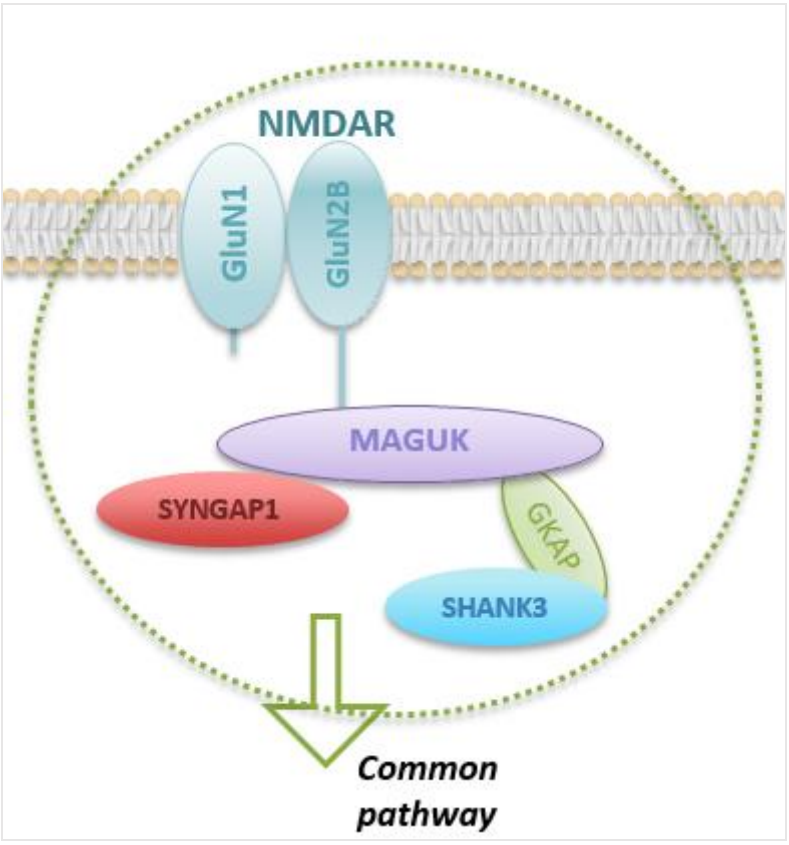

Figure 1.1 | NMDAR and its interacting proteins.

GluN2B subunit of NMDARs has a long cytoplasmic tail involved in protein-protein interactions. SYNGAP1 associates with NMDAR via MAGUK (membrane-associated guanylate kinase) proteins, while SHANK3 binds to GKAP (guanylate kinase-associating protein) which in turn associates with MAGUK. Gene mutations in the proteins illustrated here (GluN1, GluN2B, MAGUK, GKAP, SYNGAP1 and SHANK3) are all implicated in autism spectrum disorder (ASD) and/or intellectual disability, indicating a common molecular pathway.

1.2 SHANK3

SHANK3 is a synaptic scaffolding protein, which physically interacts with NMDAR complexes *in vitro* (Naisbitt et al. 1999). SHANK3 is a member of the SHANK family, which connects membrane receptors and other synaptic proteins to actin cytoskeleton and G-protein-coupled signalling pathways (Boeckers et al. 1999; Naisbitt et al. 1999). As shown in **Figure 1.1**, SHANK3 interacts with NMDARs via MAGUKs and guanylate kinase-associating protein (GKAP) (Naisbitt et al. 1999; O'Connor et al. 2014).

The SHANK3 gene is located on mouse chromosome 15 (22q13.3 in human), and has 22 exons (**Figure 1.2**). SHANK3 has a wide range of mRNA splice variants resulting from combinations of six intragenic promoters (Monteiro & Feng 2017) and several alternative splicing exons (Wang et al. 2014; Zhu et al. 2014). The full length structure of the mouse SHANK3 gene comprises 5 domains for protein-protein interactions: the ankyrin repeat domain (ANK), the SRC homology 3 (SH3) domain, the PDZ domain, the proline-rich region (PRO) and sterile alpha motif (SAM) domain (**Figure 1.3**). The N-terminal ankyrin repeat domain contains six ankyrin repeats, and interacts with the F-actin cytoskeleton via an interaction with α-fodrin (Duffney et al. 2015). The PDZ domain of SHANK3 interacts with MAGUKs via binding to GKAP (Naisbitt et al. 1999). The PRO binds to Cortactin and Homer proteins, which are involved in the regulation of the cytoskeleton, synaptic plasticity and transmission (Monteiro & Feng 2017). Lastly, the C-terminal SAM domain is required for the localisation of SHANK3 to the PSD (Boeckers et al. 2005).

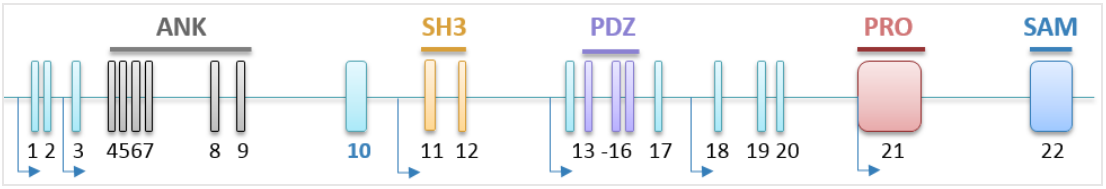

Figure 1.2 | Structure and intragenic promoters of SHANK3.

Schematic shows the structure of the mouse SHANK3 gene and the location of intragenic promoters indicated by the blue arrows. ANK: ankyrin repeat domain; SH3: SRC homology 3 domain; PRO: proline-rich region; SAM: sterile alpha motif.

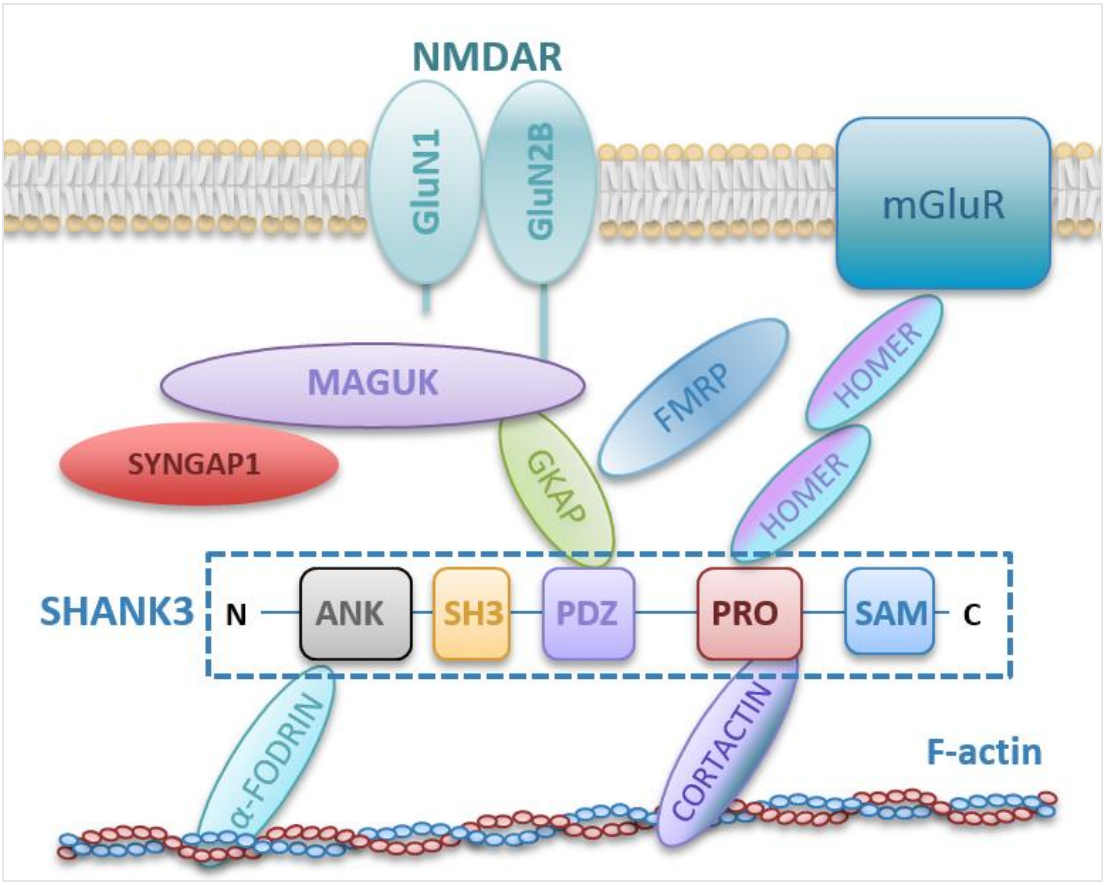

Figure 1.3 | SHANK3 interacting proteins in the PSD.

Representation of SHANK3 in the PSD is shown with its domains for protein-protein interaction. The ankyrin repeat domain (ANK) interacts with the F-actin cytoskeleton through an interaction with α-fodrin. The PDZ domain binds to GKAP, which then interacts with MAGUKs and the fragile X mental retardation protein (FMRP). The PRO domain interacts with F-actin through binding to Cortactin. The PRO domain also interacts with the metabotropic glutamate receptor (mGluR).

The SHANK3 gene was first implicated in neurodevelopmental disorders by studies of the 22q13.3 deletion syndrome, also known as Phelan-McDermid syndrome. This syndrome is characterised by autistic-like behaviours, intellectual disability, global developmental delay, and hypotonia (Prasad et al. 2001). Over 600 cases of the 22q13.3 deletion syndrome have been reported, and the SHANK3 gene is deleted in nearly all cases (Phelan & McDermid 2012). SHANK3 haploinsufficiency is thus thought to be the cause of core neurodevelopmental and behavioural impairments observed in patients (Bonaglia et al. 2001). In rare cases where the 22q13.3 deletion leaves the SHANK3 gene intact, the individuals are phenotypically normal, further supporting the hypothesis that SHANK3 haploinsufficiency is responsible for neurological defects in the 22q13.3 deletion syndrome (Phelan & McDermid 2012).

Apart from the 22q13.3 deletion syndrome, many SHANK3 mutations have been found in nonsyndromic ASD (Durand et al. 2007; Gauthier et al. 2009; Boccuto et al. 2013; Moessner et al. 2007) and schizophrenia (Gauthier et al. 2009; Durand et al. 2007; Moessner et al. 2007; Boccuto et al. 2013) (**Table 1.1**). These mutations include nonsense mutations, missense mutations and small deletions, most of which are *de novo* variants. Recently, mutations in SHANK1 and SHANK2 have also been found in ASD (Leblond et al. 2012; Boccuto et al. 2013; Sala et al. 2015). A meta-analysis of SHANK mutations show that individuals with SHANK3 mutations have more severe cognitive impairment than those with SHANK1 or SHANK2 mutations (Leblond et al. 2014). The difference in the degree of cognitive impairment might be explained by the expression pattern of the mutated SHANK3 protein in the brain, and by the extent to which the remaining two SHANK proteins can compensate for the loss (Monteiro & Feng 2017). Although all members of the SHANK protein family are widely expressed in the mouse brain including areas like cortex, thalamus and hippocampus, only SHANK3 mRNA is highly expressed at cortico-striatal glutamatergic synapses (Peça et al. 2011). Cortico-striatal dysfunction has been implicated in repetitive behaviour in mice (Welch et al. 2007) further

implicating the potential importance of SHANK3 in ASD. It is worth noting that not only SHANK3, but its numerous interacting proteins are also associated with ASD and/or intellectual disability, including GKAP (Li et al. 2014), the fragile X mental retardation protein FMRP (Steinberg & Webber 2013), Homer1 (Kelleher III et al. 2012), MAGUK protein PSD95 (Feyder et al. 2010), SYNGAP1 (Hamdan et al. 2009; Hamdan et al. 2011; Mignot et al. 2016; Kimura et al. 2018) and NMDAR subunits GluN1 and GluN2B (O'Roak et al. 2012) (see **Figure 1.3**).

Animal models of SHANK3 deficiency display ASD-like behaviours such as social avoidance, self-injurious grooming, and deficits in learning and memory (see **Table 1.2**), along with NMDAR hypofunction (Duffney et al. 2015), and altered levels of synaptic proteins including GluN2B, Homer proteins, SYNGAP1, metabotropic glutamate receptor 5 (mGluR5) (Peça et al. 2011; Zhou et al. 2016). Together these findings strongly indicate there is a common molecular pathology involving NMDAR complexes. Given a wide range of synaptic proteins that SHANK3 interacts with, it is important to investigate how mutations in SHANK3 might affect the structural and functional organisation of NMDAR complexes at the PSD. This information will provide an insight into how SHANK3 mutations might be related to the pathophysiology.

Exon affected by mutation	Diagnoses	Phenotypes and comments	References
Exon 1	ASD (1 case)	Severe ID and absence of language. Impaired social interaction. Low noise threshold.	(Durand et al. 2007)
Exon 2	ASD (1 case)	Language defects at 18 months of age.	(Gauthier et al. 2009)
Exon 4 (ANK)	ASD (1 case)	High sensitivity to touch. Developmental delay & seizures. Repetitive speech (echolalia).	(Boccuto et al. 2013)
Exon 8 (ANK)	ASD (2 cases)	Restricted interests and repetitive behaviours. Communication and social interaction deficits. Brisk reflexes and generalised hypotonia.	(Moessner et al. 2007; Durand et al. 2007)
Exon 11 (SH3)	ASD (1 case)	Individual also has mutation in Neurexin 1.	(Boccuto et al. 2013)
Exon 16 (PDZ)	ASD (1 case)	Splice site mutation (intron 15-exon 16). Asperger syndrome. Behavioural deficits and echolalia at 2 years.	(Boccuto et al. 2013)
Exon 19	ASD (1 case)	Splice site mutation (exon 19-intron 19).	(Durand et al. 2007)
Exon 21 (PRO)	ASD (8 cases) SCZ (3 cases)	Severe ID (8 cases). Mild-moderate ID (3 cases). Absence of verbal communication (4 cases). Severely impaired speech (2 cases). Global developmental delay (6 cases).	(Leblond et al. 2014; Boccuto et al. 2013; Durand et al. 2007; Gauthier et al. 2010)

Table 1.1 | Human SHANK3 mutations.

ASD: autism spectrum disorder; ID: intellectual disability; SCZ: schizophrenia.

Exon (domain) mutated	Dendritic spine	Social behaviours	Repetitive behaviours	Anxiety	Morris water maze	Rotarod test	References
Exons 4-7 (ANK)	N/A	Social novelty deficit	Normal self-grooming	N/A	N/A	N/A	(Peça et al. 2011)
Exons 4-9 (ANK)	Remodelling deficit	↓ sniffing	↑ self-grooming	N/A	Normal	Impaired	(Bozdagi et al. 2010; Yang et al. 2012)
	↓ density	Abnormal	↑ self-grooming	↑	Impaired	Impaired	(Wang et al. 2011)
	N/A	Mild deficit	↑ self-grooming	N/A	Mildly impaired	Normal	(Jaramillo et al. 2016)
Exon 9 (ANK)	N/A	Normal	↑ rearing in new environment	N/A	Normal	N/A	(Lee et al. 2015)
Exon 11 (SH3)	Normal	Abnormal	Self-injurious grooming	N/A	Impaired	Mildly impaired	(Schmeisser et al. 2012; Vicidomini et al. 2016)
Exons 13-16 (PDZ)	↓ density	Abnormal	Self-injurious grooming	↑	Normal	N/A	(Peça et al. 2011)
	↓ density	Abnormal	Self-injurious grooming	↑	N/A	Impaired	(Mei et al. 2016)
Exon 21 (PRO)	Normal	Social novelty deficit	↑ self-grooming	↑	Impaired	Impaired	(Kouser et al. 2013)
	N/A	N/A	Normal	↑	Mildly Impaired	Impaired	(Speed et al. 2015)
	↓ number	Abnormal	Self-injurious grooming	↑	N/A	Impaired	(Zhou et al. 2016)
Exons 4-22 (All domains)	↓ density in striatum	Normal	Self-injurious grooming	↑	Impaired	Impaired	(Wang et al. 2016)

Table 1.2 | Characterisation of the SHANK3 mutant mice.

Morris water maze is a test of spatial learning and memory. Rotarod testing measures motor coordination. N/A: data not available.

1.3 SYNGAP1

SYNGAP1 is another NMDAR-interacting protein, and associates with SHANK3 (Sakai et al. 2011) through NMDAR complexes (see **Figure 1.1**). SYNGAP1 directly interacts with MAGUKs such as PSD95 (postsynaptic density protein 95) and SAP102 (synapse-associated protein 102) (Kim et al. 1998), and preferentially binds to GluN2B containing NMDARs (Kim et al. 2005).

SYNGAP1 is a brain-specific Ras **G**TPase **a**ctivating **p**rotein (GAP), which negatively regulates Rap and Ras GTPases and their downstream signalling (Pena et al. 2008; Krapivinsky et al. 2004). SYNGAP1 is one of the most abundant PSD proteins (Cheng et al. 2006) and is activated by Ca^{2+}/calmodulin-dependent kinase II (CaMKII) (Krapivinsky et al. 2004). SYNGAP1 physically interacts with the small G proteins, which in turn play a role as molecular switches by cycling between an active guanosine triphosphate (GTP)-bound conformation and an inactive guanosine diphosphate (GDP)-bound conformation (**Figure 1.4**). GTPases have a slow intrinsic GTPase activity, and GAPs such as SYNGAP1 enhances the hydrolysis of GTP to GDP by 10^5-fold (Chen et al. 1998). Conversely, guanine nucleotide exchange factors (GEFs) facilitate the reverse process by exchanging GDP to GTP. The workings of GAPs and GEFs ensure appropriate levels of the small G protein activation in cells (Bos et al. 2007).

The small GTPase Ras mediates the activity of a cytoskeleton protein, F-actin, which regulates dendritic spine formation and synaptic connection (Jeyabalan & Clement 2016). Ras also activates the extracellular signal-regulated kinases (ERK) pathway, which transmits signal downstream and leads to the transcription of genes involved in neurite and spine development (Vadodaria & Jessberger 2013). The Ras-ERK pathway is an essential modulator of synaptic strength and structure during NMDAR-dependent long-term potentiation (LTP) (**Figure 1.5**). By altering the number of AMPA receptors in the cell membrane, postsynaptic neurons directly regulate its sensitivity to glutamate and the

probability to generate an action potential (Krab et al. 2008). Together these findings illustrate a potential mechanism by which SYNGAP1 regulates neurite and spine maturation (Vadodaria & Jessberger 2013), and synaptic physiology (Araki et al. 2015).

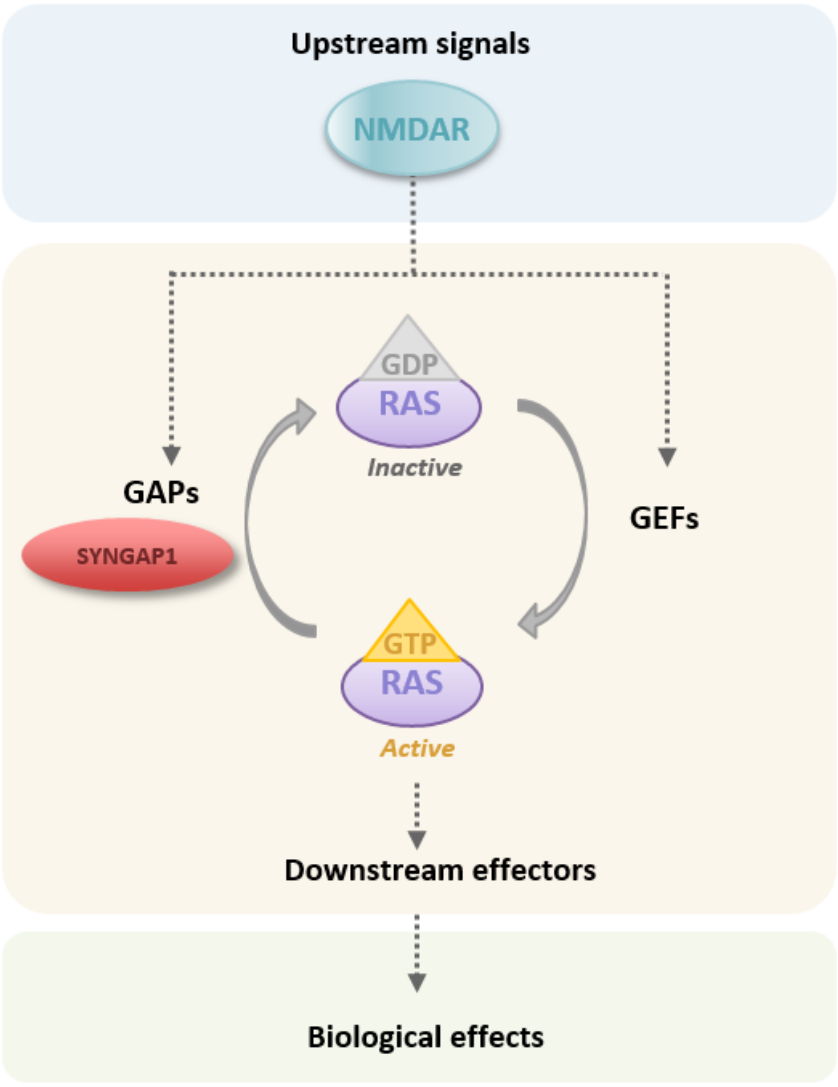

Figure 1.4 | Small GTPase signalling.

Upstream signalling such as NMDAR activation modulates the activity of GAPs (GTPase activating proteins; e.g. SYNGAP1) and GEFs (guanine nucleotide exchange factors) thereby mediating small GTPases such as Ras. GEFs promote activation (GTP-bound form), while GAPs facilitate inactivation (GDP-bound form). The active small GTPase binds to downstream effectors influencing synaptic physiology.

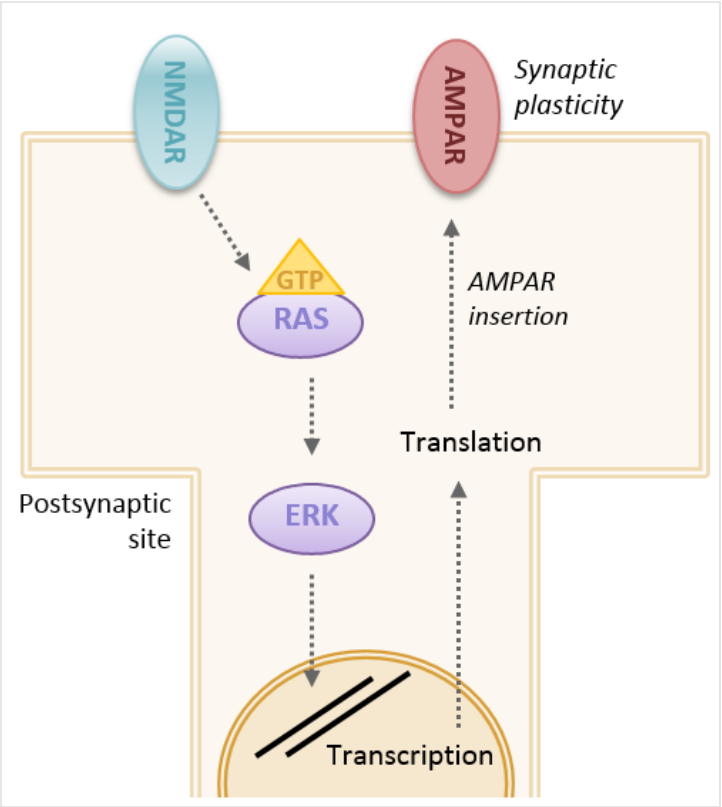

Figure 1.5 | Ras-ERK pathway in neurons.

The Ras-ERK pathway is recruited for synaptic plasticity. Synaptic strength is strongly dependent on the number of AMPA receptors present in the PSD. Upon the activation of the NMDA receptors, the ERK pathway alters synaptic strength by mediating the insertion of AMPA receptors.

Although SYNGAP1 homozygous knockout mutations in mice are lethal at early postnatal stages, heterozygous SYNGAP1 mice are viable with several behavioural and electrophysiological deficits (**Table 1.3**). NMDAR hypofunction may contribute to the altered behaviours, since lack of SYNGAP1 disrupts NMDAR-dependent synaptic transmission and learning (Komiyama et al. 2002; Clement et al. 2013). SYNGAP1 haploinsufficiency impairs the excitatory-inhibitory balance in the developing cortex and hippocampus (Aceti et al. 2015), and leads to precocious synaptic maturation (Clement et al. 2012). SYNGAP1 also plays a role in NMDAR-dependent regulations of synaptic density, spine morphology and synaptic plasticity (Kim et al. 2003; Vazquez et al. 2004; Rumbaugh et al. 2006).

Mutation (reference)	Behavioural testing	Electrophysiology	Comments
Het KO mice in a C57BL/6 background (Komiyama et al. 2002)	Slow learning.	LTP deficit	Altered levels of active form ERK and Ras.
Hom KO mice in a C57BL/6 background (Vazquez et al. 2004)	N/A	↑ mEPSC amplitude and frequency	Precocious spine maturation and larger dendritic protrusions.
Het KO mice in a C57BL/6 background (Rumbaugh et al. 2006)	N/A	↑ synaptic transmission	↑ ERK activation.
Het KO mice in a 129 and C57BL/6 mixed background (Carlisle et al. 2008)	N/A	LTD deficit	↑ Levels of Ras and Rac.
Het KO mice in a 129 and C57BL/6 mixed background (Guo et al. 2009)	Social recognition memory deficit, social isolation preference.	N/A	Less responsive to NMDAR antagonist MK-801.
Same as Vazquez et al., 2004 (Muhia et al. 2010)	Severe working and reference memory deficits.	N/A	Neurogenesis deficit.
Hippocampus-specific KO in mice in a 129 and C57BL/6 mixed background (Muhia et al. 2012)	Reversal learning impairment, spatial recognition memory deficit.	↓ sEPSC amplitude, ↑ sEPSC frequency	Conditional KO. Reduced adult neurogenesis.
Same as Guo et al., 2009 (Clement et al. 2012)	Hyperactivity, context discrimination deficit.	↑ mEPSC amplitude and frequency, abnormal synaptic transmission	Accelerated maturation of dendritic spine.
Same as Guo et al., 2009 (Clement et al. 2013)	N/A	LTP deficit, ↑ ratio of AMPAR/NMDAR current	Altered critical period of plasticity.
Forebrain glutamatergic neurons-specific KO in a 129 and C57BL/6 mixed background (Ozkan et al. 2014)	Impaired fear memory, hyperactivity	Abnormal EEG, ↑ mEPSC amplitude and frequency	Conditional KO.

Table 1.3 | Characterisation of the SYNGAP mutant mice.

Most studies used heterozygous null mutant mice maintained in a C57BL/6 background or a 129 and C57BL/6 mixed background. The mouse line from Carlisle *et al.* (2008) was maintained in the mixed background as it breeds poorly in a single C57BL/6 background.

The difference in phenotypic results might be explained by the methodological difference in phenotypic data analysis. Standardising the phenotyping analyses would be necessary for the future experiments.

LTP: long-term potentiation; mEPSC: miniature excitatory postsynaptic current; sEPSC: spontaneous excitatory currents; EEG: electroencephalography.

The SYNGAP1 gene is located on mouse chromosome 17 (6p21.3 in humans) and gives rise to multiple protein isoforms with several functional domains (**Figure 1.6**). Each isoform contains the GAP domain that enhances the activity of small GTPases. Three different isoforms (SYNGAP1 A, B, and C), which differ in their N-termini arise from multiple promoter regions, and are regulated by synaptic activity and postnatal ages (McMahon et al. 2012). SYNGAP1 A and B carry a complete pleckstrin homology (PH) domain, which mediates protein-protein interaction and lipid binding (Lemmon 2004). SYNGAP1 C has neither a unique amino acid sequence nor a complete PH domain. The C2 domain mediates binding to phospholipid and/or Ca^{2+} (Südhof & Rizo 1996), and a proline-rich region (PRO) binds to SH3 domains (Cohen et al. 1995). The C-terminal coiled-coil domain (CC) facilitates the SYGNAP1 trimerisation (Zeng et al. 2016).

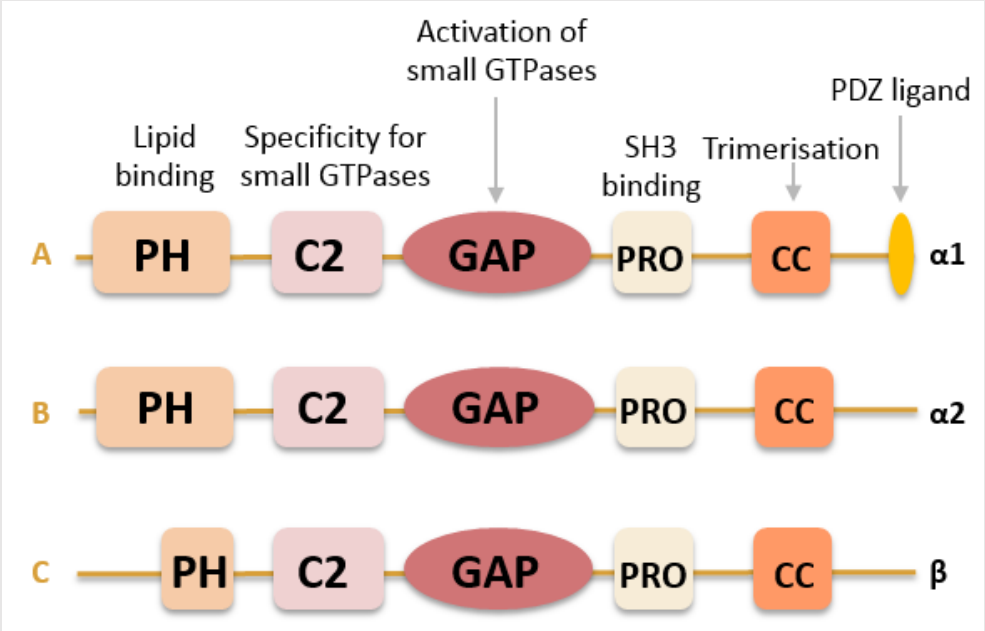

Figure 1.6 |SYNGAP1 isoforms.

Different isoforms of SYNGAP1 vary in both N-terminal and C-terminal (γ isoform not shown). PH: pleckstrin homology; GAP: GTPase activating protein; PRO: proline-rich domain; CC: Coiled-coils; SH3: SRC homology 3 domain.

Alternative splicing of SYNGAP1 also leads distinct C-terminal isoforms (α1, α2, β and γ), which modulates interactions of SYNGAP1 with other PSD proteins (McMahon et al. 2012). SYNGAP1 α1 is the most studied C-terminal isoform, as it carries the four amino acids (QTRV) necessary for binding PDZ domains (**Figure 1.6**). SYNGAP α2, β and γ lack this PDZ-binding domain. Although all these splice variants are wildly expressed throughout the brain, α2 and γ isoforms are less abundant (Li et al. 2001). Several studies have demonstrated the binding of SYNGAP1 α1 to PDZ domains of PSD95 plays an important role in regulating the composition of the PSD (Zeng et al. 2016; Walkup et al. 2016). Together the above findings indicate an additional role of SYNGAP1 in postsynaptic scaffold protein interactions.

SYNGAP1 *de novo* mutations have been identified in autism spectrum disorders (Berryer et al. 2013), intellectual disability (Hamdan *et al.*, 2009; Hamdan *et al* 2011; Rauch *et al.*, 2012; Mignot *et al.*, 2016), and epilepsy (von Stülpnagel et al. 2015) using exome sequencing or the candidate gene approach (**Table 1.4**). Deleterious mutations in SYNGAP1 are distributed throughout the gene, although the first two and last two exons (exon 1, 2 and 18, 19) are spared, as well as exons 9 and 16, which are present in all known isoforms (Mignot et al. 2016).

SYNGAP1 is one of the most common causes of intellectual disability and accounts for up to 1% of patients with intellectual disability (Mignot et al. 2016). Recently, a large genetic study analysed the exomes of 4293 families containing individuals with developmental disorders and found that SYNGAP1 is one of the six most significantly associated genes (Deciphering Developmental Disorders Study 2017). The question remains whether GAP deficiency is responsible for the pathological phenotypes observed in both human and animal models. Alternatively, or additionally, the lack of protein-protein interaction may contribute to the pathology (Zhou et al. 2016).

Patient ID	Location in gene	Mutation type	Diagnoses	Clinical features and comments
1	Intron 1- exon 9 (PH, C2, GAP)	Intragenic deletion	Severe ID, epilepsy	Developmental delay.
2	Exon 4 (PH)	Nonsense	Mild ID, ASD	Neurological examination normal.
3	Exon 5 (PH)	Nonsense	Moderate ID	Global hypotonia, gait ataxia.
4	Exon 5 (PH)	Nonsense	Severe ID, ASD	Truncal hypotonia.
5	Exon 5 (PH)	Frameshift	Severe ID, ASD	Absence of speech, clumsy gait.
6	Exon 5 (PH)	Nonsense	Severe ID, ASD	Facial and truncal hypotonia, broad-based gait.
7	Intron 5 (PH)	Splice site	Moderate ID	Truncal hypotonia.
8	Exon 8 (C2)	Frameshift	Moderate ID	Facial hypotonia with drooling, ataxic gait.
9	Exon 8 (C2)	Frameshift	Moderate ID	Truncal hypotonia, gait ataxia.
10	Exon 8 (C2)	Nonsense	Severe ID, ASD	Absence of speech, truncal hypotonia, gait ataxia.
11	Exon 10 (GAP)	Nonsense	Severe ID	Absence of speech, swallowing difficulty.
12	Exon 11 (GAP)	Missense	Severe ID	Absence of speech, mild gait ataxia.
13	Exon 12 (GAP)	Nonsense	Severe ID	Absence of speech, hyperactive deep tendon reflexes, unsteady gait.
14	Exon 13 (GAP)	Frameshift	Mild ID, ASD	Moderate akinesia, gait ataxia, truncal hypotonia.
15	Exon 15 (PRO)	Frameshift	Moderate ID	Truncal hypotonia, truncal tremor, ataxic gait.
16	Exon 15 (PRO)	Frameshift	Severe ID, ASD	Absence of speech, truncal hypotonia.
17	Intron 15 (PRO)	Splice site	Severe ID, ASD	Absence of speech, wide-based gait.

Table 1.4 | Human SYNGAP1 mutations.

Molecular and clinical features of human SYNGAP1 mutations. PH: pleckstrin homology; GAP: GTPase activating protein; PRO: proline-rich domain; ASD: autism spectrum disorder; ID: intellectual disability. Data from Mignot *et al.*, 2016.

We hypothesise GAP deficiency is the major contributor of the disease phenotypes, because molecular pathway network analyses for ASD-associated genes revealed the convergence upon the Ras-ERK pathway (Wen et al. 2016) in which SYNGAP1 is involved. Correspondingly, SYNGAP1 null mutants display abnormal levels of several components of the Ras-ERK pathway. If GAP deficiency is responsible, there is a potential to develop a new pharmacotherapy for patients with SYNGAP1 haploinsufficiency, as GAP function is more easily targetable than the structural function of SYNGAP1.

Collectively, the aforementioned findings indicate the structural and functional interplay between SHANK3 and SYNGAP1 in NMDAR complexes. Both SHANK3 and SYNGAP1 are enriched at the PSD, associate with each other, and are implicated in the same set of neurodevelopmental disorders. Despite the common features, however, SYNGAP1 and SHANK3 loss-of-function mutations significantly differ in their functional synaptic deficits: while reducing SYNGAP1 leads to premature dendritic spine formation and increased synaptic transmission (Clement et al. 2012), lack of SHANK3 reduces the size and density of the PSD, and decreases synaptic transmission (Bozdagi et al. 2010; Peça et al. 2011). In addition, while SHANK3 homozygous knockout animals are viable (Bozdagi et al. 2010), SYNGAP1 null mice die within a week (Komiyama et al. 2002; Kim et al. 2003). It remains therefore to be investigated how mutations in distinct synaptic proteins result in the same set of neurodevelopmental disorders. We hypothesise that the NMDA receptor, SHANK3 and SYNGAP1 form multi-protein complexes at the PSD, and that mutations in these genes disrupt the structural and/or functional architecture of NMDAR complexes leading to convergent clinical phenotypes.

1.4 CRISPR/Cas9 genome editing system

To create novel mouse models with mutations in SHANK3 and SYNGAP1, we used a recently developed genome editing technology, the CRISPR/Cas9 system (Ran et al. 2013). Historically, targeted gene mutation has been achieved by homologous recombination (Capecchi 2005). However, the vector construction is time-consuming, and the low efficiency of homologous recombination in mammalian cells limits the utility of this approach. Although RNA interference (RNAi) can facilitate inexpensive and high-throughput investigation of gene function (Elbashir et al. 2001), it is limited by offering only temporary inhibition of gene function (Alic et al. 2012). Other recent methods using engineered nucleases such as Zinc-finger nucleases (ZFNs) and Transcription activator-like effector nucleases (TALENs) can produce a permanent mutation by introducing a targeted double stranded break (DSB) in the chromosome (Miller et al. 2011; Urnov et al. 2010). However, engineering these nucleases is laborious and costly, hindering their widespread use (Ran et al. 2013). The CRISPR/Cas9 system is significantly easier to design and cost-effective.

CRISPR is the microbial **c**lustered **r**egularly **i**nterspaced **s**hort **p**alindromic **r**epeats (CRISPR) adaptive immune system that cleaves exogenous genetic elements using RNA-guided nucleases (Garneau et al. 2010). Three types (I-III) of CRISPR systems have been identified in a wide range of bacterial and archaeal hosts. Each system contains a group of CRISPR-associated (Cas) genes, noncoding RNAs and an array of direct repeats (**Figure 1.7**). These repeats are interspaced by protospacers, short adaptable sequences derived from foreign DNA targets, and together they comprise the CRISPR RNA (crRNA) array (Makarova et al. 2011). The protospacers are immediately preceded by a protospacer adjacent motif (PAM), which vary depending on the particular CRISPR system (Ran et al. 2013).

The Type II CRISPR interference has become the system adapted for genome editing in mammalian cells due to its relative simplicity (Sapranauskas et al.

2011), comprising of the Cas9 (**C**RISPR-**as**sociated protein **9**) nuclease, the crRNA array encoding guide RNAs, and trans-activating crRNA (tracrRNA) mediating the processing of the crRNA array into separate units (Garneau et al. 2010). Each crRNA unit comprises a partial direct repeat and a 20 nucleotide (nt) guide sequence, which directs Cas9 to the DNA target via Watson-Crick base paring. In the Type II CRISPR system derived from *Streptococcus pyogenes* (which is the system used in this study), a 5'-NGG PAM sequence must immediately follow the target DNA. The CRISPR system is reconstructed in mammalian cells by expression of human codon-optimised Cas9 and the required RNA elements (Mali et al. 2013). In addition, the crRNA and tracrRNA are fused together to make a chimaeric, single-guide RNA (sgRNA). Cas9 can therefore be directed toward any locus in the genome in immediate adjacency of PAM by selecting 20 nt guide sequences within the sgRNA.

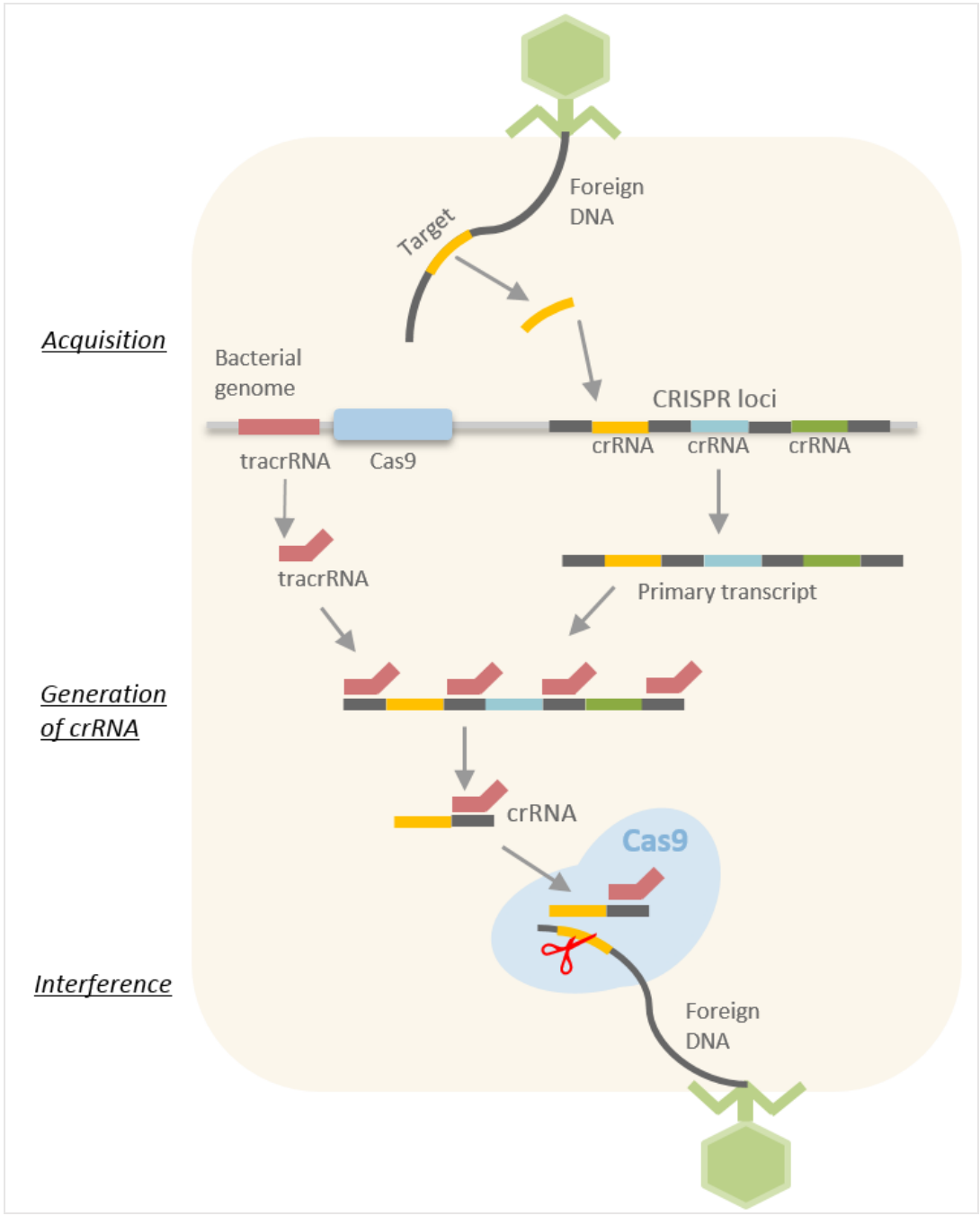

Figure 1.7 | CRISPR/Cas9-mediated immunity in prokaryotes.

During the acquisition stage, an invading foreign DNA (or RNA) is captured and cleaved by endogenous Cas9, and it is subsequently incorporated into the CRISPR loci. The CRISPR loci are then transcribed and processed into crRNAs. Upon re-infection, Cas9 complexed with the crRNA and tracrRNA cleaves the foreign DNA. crRNA: CRISPR RNA; tracrRNA: trans-activating crRNA.

Similar to ZFNs and TALENs, Cas9 facilitates genome editing by generating a double-stranded DNA break in the target locus. The resulting cellular repair mechanisms can be exploited to induce various types of mutations including deletion and point mutation (Cong et al. 2013) (**Figure 1.8**). CRISPR/Cas9 offers several advantages over ZFNs and TALENs, including the ease of design, the ability for multiplex genome editing, and higher editing efficiency (Ran et al. 2013).

Double-stranded breaks generated by Cas9 can be processed by two endogenous cellular pathways. In the error-prone end joining pathway, the break ends are re-joined by DNA repair machinery, which can result in random insertions or deletions (indels) at the site of the break (Dickinson & Goldstein 2016). These indels stem not from canonical non-homologous end joining as had been previously assumed, but from another end joining pathway that involves DNA polymerase θ (van Schendel et al. 2015) (**Figure 1.9**A). An indel mutation present within the coding region of a gene can lead to a reading frameshift generating a premature termination codon (Vicente-Crespo & Palacios 2010). Transcripts containing premature termination codons are eliminated by nonsense-mediated mRNA decay mechanisms resulting in gene knock-out (Brogna & Wen 2009) (**Figure 1.9**A). On the other hand, when homologous DNA fragments (donor DNAs) are present, another process called the homology-directed repair (HDR) can take place (**Figure 1.9**B). A crucial step in HDR is DNA end resection which creates a long 3' overhang that can invade the homologous DNA template (Liu & Huang 2016). Although HDR pathway occurs less frequently than end joining, it can be utilised to introduce precise modifications (**Figure 1.9**B) using a single-stranded DNA oligonucleotide as the donor DNA (Chen et al. 2011). The mutation in the donor DNA is copied into the genome in an error-free manner.

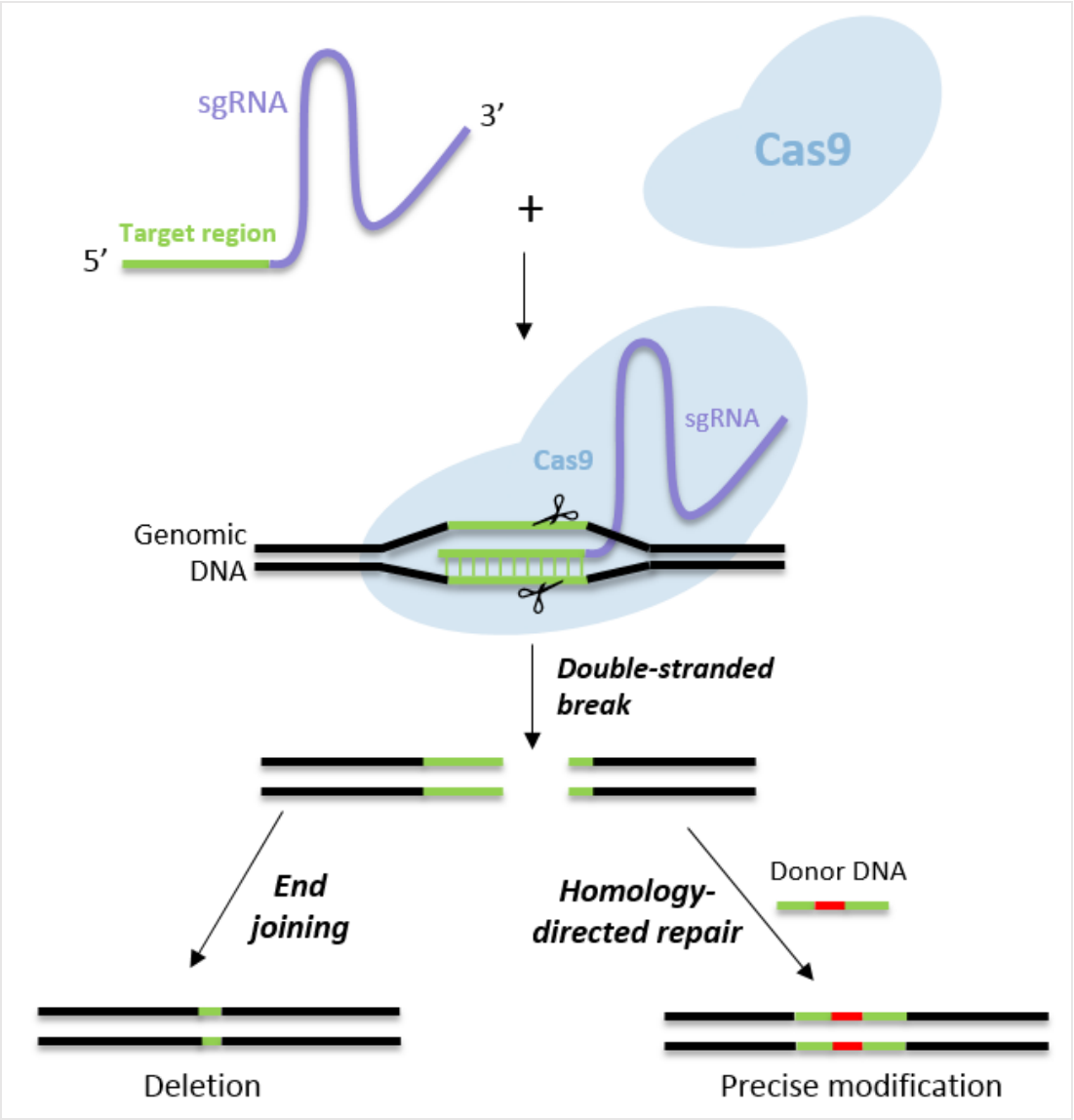

Figure 1.8 | CRISPR/Cas9 genome editing.

Double-stranded break repair facilitates gene editing. RNA-guided endonuclease, Cas9 generates targeted double-stranded break. The resulting repair pathways can be leveraged to induce deletion by the end joining mechanism as well as precise modification by the homology-directed repair.

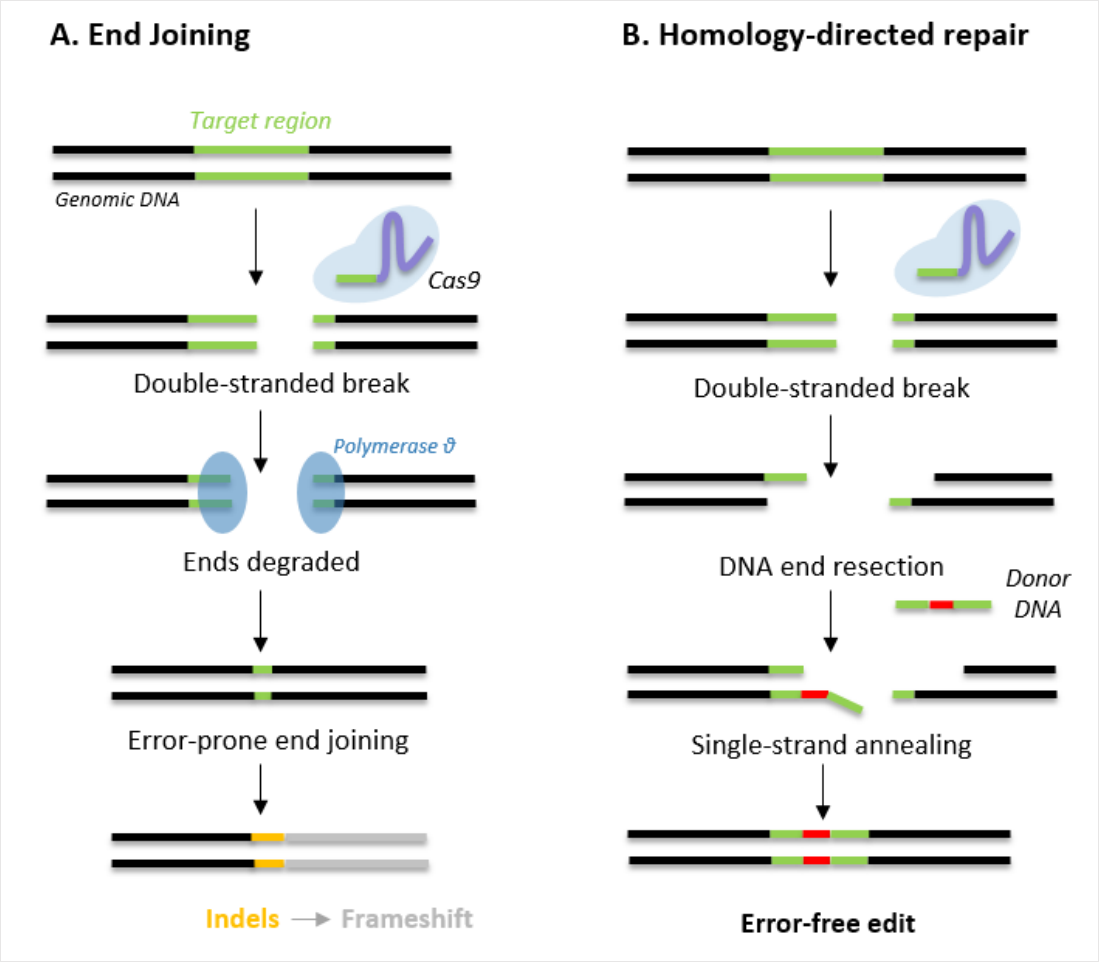

Figure 1.9 | DNA repair mechanisms.

A. End joining: Cas9 guided by short RNA generates double-stranded break at the target region. This can be repaired by the error-prone end joining pathway with DNA polymerase θ. The end joining can produce small insertions or deletions at the site of the break. If indels are generated in protein-coding sequence, it can shift the reading frame resulting in a premature stop codon. The CRISRP/Cas9 technology uses this end joining repair pathway to produce loss-of-function alleles.

B. Homology-directed repair: A donor DNA is introduced along with RNA-guided Cas9. DNA end resection generates a 3' single-strand DNA tail which can invade homologous sequence in the donor DNA (For the detailed mechanism of end resection see Liu and Huang, 2016). The mutation (in red) present in the donor DNA is copied into the genome via a single-stranded annealing mechanism resulting in an error-free edit.

The flexibility and simplicity of the CRISPR/Cas9 system has enabled the development of numerous applications and improvements. In addition to extensive use for gene modification, the CRISPR/Cas9 system has been repurposed for transcription regulation using catalytically dead Cas9 (dCas9) (Dominguez et al. 2016). This application was first demonstrated by mutating two nuclease domains of Cas9 from *Streptococcus pyogenes* (Qi et al. 2013). The resulting nuclease-deficient dCas9 allows direct regulation of DNA transcription without altering DNA sequence. dCas9 can facilitate the recruitment of various effector proteins for transcription repression or activation (Gilbert et al. 2013), DNA methylation or demethylation (Liu et al. 2016) and histone modifications (Hilton et al. 2015). Within a few years of being customised for mammalian gene editing, the CRISPR system now offers a highly versatile toolbox for robust and precise modification of genome and epigenome. Moreover, the CRISPR system has been applied to a wide range of species from a flowering plant *Arabidopsis thaliana* (Bortesi & Fischer 2015) to a free-living nematode *Caenorhabditis elegans* (Dickinson & Goldstein 2016).

The major criticism of any gene editing modalities is the possibility of unintended mutations at other sites in the genome (off-target) in addition to the targeted site (on-target) (Singh et al. 2014). As the CRISPR/Cas9 system targets genetic loci in a sequence-dependent manner, Cas9 may bind to off-target sites containing a similar sequence to the targeted sequence. However, a requisite PAM sequence limits binding to off-targets without the PAM sequence. The use of target selection software designed to minimise off-target activities is crucial (Ran et al. 2013; Naito et al. 2015). In addition, various methods for off-target detection are available including web-based prediction tools (Bae et al. 2014), deep sequencing (Cho et al. 2014), and chromatin immunoprecipitation (ChIP)-sequencing (Wu et al. 2014). The web-based software has an intrinsic limitation as the software assumes that off-target sequences are similar to the on-target site, overlooking off-target sites with low sequence similarity (Zhang et al. 2015). Deep sequencing measures off-target effects at rates ranging from 0.01

to 0.1% (Cho et al. 2014). ChIP-seq has also been adapted to find off-target binding sites for a specific sgRNA complexed with dCas9 (Wu et al. 2014). Encouragingly, most published studies report very rare, if any, off-target mutations (Yang *et al.*, 2013; Duan *et al.*, 2014; Veres *et al.*, 2014; Wu *et al.*, 2014). Overall, even with potential off-target effects, careful selection of the guide sequence will likely offer precise and effective gene modification.

Genetically modified mice are crucial tools for understanding the functions of genes in health and disease. Conventionally, gene modification is first introduced in ES cells, derived from the inner cell mass of a blastocyst. The modified ES cells are then injected into wild type blastocysts to produce germ-line chimaeras (Capecchi 2005). The CRISPR/Cas9 system offers one-step generation of genome engineered mice by directly injecting Cas9 mRNA and sgRNAs into zygotes (H. Wang et al. 2013; Yang et al. 2013; Mashiko et al. 2013). As zygote injection does not require complex and time-consuming ES cell line generation, it has been widely used in many laboratories to generate mutant mice (Oji et al. 2016). However, direct zygote injection has several limitations. The efficiency of complicated genome editing in mouse zygotes, including large deletions, gene knock-in and point mutations, varies among not only target genes but also among laboratories (Mashiko et al. 2013; Aida et al. 2015; Sakuma et al. 2015). It is therefore necessary to use cell lines to validate the efficiency of sgRNAs before the injection. Furthermore, the high incidence of mosaicism in founder mice complicates genotyping and phenotyping analyses (Yen et al. 2014; Oliver et al. 2015). Subsequent mating is necessary to produce fully homozygous mutant mice, making the amount of time similar to the conventional ES cell-mediated approach (Oji et al. 2016). The difference between zygote injection and ES cell-mediated approach is illustrated in **Figure 1.10** and summarised in **Table 1.5** and below.

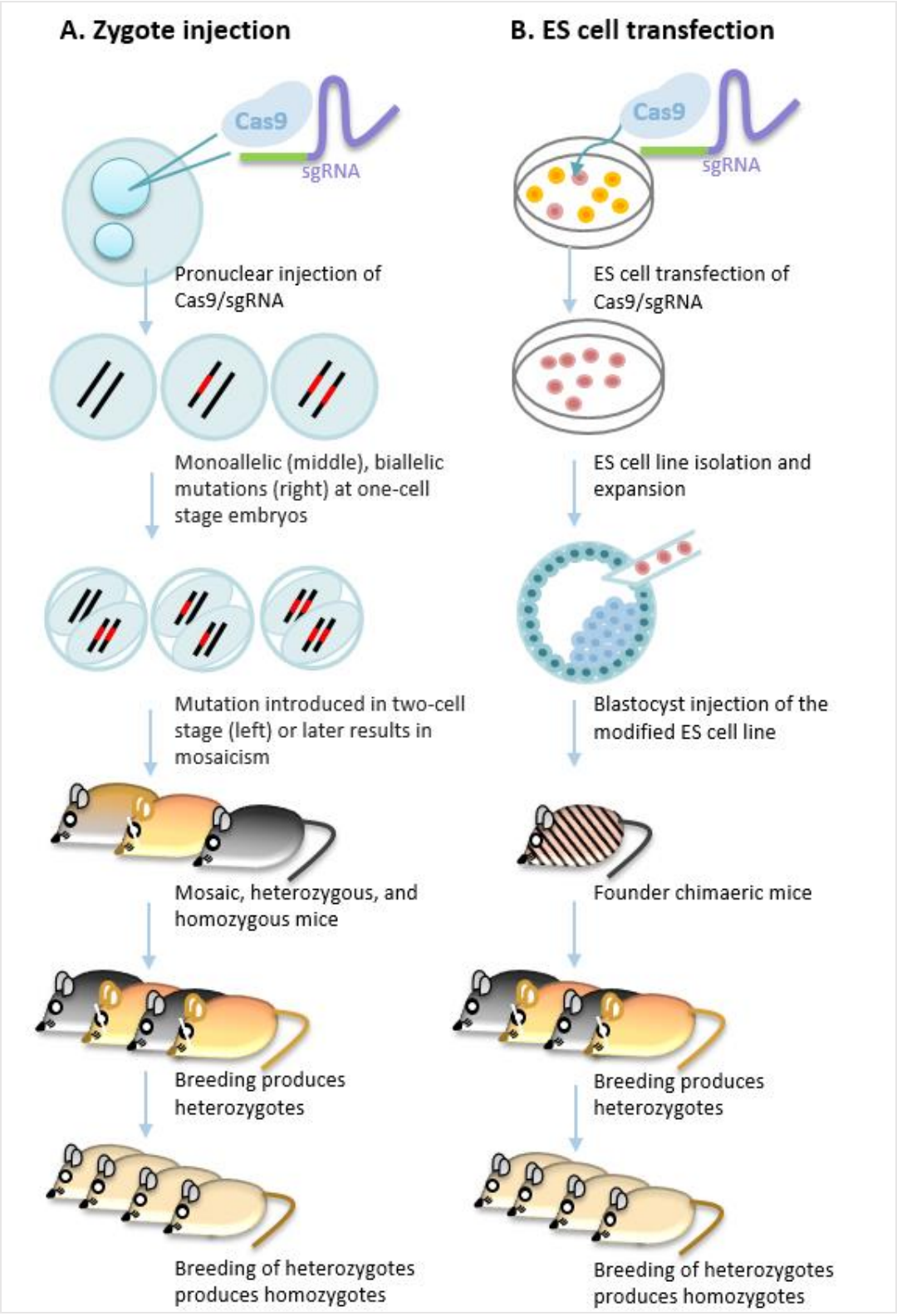

Figure 1.10 | Experimental procedures of zygote injection and ES cell transfection.

A. Zygote injection: mRNA of Cas9 and sgRNAs are directly injected to pronuclei of zygotes. The introduction of monoallelic or biallelic mutations at the one-cell stage results in mutant mice carrying a distinct mutation in all cell types. However, mutations occurred later than one-cell stage lead to mosaic founder mice.

B. ES cell transfection: ES cells are transfected with Cas9 and sgRNAs. The cell line with the desired mutation can be expanded and injected into blastocysts to generate chimaeric mice.

Both A & B: After the generation of founder mice, a series of mating follows to produce homozygous mice.

	Zygote injection	ES cell transfection
Pros	One step generation of mutant mice (Fast and efficient)	Precise and complicated genome editing Can perform control experiment, optimisation and cell differentiation analysis
Cons	Mosaicism in founder animals	Additional steps of ES cell line generation (slow and laborious)

Table 1.5 | Zygote injection and ES cell-mediated methods.

In the present study, we examined the feasibility of genome editing in mice using an ES cell-mediated approach. First, we engineered SHANK3 deletion in mouse ES cells using the CRISPR/Cas9 system. Although several studies reported the generation of SHANK3 knockout mice previously (See **Table 1.1**), these studies were solely based on gene targeting by homologous recombination. It remained therefore to be seen whether generation of CRISPR/Cas9-mediated knockout mice was possible, and the ES cells-based approach was necessary to evaluate the efficiency of the CRISRP/Cas9 system. After successfully generating a SHANK3 knockout mouse line, we introduced a novel point mutation in SYNGAP1 gene for the first time with an aim of generating a GAP-deficient mouse line. These new mouse lines will facilitate research into the structural and functional interplay of SHANK3 and SYNGAP1 proteins in NMDAR complexes *in vivo*, and how the protein-protein interaction relates to the common pathophysiology.

Chapter 2 Materials and Methods

2.1 General procedures and materials

The CRISPR/Cas9 genome editing in mouse ES cells was performed as previously described (Ran et al. 2013) with modifications detailed below. All oligonucleotides were purchased from Invitrogen with a synthesis scale of 25 nmole, desalted and dry format.

All chemicals were analytical grade and products of Sigma-Aldrich unless otherwise indicated. Molecular cloning was performed using chemically competent *Escherichia coli* DH10B (Durfee et al. 2008; Grant et al. 1990). All enzymes and buffer solutions were purchased from New England Biolabs. ES cell culture was performed using ES cell line E14TG2a (a gift from Bill Skarnes, Wellcome Trust Sanger Institute) derived from 129/Ola strain. All ES cell culture reagents were products of Thermo Scientific, except where specified. All animal procedures were performed in accordance with Institutional Animal Care and UK Home Office guidelines.

2.2 Cloning using CRISPR/Cas9 backbone plasmid

Design of sgRNAs: Mouse genomic DNA sequences were extracted from the Ensembl genome browser (http://www.ensembl.org/index.html) and analysed by Serial Cloner (Serial Basics). 20 nt guide sequences were identified by sgRNA Designer (http://www.broadinstitute.org/rnai/public/analysis-tools/sgrna-design) of which search algorithms were described previously (Doench *et al.*, 2014). In order to clone the selected target sequences into a sgRNA-expressing plasmid pX330 (Addgene plasmid # 42230), each pair of oligos (**Table 2.1**) were synthesized in the form as follows:

5′- CACC**G**NNNNNNNNNNNNNNNNNNN – 3′

3′- **C**NNNNNNNNNNNNNNNNNNNCAAA – 5′

CACC and AAAC (highlighted in grey) were appended as cloning overhangs. In addition, a G-C base pair (underscored) substituted the 5' end of the guide sequence due to the transcription initiation requirement for U6 promoter of pX330. This does not negatively affect targeting efficiency (Ran et al. 2013).

Oligonucleotide annealing with phosphorylation: Oligonucleotides were resuspended and diluted in double-distilled water to make a final concentration of 100 µM. 1 µl of each pair of oligonucleotides was mixed with one unit of T4 Polynucleotide Kinase and 1 µl of 10X T4 Ligase Buffer in a volume of 10 µl which was made up by double-distilled water. The oligonucleotide mixture was incubated at 37 °C for 30 minutes, heating to 95 °C for 5 minutes and then cooling gradually to room temperature. 1 µl of the annealed oligonucleotide was diluted in 250 µl of 1X TE buffer.

BbsI digestion: 100 ng of pX330 was added to a reaction containing 1 unit of a restriction enzyme BbsI, 1.5 µl of 10X Buffer 2.1 in a volume of 15 µl made up by double-distilled water. The digestion mixture was incubated at 37 °C for an hour and treated with 0.5 µl of Shrimp Alkaline Phosphatase for 1 hour.

Digest/ligation mixture: The resulting digestion mixture (15 µl) was mixed with 2 µl of the diluted oligonucleotide mixture, 2 µl of T4 Ligase Buffer, and 1 µl of T4 Ligase. The digest/ligation mixture was incubated at room temperature for one hour and 7 µl was used for transformation into DH10B cells.

2.3 Design of DNA repair templates

The 100 nt single-stranded DNA donor oligonucleotides (ordered from Invitrogen) were designed with homologous flanking sequence centred around the predicted Cas9 cut site, and the desired point mutation along with Cas9-blocking and restriction enzyme site mutations (see Chapter 4). Cas9-blocking and restriction enzyme site silent mutations (which do not change the amino acid sequence) were selected based on the frequency of occurrence of synonymous codon from Codon Usage Database (http://www.kazusa.or.jp/codon/).

Mouse line	Function	Name	Sequence (5' to 3')
SHANK3	Vector construction	G1-F	CACCGCCACTGTGCTACCCGCCAG
		G1-R	AAACCTGGCGGGTAGCACAGTGGC
		G2-F	CACCGTGAAGGTTCTCCGCAACGG
		G2-R	AAACCCGTTGCGGAGAACCTTCAC
		G3-F	CACCGACCCGCCAGCGGAACGCAG
		G3-R	AAACCTGCGTTCCGCTGGCGGGTC
		G4-F	CACCGCCCCAGCTATGCAAAGCGA
		G4-R	AAACTCGCTTTGCATAGCTGGGGC
		G5-F	CACCGTCAGCCCGCAGCTTCTCCA
		G5-R	AAACTGGAGAAGCTGCGGGCTGAC
	Genotyping	SH3-E5-F	GTGTTTTTGACCGGCTGGGA
		SH3-E5-R	TGCCAACCATTCTCATCAGTG
		SH3-E10-F	CGTGATAACAATGAAAATGAGGGC
		SH3-E10-R	CAGGCCCTCCTACCTGATCT
		C17W1	ACCCCCAGCTATGCAAAGCGAC
		C17M1	CAGGGAAACCCCCAGCTGGGC
		C23W1	GCTATGCAAAGCGACGGCGT
		C23W2	CAAAGCGACGGCGTCTGGCT
		C23W3	GGCGTCTGGCTGGCCCGAGTG
		C23M1	CCATTCAGGGAAACCCCCAGCC
		C24W1	TATGCAAAGCGACGGCGTC
		C24W2	TATGCAAAGCGACGGCGTCT
		C24M1	GGAAACCCCCAGCTATGCAACGG
		Rev1	ACCCCTAGCCCCAGCCTATC
		Rev2	TGTGGGGGACGACGGACAGCCA
	Off-target analysis	OT1-F	GTTCAGGTGGACAGAAGCGT
		OT1-R	CAGTGTGGCTAGGTGTAGTGG
		OT2-F	GTTCAGGTGGACAGAAGCGT
		OT2-R	CAGTGTGGCTAGGTGTAGTGG
		OT3-F	AAGGCATGGGAGGCATTTACA
		OT3-R	GTCTGGAGTACCCAGCACTCT
		OT4-F	AGCTGGCCAGGAAAGGTGTTA
		OT4-R	AACAGCTATGTGTGCAGCTCT
		OT5-F	CTCAGAATGGCTGGACAACCT
		OT5-R	ACAGTGTGGGAACACTGGATG
		OT6-F	GCGCACCTCCAGATAACACT
		OT6-R	AATATGCCCAGCGTGCAAAC
		OT7-F	GGGCTGTCTACCATGAAGCA
		OT7-R	GACCAGGGTTGGCTGAACTG
		OT8-F	GACTGCCTGTGCACCAGAAT
		OT8-R	CCCTAGAGAGGCTCACTCCT
SYNGAP1	Vector Construction	SG1-G1-F	CACCGGTAGACCGATTCATGGAGC
		SG1-G1-R	AAACGCTCCATGAATCGGTCTACC
	Genotyping	SG1-E9-F	GTGGGCGGTGAAGAGAGAAT
		SG1-E9-R	GATGTACAACAGGGAGCGGT
		SG1-XL-F	TGTGACCAACCATTACCGGA
		SG1-XL-R	ATACCCCAGAAAATGCTTTGCC

Table 2.1 | Oligonucleotide sequences for CRISPR mice generation.

2.4 Chemical transformation

Preparation of competent cells: Single DH10B colonies from lysogeny broth (LB) agar plate were inoculated into 10 ml LB media and incubated at 37 °C overnight with shaking. 100 µl of overnight culture was added into 10 ml of fresh LB media, and incubated at 37 °C for 3 hours with shaking. The cells were harvested by centrifugation at 2500g for 5 minutes at 4 °C. The supernatant was decanted, and the cell pellet was resuspended in 10 ml of ice cold $CaCl_2$ and incubated on ice for 1 hour. The cells were collected by centrifugation at 2500g for 5 minutes at 4 °C. The cell pellet was resuspended in 1 ml of ice cold $CaCl_2$.

Transformation of competent cells: 7 µl of the ligation mixture containing the targeting vectors was added to 100 µl of competent DH10B cells, incubated on ice for 1 hour and then heat treated at 42 °C for 2 minutes in a water bath. The cells were then spread onto LB agar plates containing ampicillin (0.1mg/ml) and incubated at 37 °C overnight.

2.5 Plasmid DNA preparation and sequencing

Individual colonies were selected from LB agar plates containing ampicillin and inoculated 3 ml LB media with ampicillin and incubated at 37 °C overnight with shaking. Plasmid DNA was extracted using the Wizard® Plus Minipreps DNA Purification System (Promega) according to the manufacturer's protocol. Plasmid sequencing was performed using U6 promoter primer (5' GACTATCATATGCTTA CCGT 3').

2.6 Sequence analysis

All sequencing was performed by Edinburgh Genomics, using Sanger sequencing. Reference mouse genomic DNA and peptide sequences were retrieved from Ensembl genome browser (http://www.ensembl.org/index.html) aligned using MAFFT (http://www.ebi.ac.uk/Tools/msa/mafft/) in ClustalW output format. Chromatogram data were analysed using FinchTV (Geospiza, Inc).

2.7 Embryonic stem cell culture

Feeder-free ES cells were maintained in cell culture flasks coated with 0.1% gelatin (Sigma-Aldrich) in ES cell media containing G-MEM, 10% Foetal bovine serum (Hyclone), 1% sodium pyruvate, 1% nonessential amino acid, 2 mM L-glutamine, 100 μM 2-mercaptoethanol and 1000 U/ml leukemia inhibitory factor (Chemicon) at 37 °C supplemented with 5% CO_2. Cryovials containing frozen ES cells were quickly defrosted at 37 °C and diluted and washed with the ES cell media before plating and grown at 37 °C with 5% CO_2. Culture media were changed with every 24 hours and 2-3 hours before passage. ES cells were passaged by trypsinizing (incubating with 0.25% Trypsin-EDTA for 1-3 minutes at 37 °C) and then by mechanically breaking up ES cell aggregates.

Transfection of ES cells: pX330 with the target sequence insert was co-transfected into ES cells (passage number 26) with the pPGKpuro (Addgene plasmid # 11349) encoding puromycin-resistance gene using Promega FuGENE HD transfection Kit. 3.3μg of DNA in total was transfected in 1:1 ratio of pX330 and pPGKpuro into ES cells seeded 3 x 10^5 in a 6-well plate (9 cm^2). For SYNGAP1 experiment, donor DNA oligonucleotides were co-transfected along with pX330 and pPGKpuro in 1:1:1 ratio.

One day after transfection, ES cells were split into a 100 mm petri dish (55 cm^2). 24 hours after plating, puromycin (Cayman Chemical) was applied for positive selection at a concentration of 2 µg/ml and taken off after 3 days. After recovering for seven days, the surviving cells were either harvested from the petri dish for functional testing of targeting vectors, or isolated by manual cell picking and plating into each well of a 48-well plate for clonal isolation of ES cells. Individual colonies were then expanded and duplicated into two 48-well plates for either genomic DNA extraction or freezing. To freeze, ES cell media was replaced with freezing media containing 10% DMSO and 10% Foetal bovine serum.

2.8 DNA extraction from mammalian tissues

For DNA extraction from the heterogeneous population of CRISPR/Cas9-modified ES cells, the cells were scraped off from the petri dish using a cell scraper in warmed phosphate-buffered saline (PBS), and centrifuged at 1200 rpm for 4 minutes. The cell pellet was resuspended in 500 µl of Tail Digestion Buffer (TDB; 50 mM KCl, 10 mM Tris-HCl, 0.1% Triton X100 and 0.4 mg/ml Proteinase K) and incubated at 56 °C overnight, followed by heat treatment at 95 °C for 10 minutes.

For DNA extraction from individual ES cell colonies, genomic DNA was extracted by using Wizard SV 96 Genomic DNA Purification System (Promega) according to the manufacturer's protocol in a manual format. Briefly, DNA was purified from ES cell lysates by 96-well vacuum filtration using a vacuum pump and the Vacuum Manifold.

DNA genotyping was completed using mouse ear-clips or tail samples. Biopsies were added to 100 - 300 µl of TDB and incubated at 56 °C overnight, followed by heat treatment at 95 °C for 10 minutes. 1-2µl of a DNA extract was used for Polymerase chain reaction (PCR) amplification.

2.9 PCR amplification

Oligonucleotides used as PCR primers were designed using NCBI Primer-BLAST (https://www.ncbi.nlm.nih.gov/tools/primer-blast/). The PCR primers were designed to amplify 150-300 bp on either side of the target region for a total amplicon to be 300-600 bp to facilitate clear visualisation in agarose gel. PCR reactions were carried out in DNA Engine Tetrad 2 (MJ Research) or T100TM Thermal Cycler (Bio-Rad). Oligonucleotide sequences are listed in Table 2.1.

Approximately 1 µg of genomic DNA template was added in a reaction containing 2X HotStarTaq Master Mix (Qiagen), 20 µM of forward and reverse primers in a volume of 25 µl made up by double distilled water. The standard PCR cycling protocol is shown in **Table 2.2**.

Step	Temp.	Time	Number of cycles
Initial denaturation	95°C	5 min	1
Denaturation	94°C	30 sec	
Annealing	58-68°C	30 sec	34
Extension	72°C	30 sec	
Final extension	72°C	10 min	1
	4°C	hold	

Table 2.2 |Standard PCR cycling protocol.

2.10 Restriction enzyme digestion

PCR products were digested with restriction endonucleases Sau3AI or DraI. 10 µl of PCR products were mixed with NEB 10X digestion buffer and the appropriate volume of water before adding 0.5 µl of the restriction enzyme. The digestion mixture was incubated at the 37°C for 2 hours. Restriction fragments were size-separated by agarose gel electrophoresis as described below.

2.11 Agarose gel electrophoresis

For analysis of DNA fragments, agarose gel electrophoresis was performed using Owl Mini Gel Electrophoresis Systems (Thermo Scientific) according to the manufacturer's manual unless otherwise specified below. To visualise DNA under ultraviolet light, GelRed Nucleic Acid Stain (Biotium) was added to agarose gel. 8-10 µl of samples mixed with 6X Gel Loading Dye (Thermo Scientific) were loaded on the gel along with 6 µl of GeneRuler DNA Ladders (Thermo Scientific) in 1X TBE buffer (from 10X stock solution containing 108 g Tris base, 55 g Boric acid and 9.5g EDTA disodium salt). The gel system was connected to PowerPac HC High-Current Power Supply (Bio-Rad) and run at 100-120 V for 45-60 minutes. The gel was imaged using GelDoc-It Imager (UVP) or Odyssey Fc Imaging System (LI-COR).

2.12 T7 endonuclease assay

PCR was performed using DNA from control ES cells (wild-type) and CRISPR-treated ES cells (mutant). PCR products were then purified using Qiagen PCR Purification Kit according to the manufacturer's protocol. 100 ng of WT PCR product and 100 ng of mutant PCR product were added to NEB Buffer 2 in a volume of 10 µl made up by double distilled water. The mixture was heated using PCR block at 95 °C for 5 min and cooled down to room temperature to anneal the PCR product. The annealed product was then digested with 1 µl of NEB T7 endonuclease I at 37 °C for 20 min. 2 µl of 0.25 M ethylenediaminetetraacetic acid (EDTA) was added to stop the reaction, and the digest was run on a 2.5% agarose gel as described above. The cleavage intensity was measured as previously described by Ran *et al.*, 2013 and the detail of the procedure will be provided in Chapter 3.

2.13 Off-target analysis

CRISPR/Cas9 target online predictor CCTop (Stemmer et al. 2015) was used to find potential off-target sites that differed from SHANK3 on-target sequence (5' CCCCCAGCTATGCAAAGCGA 3') by up to 4 nt. The 8 potential off-target sites (Table 2.4) were amplified by PCR from genomic DNA of the three selected ES cell lines, then purified using Qiagen PCR Purification Kit according to the manufacturer's protocol. The PCR products were subsequently subject to sequence analysis as described above.

Name	Strand	Mismatch	Position	Sequence (5' to 3')
On-target	+	0	chr15: 89521118 (SHANK3 exon10)	CCCCCAGCTATGCAAAGCGA
Off-target 1	+	3	chr6:147732596 (Intergenic)	CCaCCAGCTATGCAAAtCcA
Off-target 2	+	3	chr13:25563699 (Intergenic)	CCCaCAGCTATGCAtAGCtA
Off-target 3	-	4	chr14:66171714 (Exonic)	CCCaCAGCTATGCAtAGCtA
Off-target 4	-	4	Chr1: 24012440 (Exonic)	CCtaCAGaTATGCAAAGCcA
Off-target 5	-	4	Chr9: 73007795 (Exonic)	CGCCCAGtTcTGCAAAGCaA
Off-target 6	-	4	Chr8: 34270077 (Intergenic)	CCCaCAGtTATaCAAAGCcA
Off-target 7	+	4	Chr19: 24085323 (Intergenic)	gCCCCAcCcATGCtAAGCGA
Off-target 8	-	4	Chr18: 35884000 (Intergenic)	ttCaCAGCTATGCAAAaCGA

Table 2.3 | List of off-target sites.

Potential off-target sites that differed from on-target SHANK3 sequence by up to 4 nt. Lower cases in sequence indicate mismatches.

2.14 Mouse colony establishment

Mouse chimaeras were produced by injecting mutant ES cell lines into C57BL/6J blastocysts. The ES cell lines were cultured for at least three passages after thawing for blastocyst injection. The injection was performed in Central Bioresearch Services, University of Edinburgh. Chimaeras were crossed with C57BL/6J wild-type mice and the first heterozygotes were produced in the F1 generation. The heterozygotes were then backcrossed with C57BL/6J wild-type mice. Inter-crosses between F2 heterozygotes were used generate homozygote mutant mice in the F3 generation.

2.15 Forebrain brain extraction

Dissection: All mice were dispatched by cervical dislocation. The brain was removed from the skull immediately and placed on a plastic plate covered with filter paper on ice. The cerebellum, olfactory bulb and midbrain were removed and discarded. The remaining forebrain was snap-frozen using liquid nitrogen and stored at – 80 °C until use.

Protein extraction: Frozen brains were homogenised individually using a Dounce homogeniser with 3.5 ml of homogenisation buffer containing 10% sodium deoxycholate (DOC), 1 M Tris pH 9, 0.5 M NaF, 20 mg/ml phenylmethylsulfonyl fluoride (PMSF) made in 100 % ethanol, one protease inhibitor cocktail (Roche) tablet per 50 ml and 1% phosphatase inhibitor cocktail (Milipore). Homogenates were centrifuged at 23000 rpm for 15 minutes at 4 °C. The supernatant was then aliquoted and frozen on liquid nitrogen. All homogenates were stored at -80 °C and thawed on ice before use. Protein extracts were quantified using a Pierce BCA Protein Assay Kit (Thermo Scientific) and using The SpectraMax i3x (Molecular Devices) according to manufacturers' instructions.

2.16 Western blot

Separating proteins by SDS-PAGE: SDS-PAGE (Polyacrylamide gel electrophoresis) was performed with NuPAGE Bis-Tris 4-12% gradient gels using XCell SecureLock Mini-Cell (Invitrogen) according to the manufacturer's instruction unless otherwise indicated below. Six microliter of HiMark Pre-stained Protein Standard (Life Technologies) was loaded as molecular weight marker, and 10 μl of each 1 mg/ml protein sample (i.e. 10 μg) was loaded into each lane of the gel. The XCell SecureLock Mini-Cell was then connected to PowerPac HC High-Current Power Supply (Bio-Rad) and run at 160 V for 80 minutes.

Semi-Dry transfer: The gel was equilibrated in a small container containing 1X NuPAGE transfer buffer for 20 minutes. A nitrocellulose membrane (Bio-Rad), and blot filter papers (Bio-Rad) were soaked in 1X NuPAGE transfer buffer. The transfer stack was assembled in a Trans-Blot SD Semi-Dry Transfer Cell (Bio-Rad) according to the manufacturer's protocol. The transfer cell was connected to PowerPac HC High-Current Power Supply (Bio-Rad) and run at 15 V for 30 minutes.

Antibody probing and detection: The membrane was removed from the Western transfer assembly and inserted into a Falcon 50ml tube. The membrane was blocked with 10 ml 5% milk in PBS with Tween (PBS-T, 0.1% Tween20) for 1 hour at room temperature on a roller mixer (Stuart Scientific). The primary antibody was diluted (**Table 2.4**) in PBS-T and incubated with the membrane at 4 °C overnight. The membrane was washed in PBS-T for 3 x 5 minutes in PBS-T. The secondary horseradish peroxidase (HRP) antibody (GE Healthcare, sheep anti-mouse) was diluted to 1:50,000 in 10 ml 1% milk PBS-T and incubated with the membrane on the roller mixer at room temperature for 1 hour. SuperSignal West Femto Maxium Sensitivity Substrate (Thermo Scientific) was used as enhanced chemiluminescent substrate for HRP. Equal volumes of luminol/enhancer solution and stable peroxide solution were mixed

and protected from light. The final PBS wash (10 minutes) was poured off, and a total volume of 4 ml (i.e. 2 ml luminol + 2 ml peroxide) was incubated with the membrane for 5 minutes at room temperature. The membrane was then removed from the Falcon tube and wrapped in a clear plastic pocket (Office Depot). The membrane was imaged using Odyssey Fc Imaging System (LI-COR).

Antigen	Supplier	Antibody type	Working dilution
SHANK3 (sc-377088)	Santa Cruz	Mouse monoclonal	1:1000
Actin beta (HCA147D800)	Bio-Rad	Human monoclonal	1:5000

Table 2.4 | Primary antibodies.

Chapter 3 Design and generation of SHANK3 knockout mice

This chapter describes the design and generation of a SHANK3 knockout mouse model using ES cells modified by the CRISPR/Cas9 system. Overview of mutant mouse generation is illustrated in **Figure 3.1**, and **Figure 3.2** summarises the CRISPR/Cas9 experiment in ES cells.

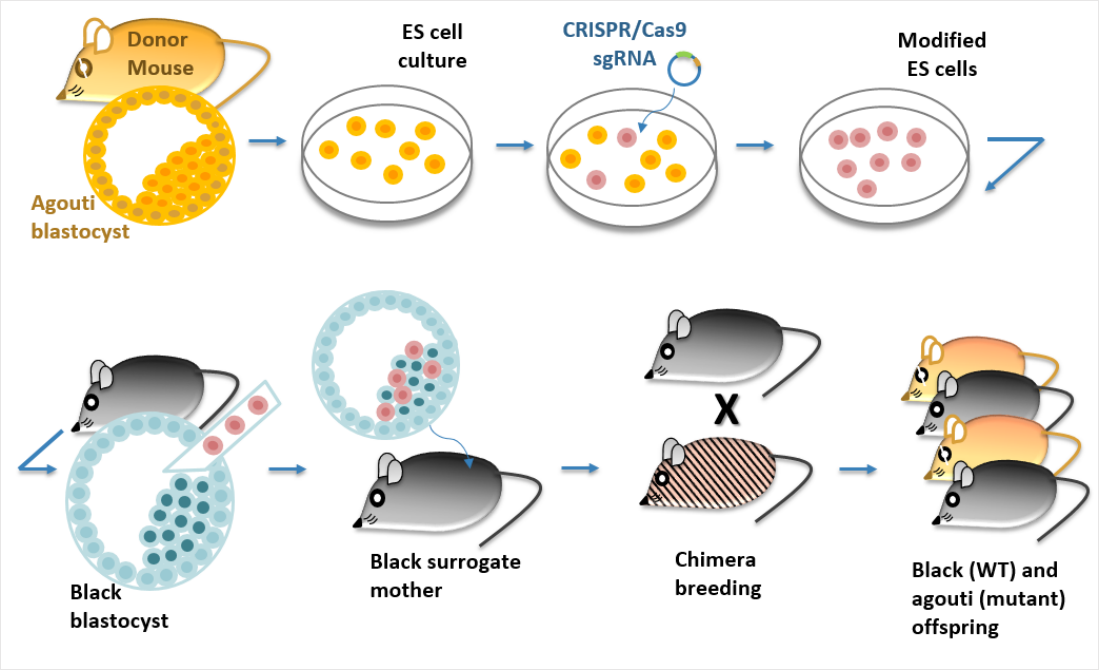

Figure 3.1 | Workflow of mutant mouse generation.

ES cells from agouti blastocysts are modified by the CRISPR/Cas9 system. ES cell lines with a desired mutation are injected into wild-type blastocysts to generate chimeric mice. Further breeding produces heterozygous and homozygous mice.

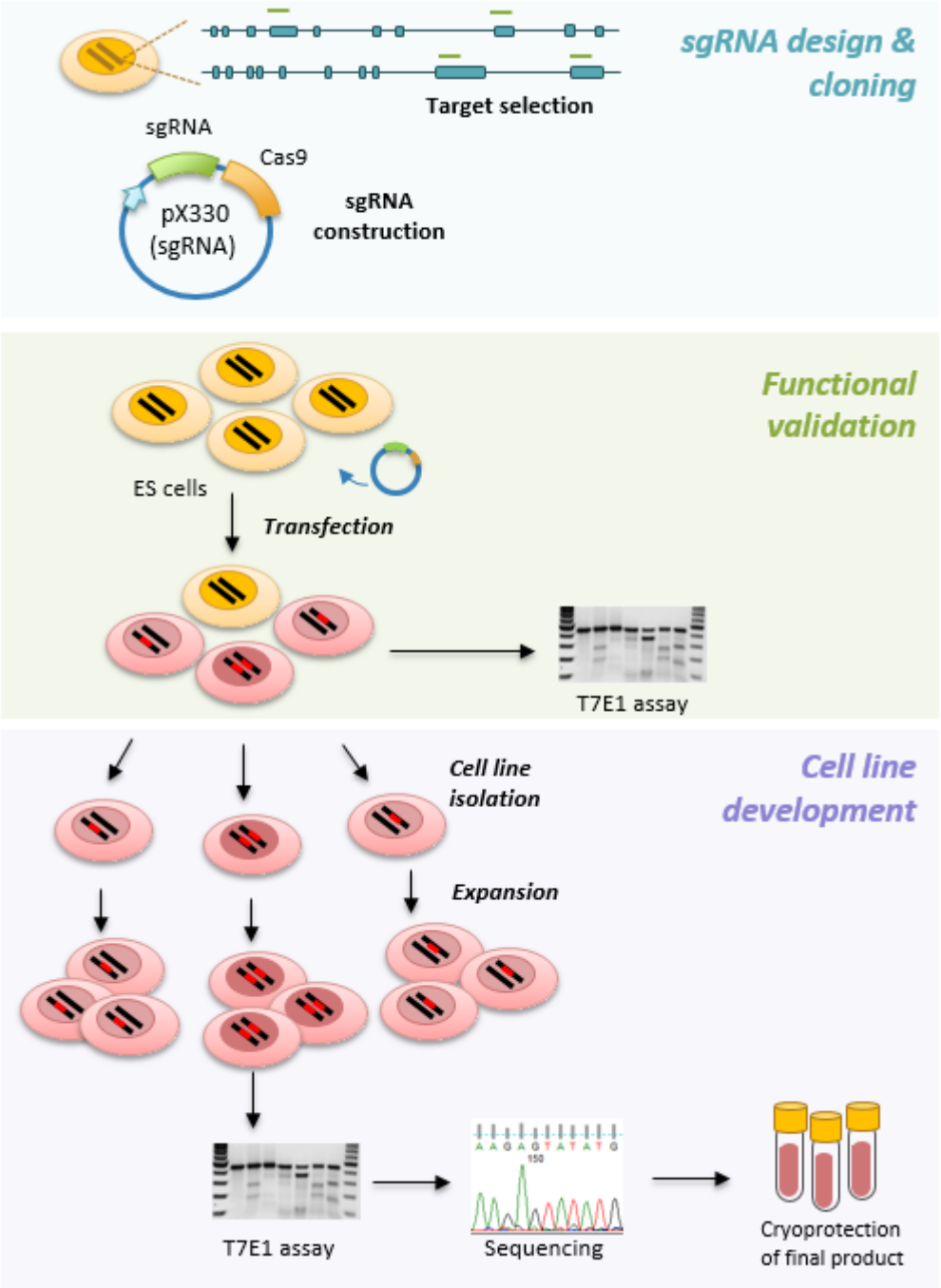

Figure 3.2 | CRISPR/Cas9-mediated gene editing in ES cells.

Illustration of stages for sgRNA design and cloning, functional validation and cell line development. The target sequence is cloned into a sgRNA expression vector pX330. Sequence-verified pX330 vectors are transfected into ES cells and assayed for their ability to introduce targeted DNA cleavage. Lastly, transfected cells are isolated individually and expanded to derive isogenic cell lines with distinct mutations.

3.1 Consideration of target sites

The efficiency of the CRISPR/Cas9 genome editing depends on the specificity of a 20 nt guide sequence within its sgRNA (Ran et al. 2013). The guide sequence must immediately precede a 5'-NGG PAM site, allowing the 20 nt guide to anneal with the opposite strand to mediate Cas9 cleavage between 3 bp and 4 bp upstream of the PAM sequence (Jinek et al. 2012) .

The mouse SHANK3 gene (ENSMUSG00000022623) sequence was obtained from the Ensembl genome browser, which lists four protein-coding transcripts (Ensembl: Shank3-201, 202, 203, and 207; **Figure 3.3**). To disrupt the expression of the major isoforms of SHANK3, three out of four protein-coding transcripts were considered for target selection (**Figure 3.3)**.

Target sites were searched using the CRISPR Design Tool provided by the protocol mentioned previously (Ran et al. 2013). Potential guide sequences were identified in the first several common exons (exon 3 to exon 10) of the three transcripts. As the first top guide sequences in exon 5 and exon 10 showed the highest guide quality scores, these sequences were incorporated into the sgRNA-expressing vector pX330. However, ES cells transfected with the resulting plasmids failed to survive after drug selection. The examination of the experimental procedures revealed that the PAM site was unintentionally added to the guide sequence in the cloning procedure. The requisite 5'-NGG PAM sequence itself should not be included in sgRNAs. Target selection was repeated and the experiment was initiated again from the very first step.

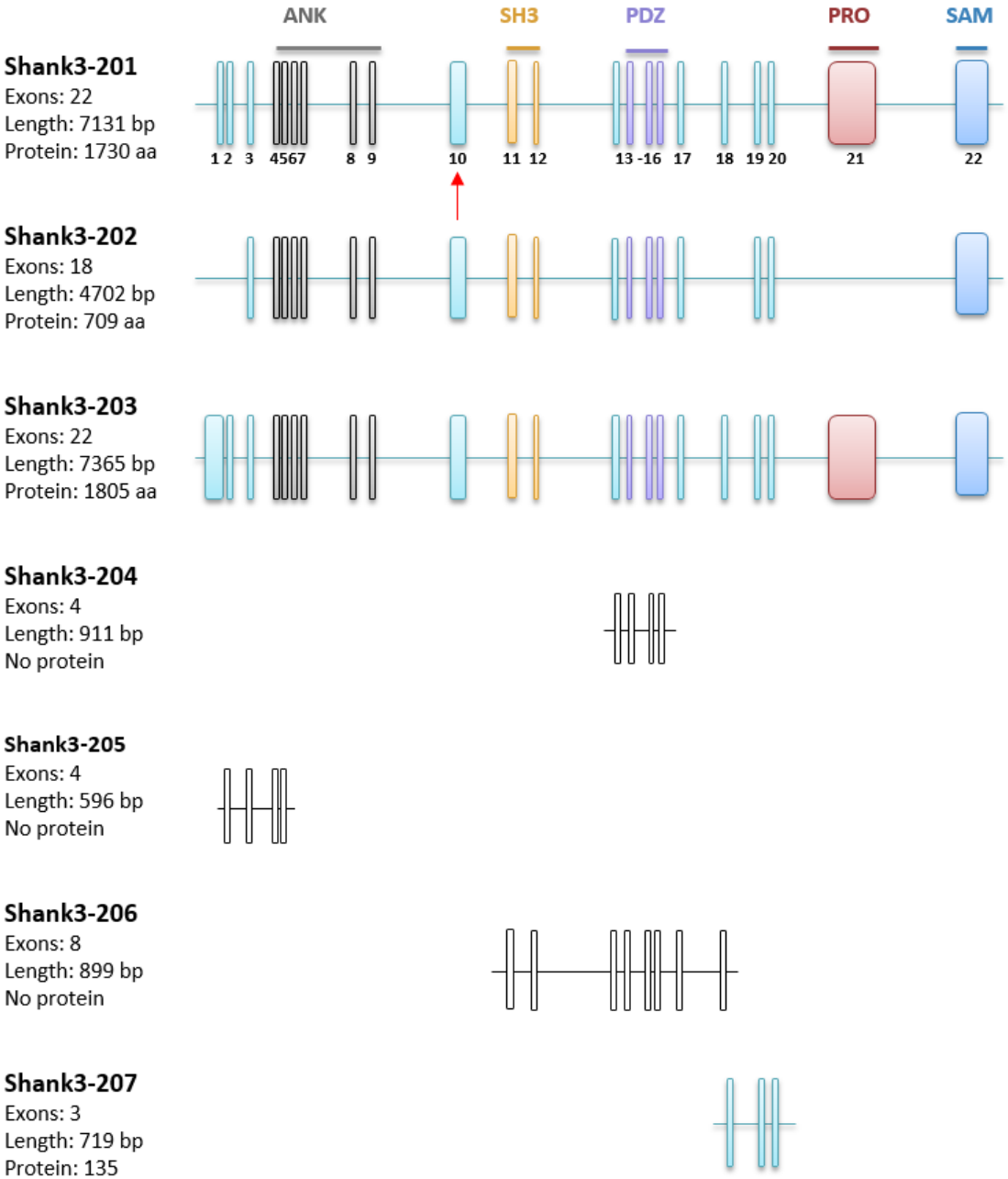

Figure 3.3 | Genomic structure and splice variants of SHANK3.

Schematic shows the full Shank3 mouse gene structure and four protein-coding transcripts listed in Ensemble database. Target exon in this study is indicated by the red arrow. Transcript Shank3-207 results in a relatively small protein (135 amino acids, aa) compared to other three transcripts (709 - 1805 aa), and lacks all of five major protein domains. Therefore, this transcript was not considered for target selection. Note that additional transcripts generated by alternative splicing and intragenic promoters are also present. aa: amino acid.

3.2 Target selection

An alternative target site finder, the sgRNA Designer, was used to search for new guide sequences. This was because, unlike the tool we previously used, the sgRNA Designer implements a published sgRNA scoring algorithm optimised for high on-site efficacy of sgRNAs (Doench et al. 2014).

As our intention was to establish gene deletion induced by premature termination, importance was focused on exons of SHANK3 that were present in all of the major isoforms. For this reason, only exon 5 and 10 were considered, as they had been previously analysed.

Five guide sequences per each exon were initially considered for cloning. The selection criteria were the sgRNA quality score, and for the sequence to be on the sense strand (**Table 3.1**). Only the sense strand sequences were chosen because of ease of targeting vector construction. The first two guides from exon 5 and the last three guides from exon 10 were selected for targeting vector construction (**Figure 3.4**) to attempt the targeting efficiency of sgRNAs with a various range of sgRNA scores (0.61-0.35).

Target	Spacer Sequence	Strand	sgRNA core	Note
Exon 5	CGTTGCGGAGAACCTTCAGG	antisense	0.71	
	TCCGCTGGCGGGTAGCACAG	antisense	0.49	
	CGTTGTCCAACTGTGCCGCA	antisense	0.48	
	TCCACTGTGCTACCCGCCAG	sense	0.39	G1
	CTGGCGGGTAGCACAGTGGA	antisense	0.38	
	CTGAAGGTTCTCCGCAACGG	sense	0.35	G2
	TACCCGCCAGCGGAACGCAG	sense	0.34	
	CTACCCGCCAGCGGAACGCA	sense	0.26	
	TGGACTTCCGGACCCGAGAT	sense	0.22	
	GCTACCCGCCAGCGGAACGC	sense	0.22	
	CAACGCCACTGACCTCCTGA	sense	0.19	
	GAGAACCTTCAGGAGGTCAG	antisense	0.15	
Exon 10	CGAGTGGCCTGGCATCCCCA	sense	0.75	
	CTTGCTCCAGAGGCTTCAGG	sense	0.65	
	TCACTGGCTGAGCGCTGTAA	antisense	0.62	
	GGAGGAGAAAGACCGTGACA	sense	0.61	G3
	CCCCCAGCTATGCAAAGCGA	sense	0.58	G4
	GGAGCAAGAGTTGATGAGGG	antisense	0.52	
	TGAGCGCTGTAAGGGCCGTG	antisense	0.52	
	TCTGGAGCAAGAGTTGATGA	antisense	0.44	
	GCTGAGCGCTGTAAGGGCCG	antisense	0.44	
	AGAGTTGATGAGGGAGGCTT	antisense	0.39	
	GGCCACCCCTGCCTGCTGAG	antisense	0.39	
	ATCAGCCCGCAGCTTCTCCA	sense	0.38	G5

Table 3.1 | SHANK3 guide sequences generated by sgRNA Designer.

Top 12 guide sequences per exon are shown above. Highlighted guide sequences indicate five highest scoring sense guides. The guide sequences highlighted in green were used for vector construction.

SHANK3 exon 5 (152 bp)

5’AGTGCCCTCTGAGCCTTGCGGCACAGTTGGACAACGCCACTGACCTCCTGAAGGTTCTCCGCAA
/**G2**/CGGCGGTGCTCATCTGGACTTCCGGACCCGAGATGGGCTGACAGCCGTCCACTGTGCTACCC
GC/**G1**/CAGCGGAACGCAGGGGCATTGACG -3’

- **G1:** TCCACTGTGCTACCCGC/cut/CAG
- **G2:** CTGAAGGTTCTCCGCAA/cut/CGG

SHANK3 exon 10 (271 bp)

5’TACCATTCAGGGAAACCCCCAGCTATGCAAAG/**G4**/CGACGGCGTCTGGCTGGCCCGAGTGGCC
TGGCATCCCCACGGCCCTTACAGCGCTCAGCCAGTGATATCAACCTGAAAGGTGATCAGCCCGCAG
CTTCT/**G5**/CCAGGGCCCACTCTCCGAAGCCTCCCTCATCAACTCTTGCTCCAGAGGCTTCAGGAG
GAGAAAGACCGTG/**G3**/ACAGGGATGGTGAACTGGAGAATGACATCAGCGGCCCCTCAGCAGGCAG
GGGTGGCCACAACAAGATCAG -3’

- **G3:** GGAGGAGAAAGACCGTG/cut/ACA
- **G4:** CCCCCAGCTATGCAAAG/cut/CGA
- **G5:** ATCAGCCCGCAGCTTCT/cut/CCA

Figure 3.4 | Loci of the selected guide sequences.

Guide sequences are highlighted in each target exon. The site of double stranded break is indicated by forward slashes.

3.3 CRISPR vector construction

Each guide sequence was cloned into pX330 carrying Cas9 and an invariant sgRNA backbone immediately downstream of the oligo cloning site (**Figure 3.5**A&B). Digestion of pX330 with BbsI enabled the replacement of restriction sites with insertion of annealed guide oligos. The resulting recombinant plasmid was extracted and purified, and the successful integration of the guide oligos was verified by Sanger sequencing (**Table 3.2**).

A. *In silico* design

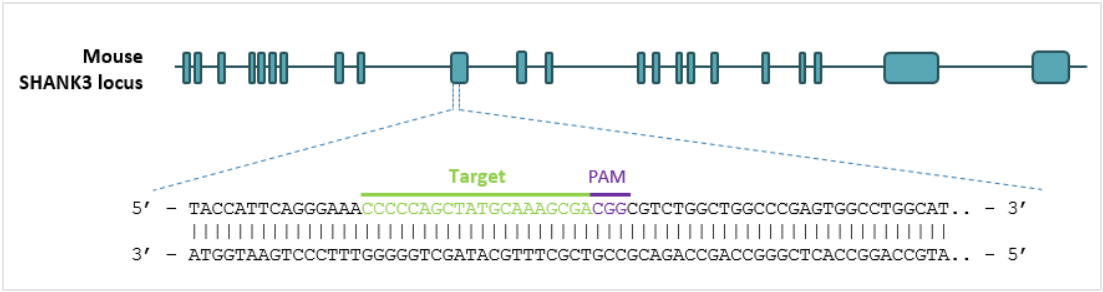

B. Reagent construction

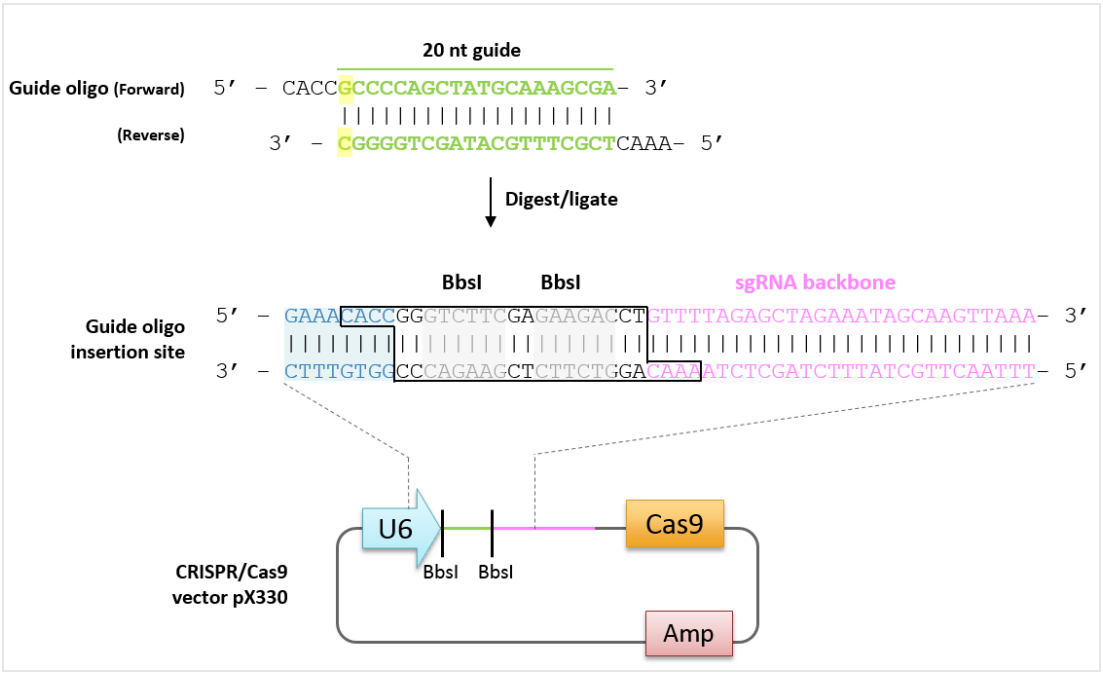

Figure 3.5 | Target selection and sgRNA expression vector construction

A. *In silico* design. 20 nt guide target (highlighted in green) must be followed by 5'-NGG at its 3' end in the mouse SHANK3 gene. DNA sequence highlights G4 guide sequence as an example.

B. Reagent construction. Cloning of the guide oligos into pX330 containing Cas9 and the sgRNA backbone. The G4 guide oligo pair (green) contains the linker sequence (cloning overhangs) for ligation into the guide oligo insertion site in pX330. A G-C base pair (yellow rectangle) is appended at the 5' end of the guide sequence for U6 transcription initiation. The vector pX330 also contains selection markers such as ampicillin (Amp) resistance gene to aid the selection of positive colonies. BbsI restriction sites are highlighted in grey.

sgRNA	Guide oligo insertion site sequence
-	GAAA CACC GGGTCTTCGAGAAGACCT GTTTTAGAGCTAGAAATAGCAAGTTAAA
G1	GAAA CACC GCCACTGTGCTACCCGCCAG GTTTTAGAGCTAGAAATAGCAAGTTAAA
G2	GAAA CACC GTGAAGGTTCTCCGCAACGG GTTTTAGAGCTAGAAATAGCAAGTTAAA
G3	GAAA CACC GGAGGAGAAAGACCGTGACA GTTTTAGAGCTAGAAATAGCAAGTTAAA
G4	GAAA CACC GCCCCAGCTATGCAAAGCGA GTTTTAGAGCTAGAAATAGCAAGTTAAA
G5	GAAA CACC GTCAGCCCGCAGCTTCTCCA GTTTTAGAGCTAGAAATAGCAAGTTAAA

Table 3.2 | Sequence validation of guide oligo insertion into pX330.

Sequence of the insertion site of the recombinant pX330. A partial sequence of U6 promoter is highlighted in blue, 20 nt guide sequence in green and sgRNA scaffold in pink.

3.4 Functional testing of sgRNAs

The five selected sgRNAs were transfected into ES cells to determine targeting efficiency in the first instance. T7 endonuclease I assay was used to detect indel mutations mediated by CRISPR/Cas9. T7 endonuclease I recognises and cleaves heteroduplex DNA formed after denaturing and annealing WT and mutant alleles (**Figure 3.6**). By measuring the fraction of cleavage DNA, Cas-mediated targeting efficiency can be estimated (Ran et al. 2013).

PCR primers were designed to amplify 150-300 bp on either side of the target for a total amplicon size of 300-600 bp to facilitate clear visualisation of cleavage bands in agarose gel. Target cleavage band sizes were determined (**Table 3.3**) based on the size of PCR product, and the fact that Cas9 cleaves between 3 bp and 4 bp upstream of the PAM of the corresponding guide sequence (Jinek et al. 2012).

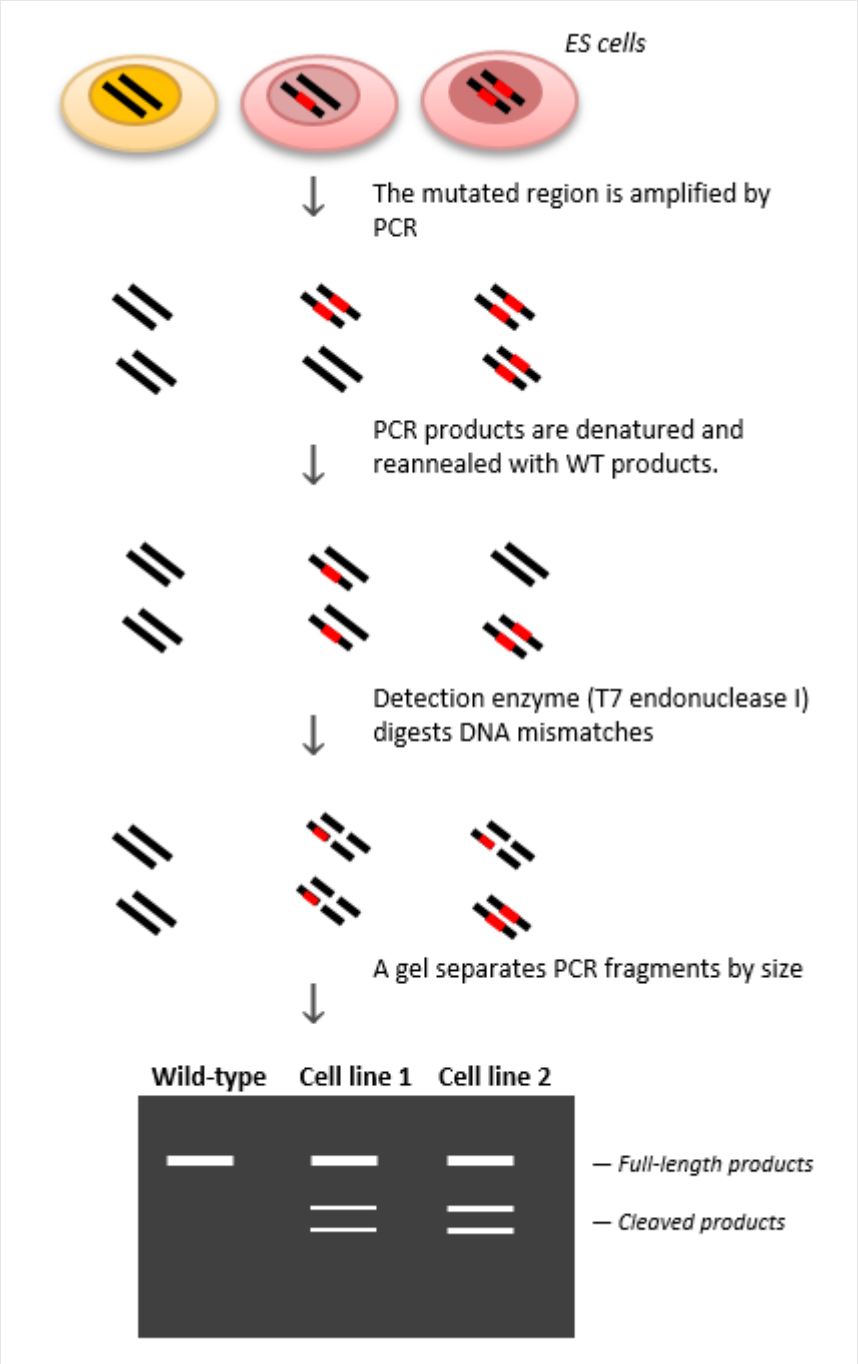

Figure 3.6 | Schematic of T7 endonuclease I assay.

Genomic DNA from the heterogeneous population of Cas9-targeted ES cells is amplified by PCR. Amplicons are denatured, and re-hybridised slowly to produce heteroduplex DNA. T7 endonuclease I cleaves heteroduplex DNA, whereas homoduplex DNA remains intact. Cas9-mediated targeting efficiency (indel percentage) is calculated on the proportion of cleaved DNA as determined by the intensity of gel bands. Highlighted in red indicates mutated sites.

sgRNAs	Target	Full PCR product (bp)	Cleavage band 1 (bp)	Cleavage band 2 (bp)
G1	Exon 5	448	271	177
G2	Exon 5	448	335	113
G3	Exon 10	437	354	83
G4	Exon 10	437	259	178
G5	Exon 10	437	284	153

Table 3.3 | Estimated cleavage band size of each sgRNA.

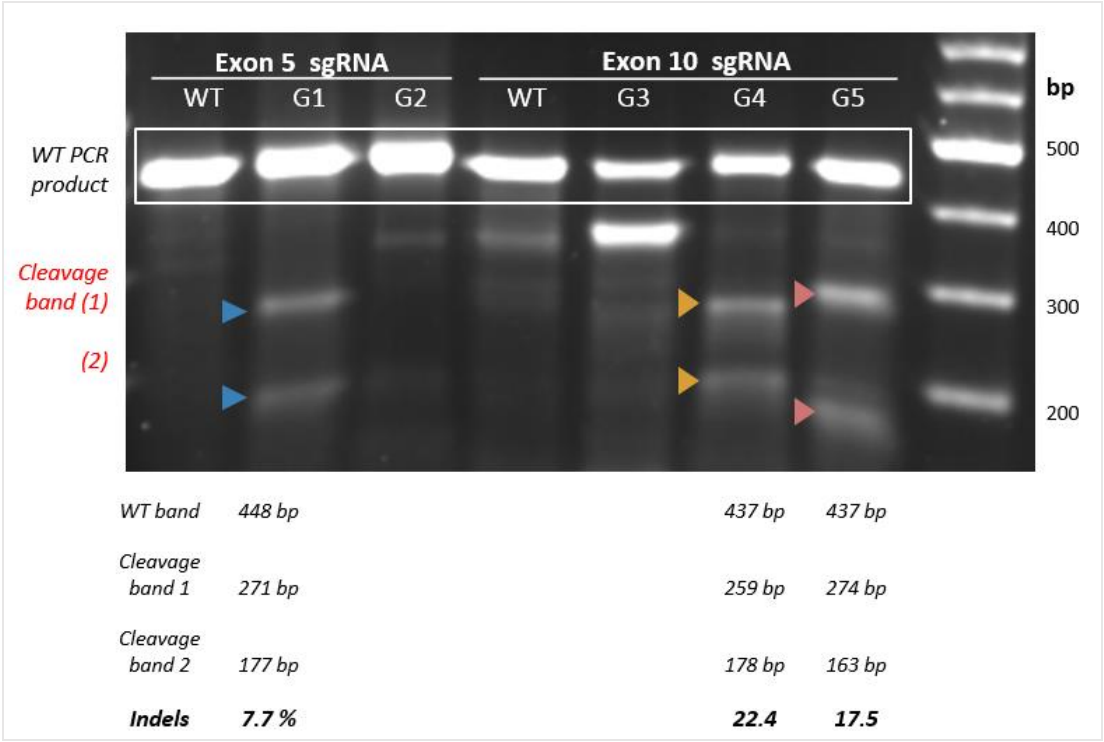

Figure 3.7 | Mutation detection on transfected ES cells.

T7 endonuclease I assay to test the efficiency of exon 5-targeting G1 and G2 sgRNAs, and exon 10-targeting G3, G4, and G5 sgRNAs. White rectangles indicate WT PCR products, and coloured arrowheads present expected fragment sizes for each locus.

sgRNAs	a	b	c	f	Indel (%)
G1	33.6	3.2	2.65	0.148	7.7
G4	14	5.81	3.44	0.398	22.4
G5	23.4	5.78	5.17	0.319	17.5

Table 3.4 | Estimation of indel percentage.

Figure 3.7 shows wild-type control for exon 5 has only one band corresponding to the size of the PCR product (448 bp), while exon 10 wild-type control has a nonspecific cleavage band (~380bp) in addition to the full size product (437 bp). This does not interfere with analysis as the size is different from the target cleavage bands. ES cells transfected with G1, G4 and G5 sgRNAs had the two clear target cleavage bands with the expected sizes. In contrast, G2 and G3 sgRNAs showed only nonspecific cleavage bands. Therefore, G2 and G3 sgRNAs were excluded from further analysis.

The intensity of the PCR product and cleaved bands was quantified by ImageStudio (**Table 3.4**). For each lane, the fraction of the cleaved amplicon (f) was calculated with the following formula: f = (b + c) / (a + b + c), where a is the intensity of the undigested PCR amplicon, and b and c are the intensities of each cleavage band. Indel percentage was estimated using the following formula: $\text{indel}\ (\%) = 100 \times (1 - \sqrt{1-f})$. **Table 3.4** lists the quantification of cleavage band intensity (a, b, and c), the fraction of cleaved amplicon (f) and indel percentage (%). The targeting efficiency ranged from 7.7 % to 22.4 % with the highest efficiency in G4 (22.4 %). It is worth noting that the targeting efficiency does not correlate with the sgRNA scores calculated by the sgRNA Designer: G3 sgRNA failed to target despite of having the highest sgRNA score of 0.61; G1 and G5 sgRNA have similar sgRNA scores of 0.39 and 0.38, respectively, but G5 sRNA was more than twice efficient as G1 sgRNA. Lastly, the efficiency estimation may be undervalued as DNA was extracted without clonal isolation. Taken together, three functional sgRNAs, G1, G4 and G5 were identified by T7 endonuclease I assay.

3.5 ES cell line generation

Having confirmed the efficiency of the sgRNAs, a second transfection was performed with the 3 functional sgRNAs: G1, G4 and G5. After transfection, each colony was picked to produce an individual cell line with a specific modification. A total of 204 colonies were isolated (G1 = 59, G4 = 73, and G5 = 72 cell lines). Among those isolated, 72 (G1 = 16, G4 = 30 and G5 = 26 cell lines) were screened through T7 endonuclease I assay. 42 cell lines (62.5 %) had the target cleavage bands. These targeted cell lines were further examined by Sanger sequencing (Edinburgh Genomics).

3.6 Sequence analyses

DNA sequence from the mutant clones (n = 42) were analysed by sequence alignment (**Figure 3.8**), examination of chromatogram (**Figure 3.9**) and translation to peptide sequences (**Table 3.5**). An example series of sequence analyses of two G4 sgRNA-treated cell lines is discussed below.

Figure 3.8 illustrates sequence alignment of two ES cell lines G4-C07 and G4-C17 with wild-type DNA. G4-C07 shows a perfect match with wild-type DNA upstream of double stranded break (DSB). After DSB, however, the sequence is poorly aligned. This suggests G4-C07 carries a heterozygous mutation. On the other hand, G4-C17 shows a precise alignment both upstream and downstream of DSB, indicating G4-C17 has a homozygous mutation of 1 bp insertion followed by 11 bp deletion.

Figure 3.9 compares DNA chromatograms of the two cell lines. Consistent with sequence alignment, G4-C07 has single peaks before DSB, then double peaks after DSB indicating either only one allele has a mutation, or each allele has a different indel mutation (i.e. compound heterozygous). G4-C17, on the other hand, has single peaks throughout suggesting both alleles have the same mutation.

Next, the homozygous DNA sequence was translated into the corresponding peptide sequence to predict if the indel mutation would change the reading frame resulting in premature termination. **Table 3.5** highlights that the indel mutation in G4-C17 leads to a frameshift, resulting in premature termination codon.

Step 1: Collect sequence data

>Wild-type
AGGGCATGAATGTGAAAGAGCAAGGAAAGGAATATGGATTGGTTTGGAGGGAGGGAAAAGAGAAAAGATGTAATTATTTAAAAAAAATCAATGAA
TCTCGAGTCTTACTCCTGCCCCTCTACTCCAGTACCATTCAGGGAAACCCCCAGCTATGCAAAGCGACGGCGTCTGGCTGGCCCGAGTGGCCTGG
CATCCCCACGGCCCTTACAGCGCTCAGCCAGTGATATCAACCTGAAAGGTGATCAGCCCGCAGCTTCTCCAGGGCCCACTCTCCGAAGCCTCCCT
CATCAACTCTTGCTCCAGAGGCTTCAGGAGGAGAAAGACCGTGACAGGGATGGTGAACTGGAGAATGACATCAGCGGCCCCTCAGCAGGCAGGGG
TGGCCACAACAAGATCAGGTAGGAGGGCCTG

>G4-C07
gtttggagggagggaaaagagaaaagatgtaattatttaaaaaaaatcaatgaatctcgagtcttactcctgcccctctactccagtaccattca
gggaaaccccagctatgcaaagacagctggtgggtcggcccagagtgctgtccccccccccctcccttcactcctctgacgatgttatcctgaa
aagagatgagccccccccttctcctcgtcccactcctctaagactcctccctcatcaactcttcctgatgattcttcaggagaaaaaaaacgacg
acgatgatgaagaacagaataataacatcatccccccctcatcaaggggggggtggccacaacaacatgaaggaggaggtgctgatgatgttgtgg
cccccgccggctgcgggggggggggctgatgttgttttgttgttgatccttgttgtggtggtgttcttcctgctgcagcaggaggaggaggaggtg
aggaggggggcggcgggggggggtgggagaagatgctgggtgctgatcttttaggtggttgttattggtggctgggcgcgggggggtggtgagg
ctgggcgcctgggagcagcaggccggggagccgtctctagatctaggtgtatgagactggagtggggtgtaggagtaggagtaggagtccataga
tatttttatgtattccgtttcctctttctccactccccccacccctc

>G4-C17
agcctgatatggattggtttggagggagggaaaagagaaaagatgtaattatttaaaaaaaatcaatgaatctcgagtcttactcctgcccctct
actccagtaccattcagggaaaccccagctgggcgtctggctggcccgagtggcctggcatccccacggcccttacagcgctcagccagtgata
tcaacctgaaaggtgatcagcccgcagcttctccagggcccactctccgaagcctccctcatcaactcttgctccagaggcttcaggaggagaaa
gaccgtgacagggatggtgaactggagaatgacatcagcggcccctcagcaggcaggggtggccacaacaagatcaggtaggagggcctaaatct
ggttgggccacccctgccggctagggggcggctaagttctttctcagttcacatcctgctgggatggttctctcggaagtgaaggcagtggagct
tgcgtgactgaggctggctgagagggggcccggagaagctgcgggctgagcacctttaggttgatatcactgggtgagcggtgtaagggccgg
ggggatgccaggccactcggggcccccacccgggggggtgtcctcgaagggcatgggggggaaaaggggggcgggagaaaaaaaccaaaaaatacc
ggggttttttttaaaaaaaaaacactcctttccctttccc

Step 2: Sequence Alignment

```
Wild-type  ACTCCAGTACCATTCAGGGAAACCCCCAGCTATGCAAAGCGACGGCGTCTGGCTGGCCCG
   G4-C07  actccagtaccattcagggaaacccccagctatgcaaa-----gacagctggtgggtcgg
           ************************************     *.*. ****. **.* *
```

⟶ **Conclusion: Heterozygous**

```
Wild-type  ACTCCAGTACCATTCAGGGAAACCCCCAGCTATGCAAAGCGACGGCGTCTGGCTGGCCCG
   G4-C17  actccagtaccattcagggaaacccccagctg-----------ggcgtctggctggcccg
           ********************************.          *****************
```

⟶ **Conclusion: Homozygous**

Figure 3.8 | SHANK3 sequence alignment.

DNA sequence of the target region of mutant ES cells are aligned with wild-type control sequence to study the nature of the mutation. Highlighted regions indicate the guide sequence of G4 sgRNA (i.e. target locus) of wild-type DNA. Asterisks (*) represent the same nucleotide between WT and mutant sequences.

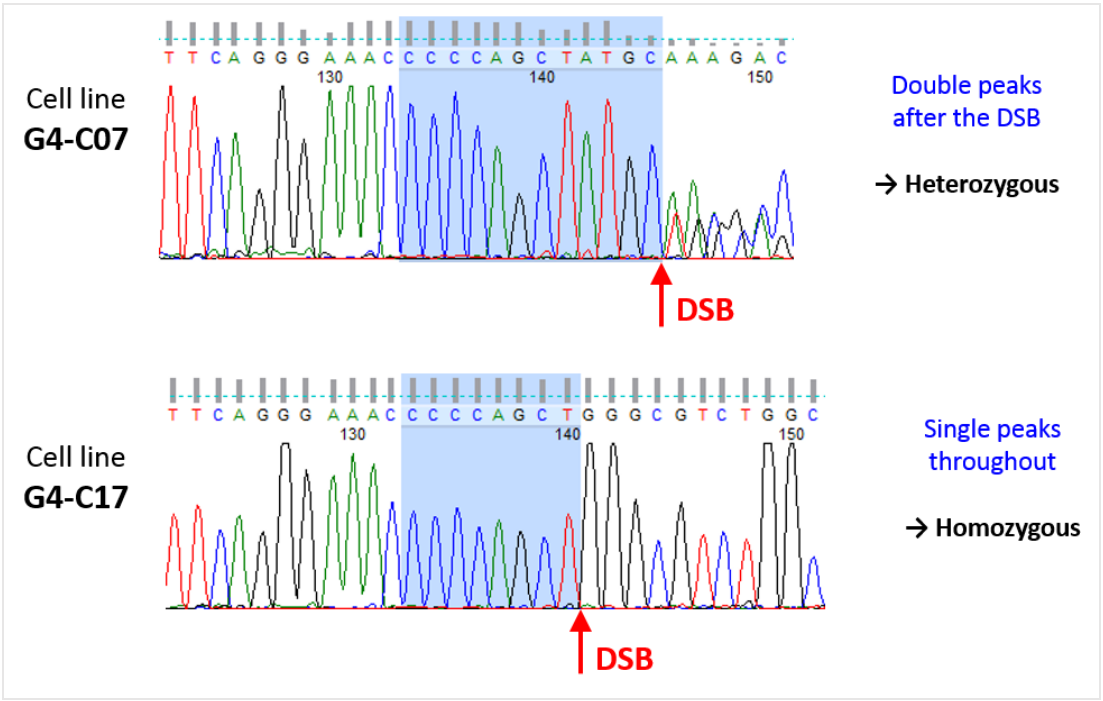

Figure 3.9 | Interpretation of chromatogram for sequence analysis.

The highlighted region indicates the G4 guide sequence. G4-C07 contains double peaks after the DSB indicating heterozygosity, whereas G4-C17 carries single peaks throughout indicating the Cas9-induced DSB resulted in the same mutation in both alleles.

Cell line	SHANK3 Exon 10 peptide sequence
Wild-type	VPFRETPSYAKRRRLAGPSGLASPRPLQRSASDINLKGDQPAASPGPTLRS LPHQLLLQRLQEEKDRDRDGELENDISGPSAGRGGHNKIS
G4-C17	VPFRETPSWASGWPEWPGIPTALTALSQ*

Table 3.5 | DNA translation of G4-C17 cell line.

Highlighted region indicates the reading frame shift and the asterisk (*) indicates premature termination codon. Nucleic acid translation performed using EMBOSS Transeq.

Table 3.6 summarises the results from all ES cell lines analysed. 62.5% of transfected ES cells carried targeted mutations and 26.4% were homozygous mutations (**Figure 3.10**). The type of homozygous mutations varied including insertion (1- 3 bp), deletion (1-36 bp), and deletion (11-12 bp) with extra insertion (1 bp) (**Table 3.7** and **Table 3.8**). All 19 homozygous mutations lead to the frameshift resulting in premature termination.

sgRNA	Targeted ES cells/ Total transfected	Homozygous/ Total targeted
G1 (Exon 5)	13/16 (81.3%)	7/13 (53.8%)
G4 (Exon 10)	20/30 (66.7%)	8/20 (40 %)
G5 (Exon 10)	12/26 (46.2%)	4/12 (33.3%)
Total	45/72 (62.5%)	19/45 (42.2%)

Table 3.6 | Result of CRISPR-SHANK3 transfection.

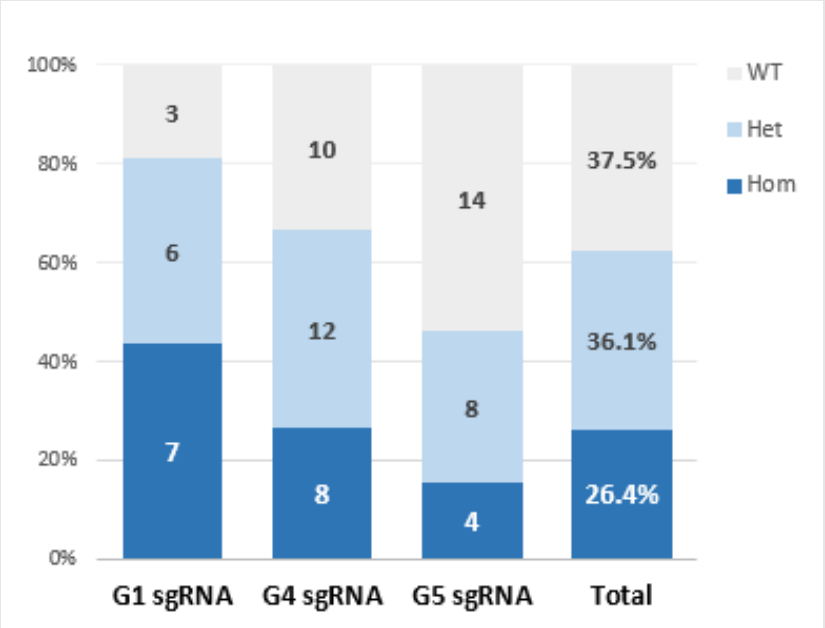

Figure 3.10 | CRISPR/Cas9-mediated SHANK3 targeting in ES cells.

Introduction of heterozygous (Het) and homozygous (Hom) mutations into ES cells with three sgRNAs (G1, G4 and G5). The number of cells is labelled for each genotype. Overall data from all three sgRNAs are represented in percentage on the right most bar (Total). WT: wild-type control.

Mutation	Cell line	SHANK3 exon 5 peptide sequences
N/A	Wild-type	ECPLSLAAQLDNATDLLKVLRNGGAHLDFRTRDGLTAVHCATRQRNAGALT
1bp del	G1-C02	ECPLSLAAQLDNATDLLKVLRNGGAHLDFRTRDGLTAVHCATRSGTQGH*
	G1-C07	ECPLSLAAQLDNATDLLKVLRNGGAHLDFRTRDGLTAVHCATRSGTQGH*
	G1-C11	ECPLSLAAQLDNATDLLKVLRNGGAHLDFRTRDGLTAVHCATRSGTQGH*
3bp ins	G1-C10	ECPLSLAAQLDNATDLLKVLRNGGAHLDFRTRDGLTAVHCAHTYCGTQGH*
4bp del	G1-C15	ECPLSLAAQLDNATDLLKVLRNGGAHLDFRTRDGLTAVHCATRGTQGH*
10bp del	G1-C09	ECPLSLAAQLDNATDLLKVLRNGGAHLDFRTRDGLTAVHCATTQGH*
11bp del	G1-C14	ECPLSLAAQLDNATDLLKVLRNGGAHLDFRTRDGLTAVHCATRRGIDG*

Table 3.7 | SHANK3 exon 5 peptide sequences of homozygous G1 cell lines.

Highlighted peptide sequences indicate missense mutations. All G1 cell lines contain premature termination codon indicated by asterisks. ins: insertion mutation; del: deletion mutation.

Mutation	Cell line	SHANK3 exon 10 peptide sequences
N/A	WT	VPFRETPSYAKRRRLAGPSGLASPRPLQRSASDINLKGDQPAASPGPTLRSL PHQLLLQRLQEEKDRDRDGELENDISGPSAGRGGHNKIS
1bp ins	G4-C37	VPFRETPSYAKATASGWPEWPGIPTALTALSQ*
1bp del	G4-C22	VPFRETPSYANDRVWLARVAWHPHGPYSAQPVIST*
2bp ins	G4-C19	VPFRETPSYAKSEGGGLARVAWHPHGPYSAQPVIST*
3bp del	G4-C15	VPFRETPSYARRRLAGPSGLASPRPLQRSASDINLKGDQPAASPGPTLRSLP HQLLLQRLQEEKDRDRDGELENDISGPSAGRGGHNKIR*
6bp del	G4-C34	VPFRETPSYRRRLAGPSGLASPRPLQRSASDINLKGDQPAASPGPTLRSLPH QLLLQRLQEEKDRDRDGELDNEISGPSAGRGGHNKIR*
11bp del + 1 bp ins	***G4-C17***	VPFRETPSWASGWPEWPGIPTALTALSQ*
12 bp del + 1 bp ins	***G4-C24***	VPFRETPSYATAGPSGLASPRPLQRSASDINLKGDQPAASPGPTLRSLPHQL LLQRLQEEKDRDRDGELENDISGPSAGRGGHNKIR*
36bp del	***G4-C23***	VPFRETPSLASPRPLQRSASDINLKGDQPAASPGPTLRSLPHQLLLQRLQEE KDRDRDGELENDISGPSAGRGGHNKIR*
1bp ins	G5-C30	VPFRETPSYAKRRRLAGPSGLASPRPLQRSASDINLKGDQPAASSRAHSPKP PSSTLAPEASGGERP*
	G5-C33	VPFRETPSYAKRRRLAGPSGLASPRPLQRSASDINLKGDQPAASSRAHSPKP PSSTLAPEASGGERP*
	G5-C34	VPFRETPSYAKRRRLAGPSGLASPRPLQRSASDINLKGDQPAASSRAHSPKP PSSTLAPEASGGERP*
5bp del	G5-C27	VPFRETPSYAKRRRLAGPSGLASPRPLQRSASDINLKGDQPAASAHSPKPPS STLAPEASGGERP*

Table 3.8 | SHANK3 exon 10 sequences of homozygous G4 and G5 cell lines.

All homozygous mutant cell lines contain missense mutations (highlighted in grey) followed by premature termination codons (asterisks). Note G5-G5-C30, G5-C33, G5-C34 contain identical peptide sequences implying they were derived from a single colony. Three ES cell lines highlighted in italic (G4-C17, G4-C24 and G4-C23) were chosen for blastocyst injection.

Antisense mediated exon skipping is a form of alternative RNA splicing causing the mutated exon to be skipped over, which can restore the disrupted reading frame (Harding et al. 2007). Cells will express the truncated, but still functional SHANK3 protein, had exon skipping restored the reading frame. It is therefore necessary to investigate the possibility of exon skipping-mediated reading frame restoration in the targeted ES cells. DNA sequence of flanking exons without each target exon (exon 5 or 10) was identified and translated into peptide sequence (**Table 3.9**). In case exon 5 is skipped over, exon 4 and 6 will be spliced together, and this will still change the reading frame leading to premature termination. Similarly, exon 10 skipping will result in premature termination. The results demonstrate even if exon skipping occurs in the targeted ES cells, there will be premature termination leading to the intended knockout mutation.

	DNA sequence	Peptide sequence
Exon5-WT	GAGTGCCCTCTGAGCCTTGCGGCACAGTTGGACAACGCCACTGACC TCCTGAAGGTTCTCCGCAACGGCGGTGCTCATCTGGACTTCCGGAC CCGAGATGGGCTGACAGCCGTCCACTGTGCTACCCGCCAGCGGAAC GCAGGGGCATTGACG	ECPLSLAAQLDNATDLLKVLR NGGAHLDFRTRDGLTAVHCAT RQRNAGALTECPLSLAAQLDN ATDLLKVLRNGGAHLDFRTRD GLTAVHCATRQRNAGALT
Exon5-Skip (Exon 4 and Exon 6)	GCAAACCTGAAGAAGTTCATGGACTATGTCCAGCTACACAGCACAG ATAAGGTGGCCCGCCTGCTGGACAAGGGGCTGGACCCCAATTTCCA TGACCCTGACTCAGGAGACCCTGCTGGACCTGGGGGCTTCGCCTGA CTACAAGGACAGCCGCGGCCTGACGCCCCTGTACCATAGTGCCCTA GGGGGCGGGGATGCCCTCTGTTGCGAGCTGCTTCTCCATGATCATG CACAGCTGGGGACCACTGATGAGAATGGTTGGCAAGAGATCCATCA G	ANLKKFMDYVQLHSTDKVARL LDKGLDPNFHDPDSGDPAGPG GFA*
Exon10-WT	GTACCATTCAGGGAAACCCCCAGCTATGCAAAGCGACGGCGTCTGG CTGGCCCGAGTGGCCTGGCATCCCCACGGCCCTTACAGCGCTCAGC CAGTGATATCAACCTGAAAGGTGATCAGCCCGCAGCTTCTCCAGGG CCCACTCTCCGAAGCCTCCCTCATCAACTCTTGCTCCAGAGGCTTC AGGAGGAGAAAGACCGTGACAGGGATGGTGAACTGGAGAATGACAT CAGCGGCCCCTCAGCAGGCAGGGGTGGCCACAACAAGATCAGC	VPFRETPSYAKRRRLAGPSGL ASPRPLQRSASDINLKGDQPA ASPGPTLRSLPHQLLLQRLQE EKDRDRDGELENDISGPSAGR GGHNKIS
Exon10-Skip (Exon 9 and Exon 11)	GTGGCCATTATTGCAGGGAACTTTGAGCTTGCCGAGGTAATCAAGA CCCACAAAGACTCCGATGTCGCCCCAGTGGGCCCGGCGGATCCGGC CCCGCGCCCGGCCCCGGCCCGGCGTCTCCCGCGCCCCCCGCGCCGC CGCCCCGGGGCCCGAAGCGGAAACTTTACAGTGCCGTCCCCGGCCG CAAGTTCATCGCTGTGAAGGCGCACAGCCCGCAGGGCGAGGGCGAG ATCCCGCTGCACCGCGGCGAGGCCGTGAAGG	VAIIAGNFELAEVIKTHKDSD VAPVGPADPAPRPAPARRLPR PPRRRPGARSGNFTVPSPAAS SSL*

Table 3.9 | Exon skip analysis.

DNA sequence and the corresponding peptide sequence are compared between wild-type target exon (exon 5 and exon 10) and its respected skip. Both exon 5 and exon 10-skip lead to premature terminations indicated by asterisks.

3.7 Design of PCR primers for genotyping

As mutant alleles with large deletions allow rapid and effective PCR genotyping, the top three G4 cell lines (G4-C17, G4-C23 and G4-C24) were chosen for blastocyst injections. These cell lines will be referred as C17, C23, and C24 respectively henceforward.

Two pairs of primers for each mutation were designed for a simple PCR-based genotyping of mice, with one pair to amplify wild-type DNA but not mutant DNA, and vice versa for another pair.

The 3' end of the PCR primer is critical for amplification as it is highly sensitive to mismatches (Yu et al. 2014). Theoretically, the indel mutation will disrupt the PCR amplification if the 3' end of primers were designed to exactly cover the indel region. Conversely, primers skipping the indel region at its 3' end will only be able to amplify mutant alleles. In view of this hypothesis, we designed wild-type primers to overlap the indel site at the 3' end, and mutant primers to skip the indel site but to cover 3 nucleotides immediately after DSB at the 3' end (**Figure 3.11**). Thus, WT primers can amplify only wild-type alleles, while mutant primers can only amplify mutant alleles.

Table 3.10 summarises how each primer was designed. As the indel mutation in C23 is 36 bp deletion, which is larger than one primer can cover, three different wild-type primers were designed, covering the beginning (C23W1), the middle (C23W2) or the end (C23W3) of the deletion. For C24, an additional wild-type primer (C24W2) was designed to accommodate extra 1 nucleotide (thymine, T) at the 3' end, which is absent in the mutant allele. The same reverse primer (Rev1) was used for all forward primers leading to PCR product size ~ 376 bp. DNA was extracted from the corresponding ES cell lines and wild-type ES cell. The annealing temperature of PCR was set to 65 °C in order to increase the sensitivity.

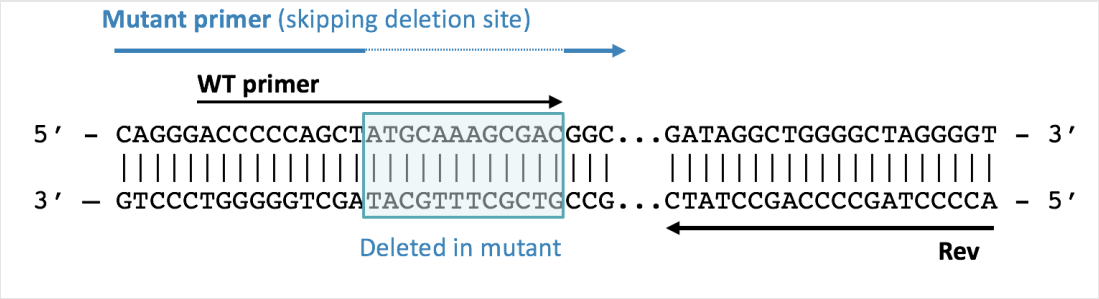

Figure 3.11 | PCR primer design.

Example primer design for ES cell line C17. A wild-type (WT) primer amplifies only wild-type DNA as it contains a region which is deleted in mutant, whereas a mutant primer amplifies the mutant allele only, as it skips the deletion site followed by three additional nucleotides at the 3' end.

Primer	Sequence	Note
C17W1	ACCCCCAGCTATGCAAAGCGAC	Covers C17 mutation (with insertion).
C17M1	CAGGGAAACCCCCAGCTGGGC	Skips C17 mutation with 3 nt at the 3' end.
C23W1	GCTATGCAAAGCGACGGCGT	Covers the beginning of C23 deletion.
C23W2	CAAAGCGACGGCGTCTGGCT	Covers the middle of C23 region.
C23W3	GGCGTCTGGCTGGCCCGAGTG	Covers the end of C23 region.
C23M1	CCATTCAGGGAAACCCCCAGCC	Skips C23 deletion, includes 3 nt at the 3' end.
C24W1	TATGCAAAGCGACGGCGTC	Overlaps C24 deletion excluding insertion.
C24W2	TATGCAAAGCGACGGCGTCT	Covers the exact C24 mutation (with insertion).
C24M1	GGAAACCCCCAGCTATGCAACGG	Skips the 24 mutation with 3 nt at the 3' end.
Rev1	ACCCCTAGCCCCAGCCTATC	Results in PCR amplicon size 376 bp.

Table 3.10 | Genotyping primers.

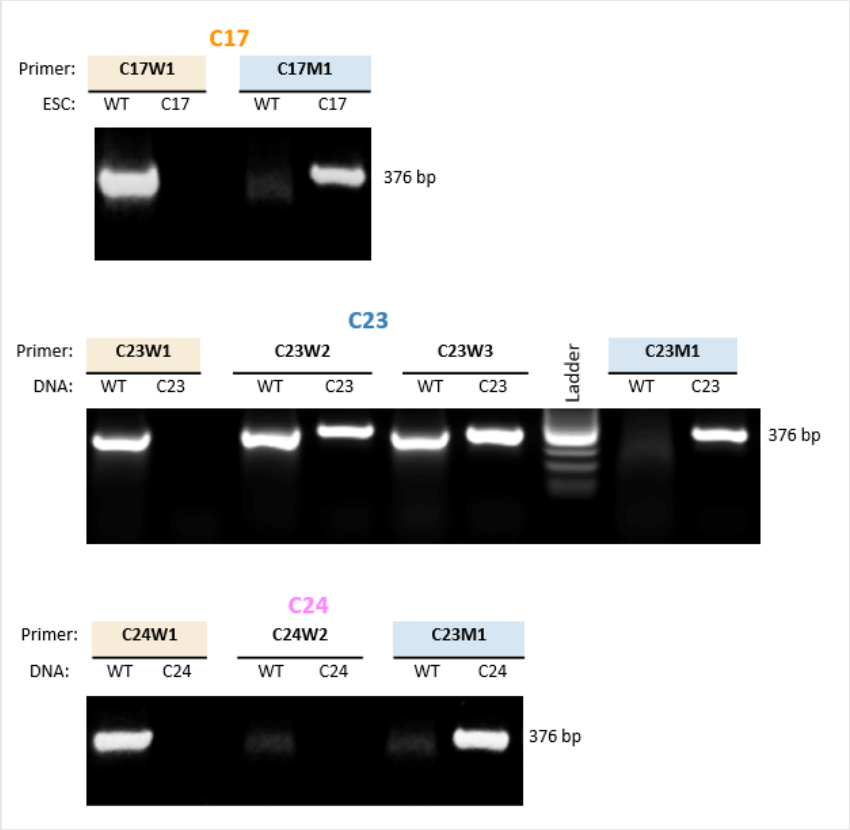

Figure 3.12 | PCR genotyping.

PCR genotyping result using the designed primers. Two pairs of allele-specific primers were identified per each cell line and highlighted in yellow for wild-type-specific and in blue for mutant-specific.

Figure 3.12 shows the result of PCR genotyping using the designed primers (9 pairs in total). Six primer pairs (2 pairs for each cell line, highlighted) had the intended selectivity. C17W1, C23W1 and C24W1 (highlighted in yellow) amplified wild-type DNA but not the respective mutant cell line. C17M1, C23M1 and C24M1 (highlighted in blue) amplified each mutant DNA but not wild-type DNA. The additional wild-type primers did not show specificity: the C23W2 and C23W3 primers amplified both wild-type and mutant alleles, whereas the C24W2 primer failed to amplify any allele. This means wild-type primers designed with the same principle for the similar mutations had different results. For example, both C17 and C24 mutations consist of 11-12 bp deletion with extra 1 bp insertion. While the C17W1 primer covering the C17 mutation

exactly had the intended specificity, the C24W2 primer of the C24 mutation failed. If the extra insertion was removed from the C24W2 primer, however, there was the intended specificity (C24W1). It is therefore advisable to consider designing several different wild-type specific primers when the indel mutation overlaps a larger region and/or contains both insertion and deletion.

Together, an efficient PCR genotyping protocol was developed using two allele-specific primers per each mutation: one for wild-type and the other for mutant. This means genotype of mice will be determined twice independently, once by a WT primer and again by a mutant primer. Thus, genotyping results will be less susceptible to false positive or negative results.

3.8 Off-target analysis

A major concern of CRISPR/Cas9 is off-target effects. Thus, we characterised all genomic loci containing up to three bp mismatches compared to G4 guide sequence (**Table 3.11**). Only two off-target sites were identified by CRISPR/Cas9 off-target predictor (Stemmer et al. 2015). All potential off-target sites have 3 or more bp mismatches demonstrating the high specificity of G4 sgRNA to the target sequence. Six additional off-target sites with 4 bp mismatches were also identified for reassurance (**Table 3.11**).

The eight off-target sites were amplified by PCR from genomic DNA of the selected ES cell lines and subsequently analysed by Sanger sequencing. No off-target mutation was identified in any locus (**Figure 3.13**). This result is consistent with the previous finding that three or more bp mismatches abolish the Cas9 activity (Yang et al. 2013). Recent publications demonstrated the rate of off-target mutations is sufficiently low and thus not a significant concern (Wu et al. 2014; Veres et al. 2014).

Site name	Direction	MM	Position	Sequence (5' to 3')
On-target (sgRNA G4)	Forward	0	chr15: 89521118 (Shank3)	CCCCCAGCTATGCAAAGCGA
Off-target 1	Forward	3	chr6:147732596 (Intergenic)	CCaCCAGCTATGCAAAtCcA
Off-target 2	Forward	3	chr13:25563699 (Intergenic)	CCCaCAGCTATGCAtAGCtA
Off-target 3	Reverse	4	chr14:66171714 (Exonic)	CCCaCAGCTATGCAtAGCtA
Off-target 4	Reverse	4	Chr1: 24012440 (Exonic)	CCtaCAGaTATGCAAAGCcA
Off-target 5	Reverse	4	Chr9: 73007795 (Exonic)	CGCCCAGtTcTGCAAAGCaA
Off-target 6	Reverse	4	Chr8: 34270077 (Intergenic)	CCCaCAGtTATaCAAAGCcA
Off-target 7	Forward	4	Chr19: 24085323 (Intergenic)	gCCCCAcCcATGCtAAGCGA
Off-target 8	Reverse	4	Chr18: 35884000 (Intergenic)	ttCaCAGCTATGCAAAaCGA

Table 3.11 | Off-target analysis of three targeted ES cells (C17, C23 & C24).

Lower cases in sequence indicate mismatches. MM: number of base-pair mismatches.

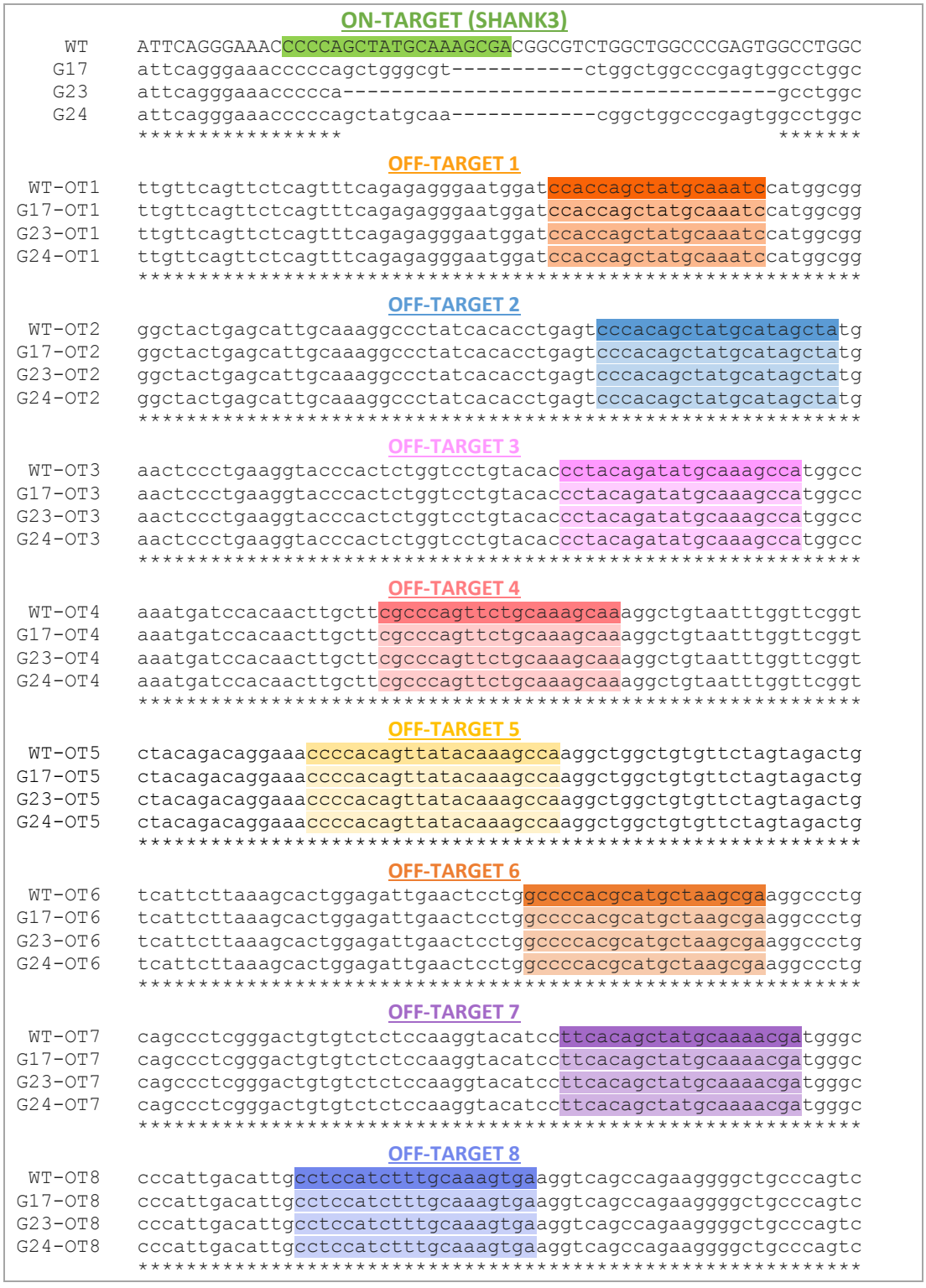

Figure 3.13 | Off-target analysis of three targeted ES cells.

Multiple sequence alignment of potential off-targets as well as on-target are shown. Each target site is highlighted. All off-target sights display a perfect alignment with WT indicating there is no off-target mutation. Note on-target (G4 sgRNA) shows the deletions as previously confirmed. Multiple Sequence alignment was performed using EMBL-EBI MAFFT.

3.9 Blastocyst injection and mouse generation

Microinjection and subsequent chimera generation were performed in Central Bioresearch Services, University of Edinburgh. The three ES cell lines were injected into C57BL/6J mouse blastocysts in separate batches, which were then transferred into a pseudopregnant recipient mouse (**Table 3.12**). The ES cells were derived from the 129/Ola mouse strain carrying genes coding for agouti coat colour, which is dominant over black coat colour of the recipient C57BL/6J. Therefore, the resulting chimaeras presents patches of agouti.

Adult male chimaeras with >50% agouti coat colour were mated with C57BL/6J mouse. Coat colours of the progeny are either agouti if 129/Ola ES cells contribute to chimaeras' germ cells, or black if the recipient C57BL/6J blastocyst contribute to the germ cells. To confirm germline transmission of ES cell-derived mutations, genomic DNA was extracted from ear clip biopsies of agouti pups and the target region was amplified by PCR, then sequenced using Sanger method. Those F1 agouti pups carrying the intended SHANK3 deletion were identified as germline transmitted heterozygous.

ES cell line (Injection date)	Transferred Embryos	Recipients	New-borns	Chimaeras (F0)	Pups (F1)	Germline (F1 Het)
C23 (25/09/2015)	67	4	6	1	0	n/a
C17 (02/10/2015)	19	1	1	0	n/a	
C24(09/10/2015)	60	4	6	2	14	0
C17 (23/10/2015)	62	4	0	n/a		
C23(22/01/2015)	60	4	12	1	42	2
C17 (29/01/2015)	8	1	4	1	22	5
C17 (23/02/2015)	12	22	2	1	46	3
C17 (24/02/2015)	63	3	6	0	n/a	
C23(01/03/2015)	43	2	0	n/a		

Table 3.12 | Blastocyst injection of the selected ES cell lines.

Table 3.12 summarises the results of blastocyst injections of the ES cell clones. The initial microinjection of the C24 cell line produced two chimaeras, while the C17 cell line generated only one infertile chimaera and no chimaera were produced from the C23 cell line. Thus, microinjections of the C17 and C23 ES cell lines were repeated while waiting for F1 offspring of C24 to be sequenced. Later we found that the C24 cell line did not reach germline transmission, since no heterozygous mouse was produced from chimaera breeding. As the C17 and C23 cell lines contributed to germline, we focused our attention to these two lines to establish the working mouse colonies. Those F2 or F3 heterozygotes were used as founder mice to establish the working mouse colony.

To examine the potential synaptic changes induced by SHANK3 deletion, F1 heterozygous mice were further crossed with a mouse line carrying a double fluorescent tags in endogenous PSD95 and SAP102 proteins. PSD95 and SAP102 are the members of MAGUK and integral part of NMDAR complexes (see **Figure 1.1**). From this cross we have obtained multiple triple heterozygous mice. Further experiments using triple homozygous mice will investigate the effect of SHANK3 deletion in PSD95 and/or SAP102 carrying synapses.

3.10 Review of PCR genotyping

When the designed genotyping primers were used for identifying F2 mice, PCR produced poor results including no amplification, smear bands or unspecific bands. To resolve this issue, the primer design was reviewed.

The melting temperature (Tm) of a primer is a critical value in performing a successful PCR, and Tm difference (ΔTm) of a pair of primers is to be less than 5 °C (Chuang et al., 2013). We found that the Tm of the designed forward primers ranged from 65 – 72 °C, whereas the reverse primer's Tm was 59 °C, resulting in ΔTm of 6 – 13 °C (**Table 3.13**). This finding led us to consider reducing the Tm by redesigning primers. As the forward primers carrying unique designs confer the specificity to each genotype, we designed a new reverse primer with the higher Tm of 70 °C, which results in PCR product size ~ 567 bp. The annealing temperature (Ta) of PCR was set to 65 °C for wild-type reaction, and 69 °C for mutant reaction to accommodate the raised average Tm.

With the new reverse primer, PCR genotyping was performed and clear bands were obtained (**Figure 3.14**). The PCR genotyping results were subsequently compared with Sanger sequencing for validation. The sequencing results of more than eight F2 matched with the genotypes determined by PCR. Therefore, mouse genotype was determined by PCR only henceforth.

Primer	Sequence 5'-3'	Tm (°C)	ΔTm 1	ΔTm 2
C17W1	ACCCCCAGCTATGCAAAGCGAC	65	6	5
C17M1	CAGGGAAACCCCCAGCTGGGC	72	13	1
C23W1	GCTATGCAAAGCGACGGCGT	66	7	4
C23M1	CCATTCAGGGAAACCCCCAGCC	70	11	0
Rev1	AGGCCCTCCTACCTGATCTT	59	-	-
Rev2	TGTGGGGGACGACGGACAGCCA	70	-	-

Table 3.13 | Genotyping primers.

Tm was calculated by Tm Calculator (http://www6.appliedbiosystems.com/support/techtools/calc/). Tm 1: Tm difference with Rev1; Tm2: Tm difference with Rev2.

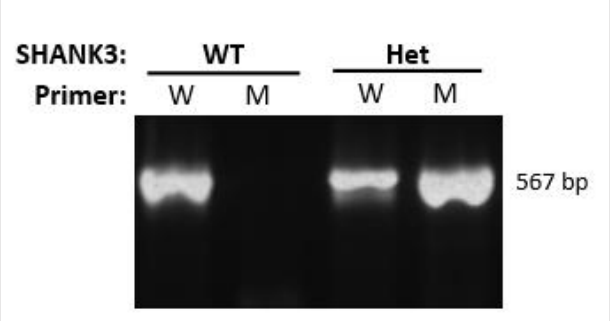

Figure 3.14 | PCR genotyping of F2 mice (C17).

Example of genotyping PCR results using genomic DNAs from wild-type SHANK3 (WT) and heterozygous (Het), using either wild-type (W) or mutant (M)-specific forward primers and the new reverse primer (Rev2).

3.11 Western blot validation

To confirm SHANK3 deficiency in the newly generated mouse lines, total protein was extracted from forebrains of adult wild-type and SHANK3 KO mice and analysed by Western blot with an antibody raised against endogenous SHANK3. As shown in

Figure 3.18, probing with the SHANK3 antibody (Santa Cruz, sc-377088) in all genotypes showed specific bands at approximately 200 kDa, 185 kDa, and 165 kDa, and the 200 kDa band corresponding to transcript SHANK3-203 (200 kDa; See **Figure 3.15**) was most robustly detected. The smaller two bands might be splice variants of SHANK3-203 or SHANK3-201 (190 kDa). Note another protein-coding isoform SHANK3-202 (78 kDa) was not visible.

The expression of the largest 200 kDa SHANK3 isoform is reduced in the C17 heterozygous mice (**Figure 3.166A)** and completely absent in the homozygous mice (**Figure 3.176C**). The C23 heterozygous mice, however, showed no reduction in SHANK3 protein expression (note C23 homozygous mice were not available). To eliminate genotyping errors, each mouse was re-sequenced and the original genotype was confirmed. Therefore, the C23 mouse line was terminated and only the C17 mouse line were used for breeding.

The above findings indicate although both mouse lines carry the indel mutations leading to premature termination codons, only one deletion (C17, 11 bp deletion) led to reduction in SHANK3 protein expression. A potential explanation for the discrepancy is that in C23 (36 bp deletion), translation termination at the premature stop codon could have been suppressed resulting in the full-length SHANK3 protein. Although translation termination is usually accurate, an error can occur (Keeling et al. 2012). In fact, suppression of translation termination is more frequent at premature termination codons at a rate of 0.01 to 1% (Bonetti et al. 1995; Cassan & Rousset 2001) than at normal stop codons at 0.001-0.1% (Parker 1989) respectively. cDNA synthesis by reverse transcription will allow detailed examination into the SHANK3

translation product of C23 mutation. Taken together, these data demonstrate successful generation of knockout mice using ES cells modified by CRISPR/Cas9 technology.

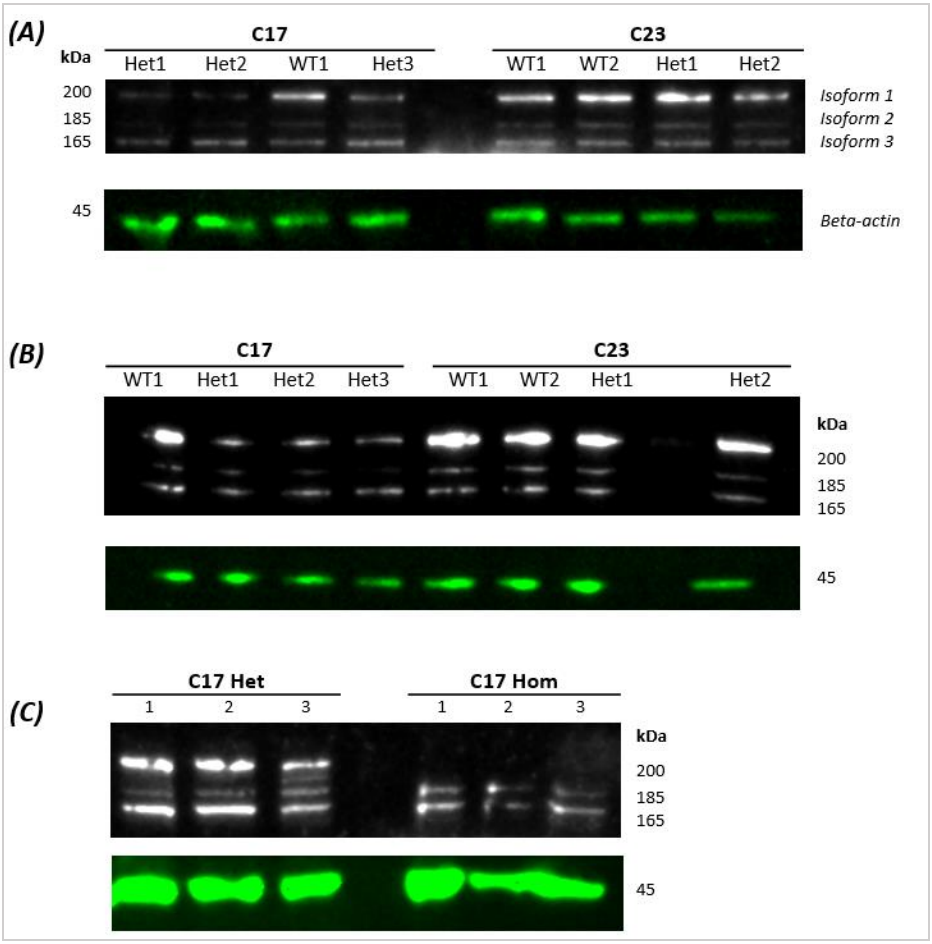

Figure 3.18 | Western blot of forebrain homogenates from the new SHANK3 mouse lines.

Forebrain homogenates from wild-type, heterozygous and homozygous SHNAK3 knockout mice were subjected to Western blot with the SHANK3 antibody and the beta-actin antibody as a loading control (45 kDa). **(A)** The full length SHANK3 (~200 kDa; SHANK3-203) expression is reduced in the C17 heterozygous mice. However, the C23 heterozygous mice show the similar level of SHANK3 expression to the wild-type mice. **(B)** The second blot was performed Cathy McLaughlin using the same brain samples. Similar to the first blot, only C17 shows the reduction in the full length SHANK3. **(C)** Blot of heterozygous and homozygous C17 mice. The SHANK3-203 isoform was absent in the homozygous C17 mice. WT: wild-type. Het: SHANK3 KO heterozygous mice. Hom: SHANK3 KO homozygous mice. White = Shank3 antibody, green = Beta-actin loading control.

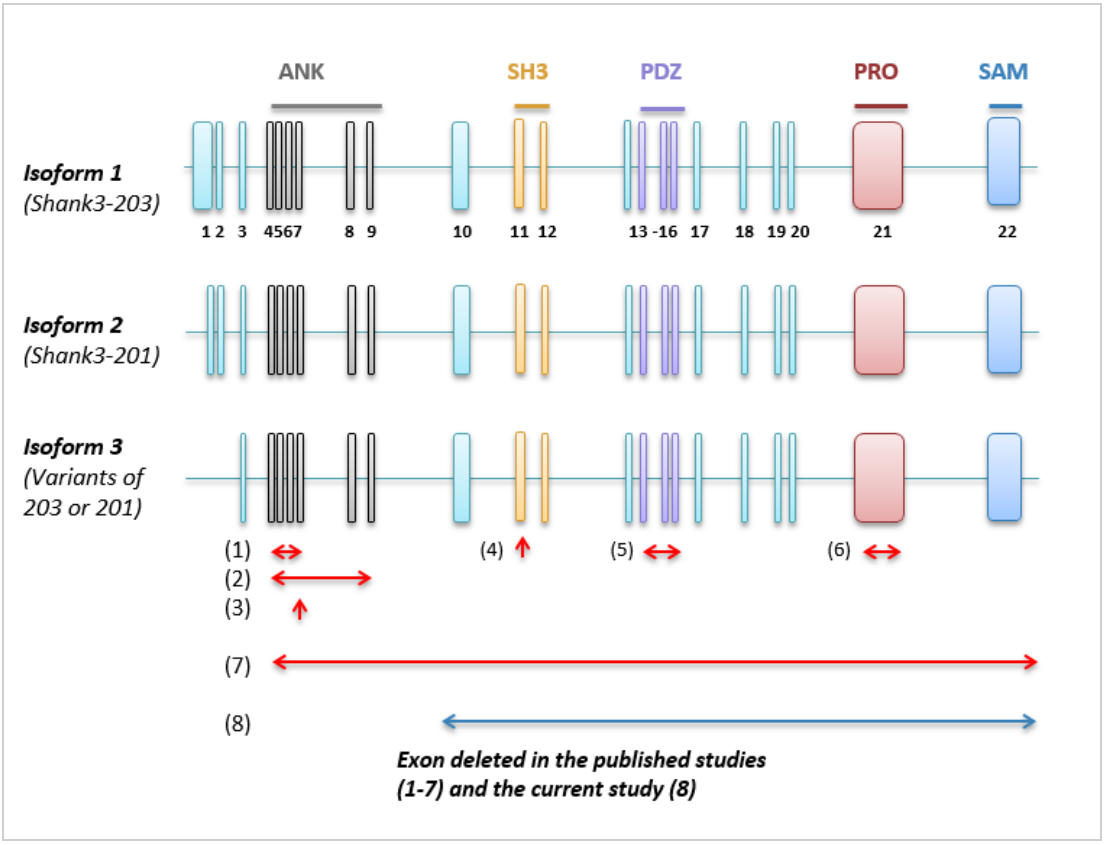

Figure 3.16 |The observed isoforms of SHANK3.

The schematic of the observed isoforms which are likely to be affected by the deletion. The corresponding transcripts are predicted based on size (see Figure 3.3). Exons deleted in each of the existing mutant lines are indicated by red arrows (see Table 1.2), and the blue arrow indicates the exons deleted in the current study.

References:

(1) Peça et al., 2011
(2) Bozdagi et al., 2010; Yang et al., 2012; Wang et al., 2011; Jaramillo et al., 2016
(3) Lee et al., 2015
(4) Schmeisser et al., 2012; Vicidomini et al., 2016
(5) Peça et al., 2011; Mei et al., 2016
(6) Kouser et al., 2013; Speed et al., 2015; Zhou et al., 2016
(7) Wang et al., 2016

Chapter 4 SYNGAP1 GAP-deficient mouse model generation

This chapter describes the design and generation of a mouse model containing a mutation in the GAP domain of SYNGAP1 using ES cells modified by the CRISPR/Cas9 system. The mutation was intended to selectively disrupt the Ras-GTPase activating function of SYNGAP1 and thereby provide insight into the potential role of GAP-mediated catalysis in the pathophysiology of SYNGAP1 haploinsufficiency. We refer to this mutation as GAP-deficient SYNGAP1 hereinafter.

4.1 Mutation rationale and design

The GAP function of Ras-GAPs, including SYGNAP1, requires a highly conserved arginine amino acid in the active site of the Ras-GTPase domain (Ahmadian et al. 1997; Scheffzek et al. 1997) (**Figure 4.1**). This "arginine finger" binds to the γ–phosphate and the β-phosphate of GTP, thereby neutralising the negative charge of the γ–phosphate that is removed during hydrolysis into GDP (Rehmann & Bos 2004). The arginine finger also helps to stabilise glutamine at position 61 in the GTPase, which in turn places a water molecule for a nucleophilic attack on the γ–phosphate (Scheffzek et al. 1997).

The replacement of the invariant arginine finger by alanine *in vitro* dramatically reduces GAP-enhanced GTPase activity of other Ras-GAPs including p120GAP (Scheffzek et al. 1997) and neurofibromin (NF1) (Ahmadian et al. 1997). We therefore reasoned that changing the catalytic arginine (R470) of SYNGAP1 to alanine (R470A) will impair the GAP activity, while keeping other functions such as a structural role intact. Two additional amino acids, lysine and proline were also considered to substitute the SYNGAP1 catalytic arginine, as R470K and R470P mutations have been previously shown to disrupt the GAP activity *in vitro* (Pena et al. 2008). Consistently, all three mutations (R470A, R470K and R470P) resulted in the almost complete deficiency of the GAP function in Malachite Green Phosphate assay (personal communication, Dr. Satou Unzai).

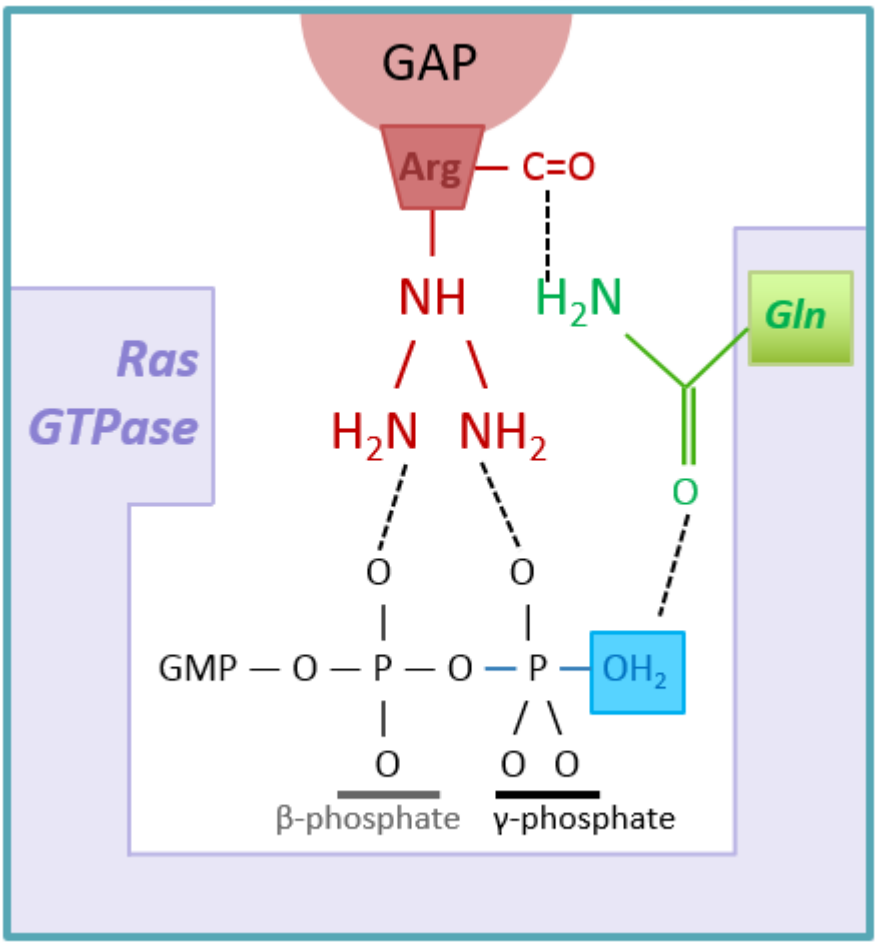

Figure 4.1 | Active site of Ras GTPase-GAP complex.

The arginine finger (Arg) moves into the active site of Ras, stabilising the transition state (i.e. the GTP hydrolysis process) of the Ras-GTPase activity. The carbonyl (C=O) group of the arginine finger forms a hydrogen bond with NH_2 group of the Glutamine-61 (Gln, in green) of Ras. The glutamine-61, in turn, positions a water molecule (H_2O, in blue) facilitating the attack on the γ–phosphate of GTP. The arginine finger also binds to the γ–phosphate and the β-phosphate and neutralises the negative charge of the γ–phosphate. GMP: guanosine monophosphate.

To introduce these mutations, we used the CRISPR/Cas9 system, which allows the introduction of a point mutation by the homology-directed repair (HDR) pathway. This results in error-free edits using an exogenous DNA as a donor DNA (see **Figure 1.9**B). The HDR process occurs most efficiently when the donor DNA contains at least 40 bp homology arms flanking the desired mutation (Chen et al. 2011; Ran et al. 2013).

The design and construction of sgRNA-expressing vectors and donor DNAs were performed by David Kerrigan, a former technician in our lab. Briefly, the CRISPR Design Tool (Ran et al. 2013) was used to identify potential guide sequences for exon 9 of mouse SYNGAP1 (ENSMUSG00000067629, chromosome 17) where the codon for arginine-470 is located. The highest scoring guide (5'-GGTAGACCGATTCATGGAGC-3') was 17 bp upstream of arginine-470 (**Figure 4.2**A). Note this guide sequence scored the second best (0.63/1.0) in the alternative target search programme, the sgRNA designer (Doench et al. 2014), which was used for the SHANK3 guide selection (see Chapter 3). The SYNGAP guide was cloned into the sgRNA-expressing vector pX330 and the functional validity of the sgRNA was confirmed by T7 endonuclease I assay following the procedures described in the last chapter.

The 100 nt single-stranded DNA oligonucleotides were designed to serve as the donor DNAs (**Figure 4.2**B). The donor DNAs contained ~40 bp homology arms flanking the desired mutation on each side. The original arginine codon CGA (R470 in A0A0A6YVS6_MOUSE in Uniprot; https://www.uniprot.org/uniprot/A0A0A6YVS6) was substituted to GCC (alanine), AAA (lysine) or CCT (proline). Additionally, all of the donor DNAs contain two silent mutations, which do not result in a change in the amino acid sequence. First, a restriction site, Sau3AI (for alanine and proline) or DraI (for lysine) was introduced to enable easy genotyping using restriction enzyme digestion. Secondly, the NGG PAM site was substituted (CGG to CGC) to prevent the Cas9 cleavage after correct editing (**Figure 4.2**C).

A. Target region

> Wild-type exon 9 (145 bp)

GACTTCCTTTCAGACATGGCCATGTCAGAGGTAGACCGATTCATGGAGCGGGAACACCTCATATTC
CGAGAGAACACGCTCGCCACTAAAGCCATAGAAGAGTATATGAGACTGATTGGCCAGAAATACCTC
AAGGATGCCATT

- CGG: PAM site to be abolished (Cas9-blocking)
- CATATTC: Restriction site to be introduced
- CGA: R470 codon to be changed

B. Donor DNA sequences

> R470A

CCATGTCAGAGGTAGACCGATTCATGGAGCGcGAACACCTgATcTTCgccGAGAACACGCTCGCCACTAAAGCC
ATAGAAGAGTATATGAGACTGATTGG

> R470K

CCATGTCAGAGGTAGACCGATTCATGGAGCGcGAACACCTgATcTTCCctGAGAACACGCTCGCCACTAAAGCC
ATAGAAGAGTATATGAGACTGATTGG

>R470P

CCATGTCAGAGGTAGACCGATTCATGGAGCGcGAACACCTCATATTtaaaGAGAACACGCTCGCCACTAAAGCC
ATAGAAGAGTATATGAGACTGATTGG

C. R470A donor DNA design

WT DNA	CGG	GAA	CAC	CTC	ATA	TTC	CGA
Mutant DNA	CGc	GAA	CAC	CTg	ATc	TTC	gcc
Amino acid	R	E	H	L	I	F	R>A
	464	465	466	467	468	469	470

- R470 codon to be changed: CGA to gcc (Arginine → Alanine)
- Introduction of Sau3AI site: CTC to CTg (Leucine); ATA to ATc (Isoleucine)
- Cas9-blocking: CGG to CGc (Arginine)

Figure 4.2 | Design of the donor DNAs.

A & B. Target region and donor DNA sequences. DNA sequence data of wild-type exon 9 and the three donor DNAs. The guide sequence, the PAM site, the R470 codon, and the restriction site are indicated in a distinct colour.

C. R470A donor design. Mutations introduced in the donor DNA. An example R470A (alanine) donor DNA contains one missense mutation for substituting arginine-470 with alanine and two synonymous mutations for the introduction of a restriction site and for the removal of the PAM site. Lower cases in DNA sequence indicate substitutions.

4.2 ES cell line generation

ES cells were transfected with the SYNGAP1-targeting sgRNA along with the donor oligos (each carrying the R470A, R470K or R470P mutation). A total of 572 colonies were isolated (R470A = 204, R470K = 144, and R470P = 224 colonies) and screened by restriction enzyme digestion. DNA was extracted from each colony and the presence of the mutations was determined by analysis of PCR amplicons. PCR primers (SG1-E9-F and SG-E9-R) were designed to amplify ~130 bp on either side of exon 9 for a total amplicon size of 414 bp. PCR products were digested with the corresponding restriction enzymes, and separated by agarose gel electrophoresis for fragment size analysis (**Figure 4.3**). A total of 147 cell lines (25.7%) had the expected fragment sizes (**Table 4.1**) indicating these cells contain SYNGAP1 mutations (**Figure 4.4**A). These mutant cell lines were further examined by sequence analyses.

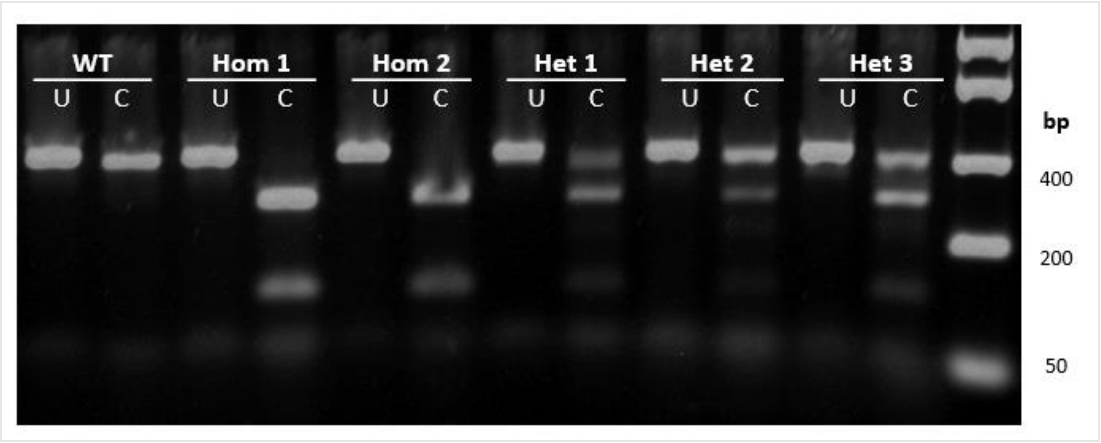

Figure 4.3 | The R470A cell lines genotyping using restriction digestion.

Gel electrophoresis of Sau3AI-digested DNA fragments of the R470A ES cells. The undigested (U) control bands were slightly bigger (414bp) than the digested (C) full-length bands (391 bp) due to an endogenous Sau3AI site at position 23 of the PCR product. The homozygous R470A cell lines (n=2) show two cleavage bands of 277 bp and 113 bp while heterozygous cell lines (n=3) present three bands of, 391 bp, 277 bp and 113 bp. Wild-type ES cells show only one band of 391 bp. Note 113 bp bands are only visible in the electronic copy of this thesis; the smallest 23 bp fragment was not visible either due to small size. WT: wild-type control DNA. Hom: homozygous R470A cell line. Het: heterozygous R470A cell line. U: uncut (undigested) control PCR products. C: cut (digested) PCR products.

Enzyme	DNA	Cleavage bands (bp)
Sau3AI	WT	391, 23
	R470A or R470K	Het: 391, 277, 113, 23
		Hom: 277, 113, 23
DraI	WT	414
	R470P	Het: 414, 272, 142
		Hom: 272, 142

Table 4.1 | Size determination of DNA restriction fragments.

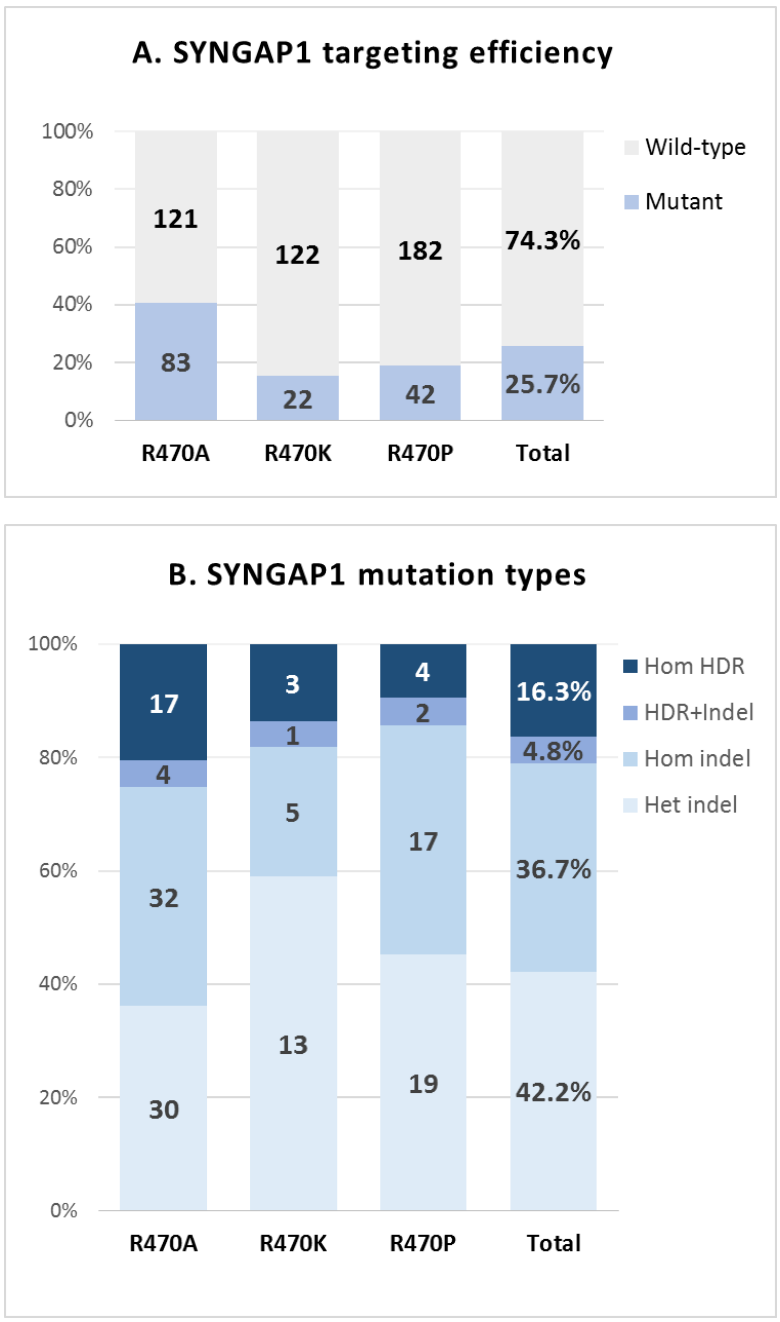

Figure 4.4 | CRISRP/Cas9-mediated SYNGAP1 mutations in ES cells.

The number of cell lines is indicated per each donor (R470A, R470K and R470P), and the overall frequencies (total) were shown in percentage. Overall, 25.7% of transfected cells carried SYNGAP1 mutations. 16.3% of targeted cells contain the accurate HDR mutation.

4.3 Sequence analyses

DNA sequence analyses of the PCR amplicons from each mutant cell line were performed as described in the previous chapter. Briefly, the undigested PCR products (414 bp) were purified, and sequenced by the Sanger method. DNA sequences from the mutant cells were aligned with wild-type DNA to identify any nucleotide mismatches (**Figure 4.5**). Additionally, DNA chromatograms were examined to confirm genotype.

The results of sequence analyses are summarised in **Figure 4.4**B. The majority (78.9%) of the mutant cells contain either mono-allelic (36.7%) or bi-allelic indel mutations (42.2%). Six HDR events (4.8%) contained additional indel mutations. This might be due to the high nuclease activity of Cas9, which may continuously re-edit targeted sites until sufficient modification by the end joining pathway prevents further cleavage (Cong et al. 2013; H. Wang et al. 2013; Paquet et al. 2016).

A total of 24 clones contained the precise HDR editing, making the overall HDR efficiency of 4.2% (24/572 cell lines). Notably, all accurate HDR mutations were homozygous. A potential explanation for the lack of heterozygous HDR mutations may be the high efficiency of Cas9, which leads mostly to bi-allelic HDR editing (Yang et al. 2013; Paquet et al. 2016). Together, the frequency of targeted cleavage and HDR mutation was in line with previous literature (C.-C. Wang et al. 2013; Yang et al. 2013; Inui et al. 2014; Oji et al. 2016).

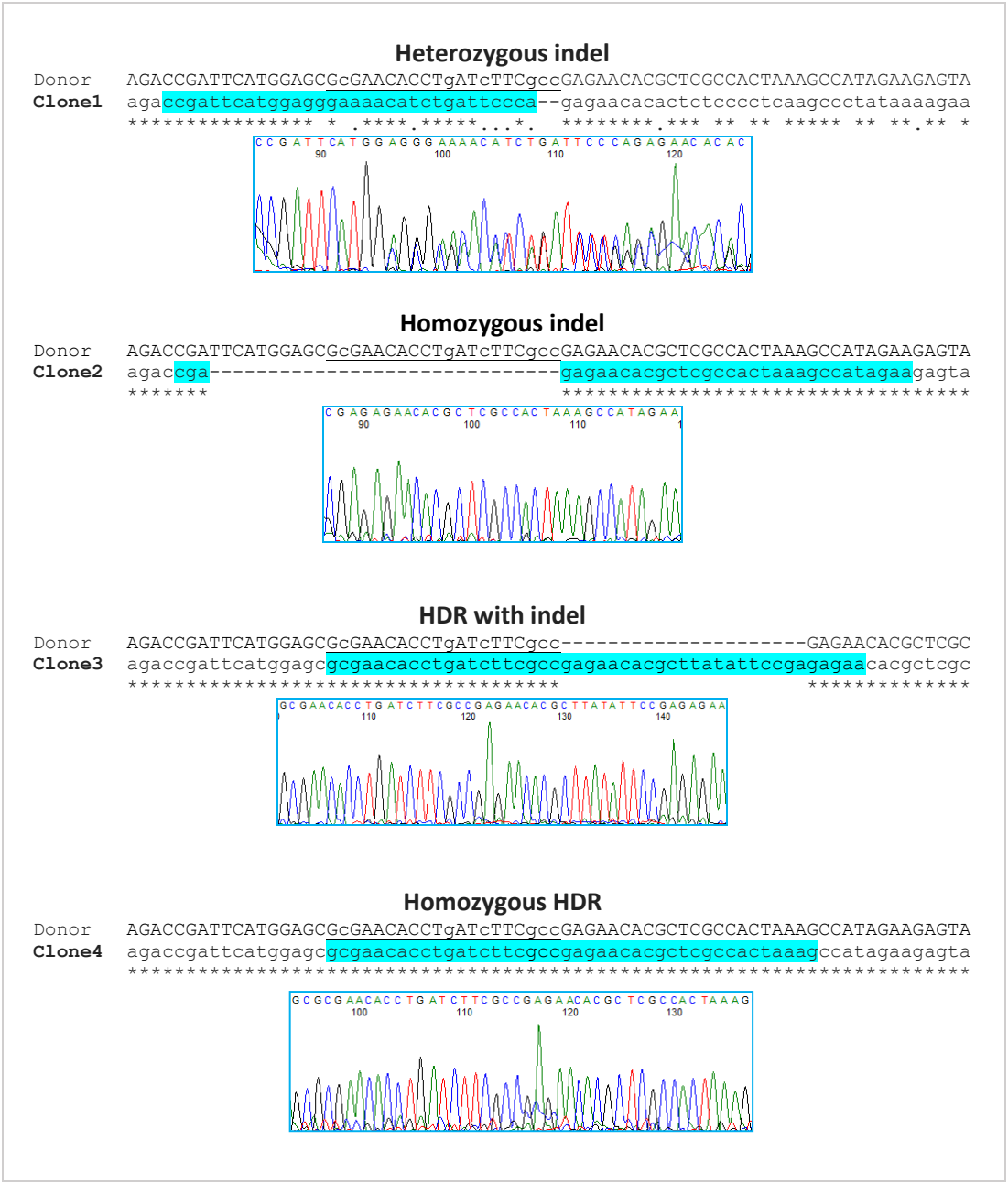

Figure 4.5 | Sequence analyses of each genotype.

SYNGAP1 sequence alignment of R470A cell lines. DNA sequences of four example mutant cell lines were compared with the R470A donor DNA sequence. In heterozygous indel Clone1, a perfect match in upstream of the target region is followed by a poor alignment and double peaks in the chromatogram. Homozygous indel Clone2 shows a perfect match both upstream and downstream of the target region. Clone3 has a perfect alignment in the target with an additional insertion. Finally, Clone4 shows a complete match with the donor DNA indicating the introduction of biallelic HDR mutation. Each chromatogram represents a region of sequence highlighted in blue.

The transfection using the R470A donor has a highest targeting efficiency (**Figure 4.4**A) as well as a highest frequency of HDR mutation (**Figure 4.4**B). In addition, a further examination of the Malachite Green Phosphate assay mentioned earlier revealed that the R470A mutation led to a slightly greater reduction in the GAP activity than the R470K or R470P mutations (personal communication, Dr. Satou Unzai). Therefore, we considered only the R470A mutant lines for blastocyst microinjection. Two homozygous cell lines with the R470A mutation were further examined by amplifying and sequencing a larger region (~ 800 bp) at around the target site using primer SG1-XL-F and SG1-XL-R. As shown in **Figure 4.6,** these cell lines were free of unwanted mutations around the target exon 9.

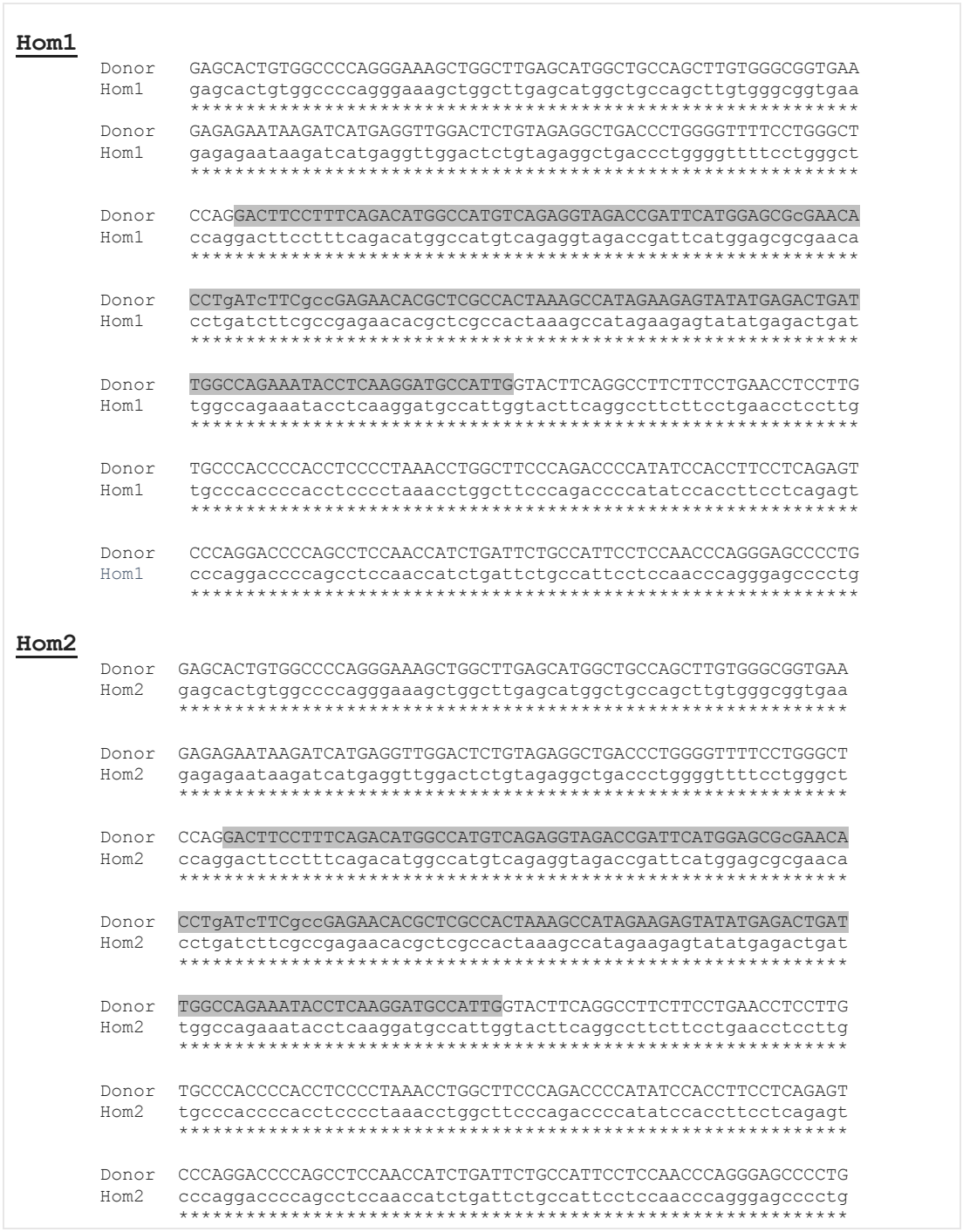

Figure 4.6 | Extended sequence alignment of the selected R470A cell lines.

SYNGAP1 sequence alignment of donor (R470A) DNA and the selected cell lines (Hom1 and Hom2) showing the exon 9 (highlighted in grey) flanking region. No unwanted mutation is found at around the target region. The intended mutation is indicated in lower cases in the donor sequence.

4.4 Introduction of specific homozygous and heterozygous mutations

Considering homozygous SYNGAP1 knockout mice die soon after birth, a precaution measure needed to be implemented in case the homozygous GAP-deficiency does the same as the knockout mice, thereby limiting chimaera generation derived from homozygous ES cell clones. Therefore, heterozygous mutation was introduced in ES cells by a second transfection. However, the resulting heterozygous ES cell lines were not used for mouse generation, as the initial microinjection of homozygous HDR ES cell lines produced a viable germline chimaera. The following paragraph describes generation of a heterozygous R470A mutant ES cells.

As our first transfection yielded only homozygous mutation, a new strategy was required to generate heterozygous mutants efficiently. Two methods could be applied to introduce heterozygous mutation. The first approach is to design a new donor DNA with a longer cut-to-mutation distance (that is a distance between Cas9 cleavage site and the desired mutation). There is an inverse relationship between a rate of HDR mutation and the mutation's distance to Cas9 cut site (Paquet et al. 2016). In other words, a homozygous mutation can be introduced by a sgRNA targeting close to the mutation, while a heterozygous mutation is achieved by distant-dependent suboptimal rate of HDR. An alternative approach is to use a mix of two donor DNA templates, both contain the Cas9-blocking silent mutation, but only one possesses the desired R470A mutation (**Figure 4.7**). The latter approach was chosen for the second transfection, since this strategy does not require the construction of a new sgRNA plasmid and subsequent functional validation. The equimolar amount of R470A and wild-type donor oligos ("mixed donor") were co-transfected with SYNGAP1-targeting pX330 as well as pPGKpuro plasmids. A control experiment using only the R470A donor ("single donor") was performed in parallel.

DNA from a total of 335 cell lines (double = 192; single = 143) were screened by restriction enzyme digestion. The SYNGAP1-targeting efficiency was 37.5% (72/192 cells) for the mixed donor and 32.9% (47/143 cells) for the single donor experiment (**Figure 4.8**A). Sequencing analysis of mutant clones revealed that only the mixed donor experiment introduced heterozygous HDR mutation in three clones (**Figure 4.8**B & **Figure 4.9**). Consistent with the previous experiment, there was no heterozygous HDR in the single donor condition. Together, the results demonstrate efficient introduction of a specific mono-allelic mutation using WT and mutant donor templates. Although incorporating Cas9-blocking mutations along with pathogenic mutations has been widely used to increase HDR accuracy (Doench *et al.*, 2014; Paquet *et al.*, 2016), the efficiency of the use of mixed donor templates has not been tested previously. Therefore our findings provide the first direct comparison between the use of single and mixed donor templates. Facilitating control experiments at low cost can be a key advantage of using ES cell-mediated approach for generation of mutant lines (See Table 4.2).

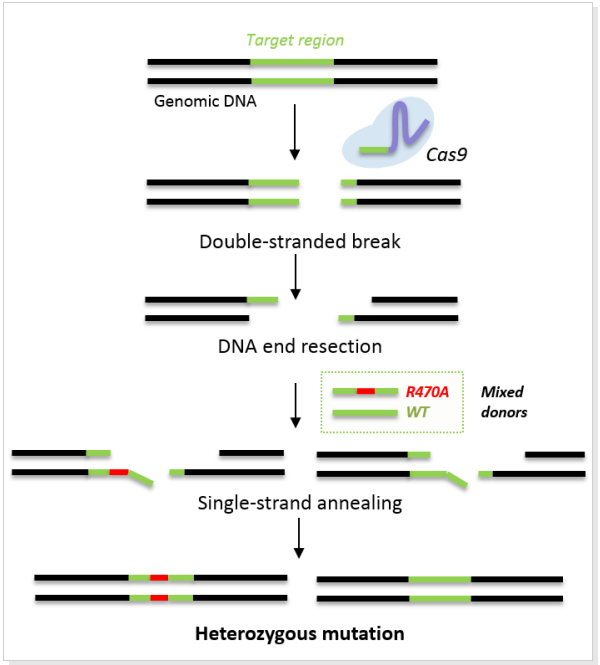

Figure 4.7 | Use of mixed donor templates to introduce heterozygosity.

Schematic describing introduction of heterozygous mutation using mixed donor templates, only one of which possesses the R470A mutation.

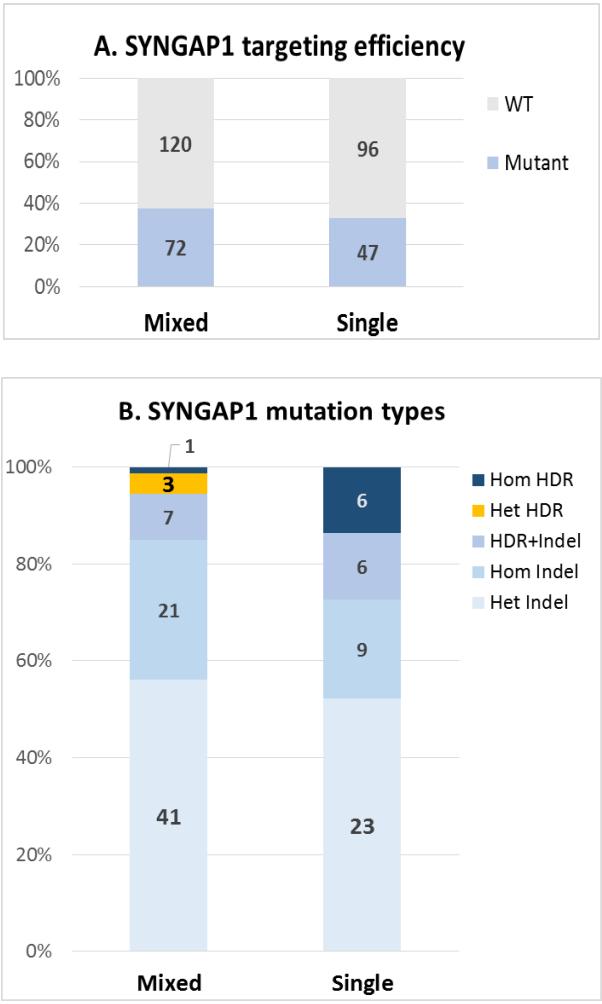

Figure 4.8 | Comparison between mixed and single donor experiments.

A. SYNGAP1 targeting efficiency. The number of cell lines is indicated in bars. The mixed and single donor experiments show the similar targeting efficiency (37.5% and 32.9% respectively).

B. SYNGAP1 mutation types. Only the mixed donors experiment introduced heterozygous HDR indicated in yellow. Data were presented in the number of cells.

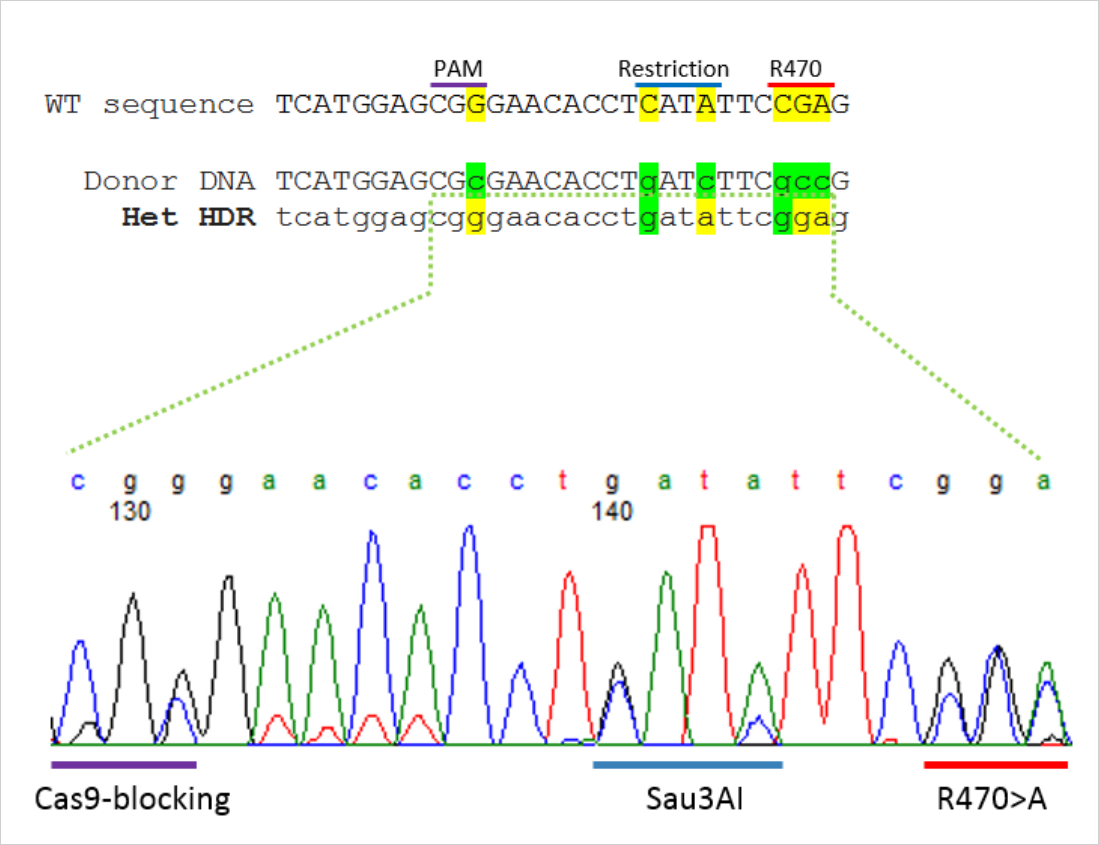

Figure 4.9 | Sequence analysis of a heterozygous HDR cell line.

Sequencing alignment and DNA chromatogram of a heterozygous HDR cell line (Het HDR) from the mixed donor experiment. The R470A mutation was introduced together with Cas9-blocking and Sau3AI silent mutations, and all mutations were represented as double peaks in the chromatogram below.

4.5 Mouse generation

Microinjection and subsequent chimaera generation were performed as described in Chapter 3. As mentioned previously, the microinjection of homozygous HDR ES cell lines generated a viable germline chimaera (**Table 4.3**); thus the heterozygous HDR cell lines were not used any further. F1 agouti pups were genotyped using restriction enzyme digestion as explained above and a female heterozygous mouse was identified (**Figure 4.10**A). Subsequent sequencing analysis confirmed germline transmission of the R470A mutation (**Figure 4.10**B). Intercross between the heterozygous offspring failed to produce homozygous mutants; 76 % (59 mice) were heterozygous, and 24% (19 mice) were wildtype indicating the homozygous R470A SynGAP1 mutation causes lethality similar to the homozygous SynGAP1 knockout mutation. SynGAP1 protein expression level of heterozygous R470A mutants was the same as that of the wildtype (**Figure 4.10**, produced by Sarah Lempriere). Together these findings support the hypothesis that GAP deficiency is responsible for neurological deficits in SynGAP1 knockout mutations in both animal models and humans. Further validation of GAP-deficiency in the R470A mutants by malachite green phosphate assay needs to be performed.

ES cell line (Injection date)	Transferred Embryos	Recipients	New-borns	Chimaeras (F0)	Pups (F1)	Germline (F1 Het)
R470A-Hom1**6)**	60	4	3	0	n/a	
R470A-Hom2	58	4	11	1	30	1

Table 4.3 | Blastocyst injection of homozygous HDR cell lines.

Two homozygous HDR cell lines (R470A-Hom1 & Hom2) were injected into C57BL/6J mouse blastocysts, which were then transferred into recipient mice. An adult male chimaera from Hom2 microinjection was mated with C57BL/6J mice and agouti pups were genotyped and subsequently sequenced to identify germline heterozygous mice.

A.

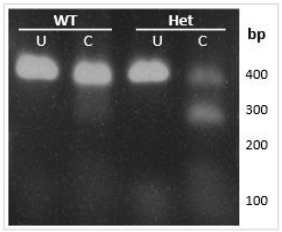

B.

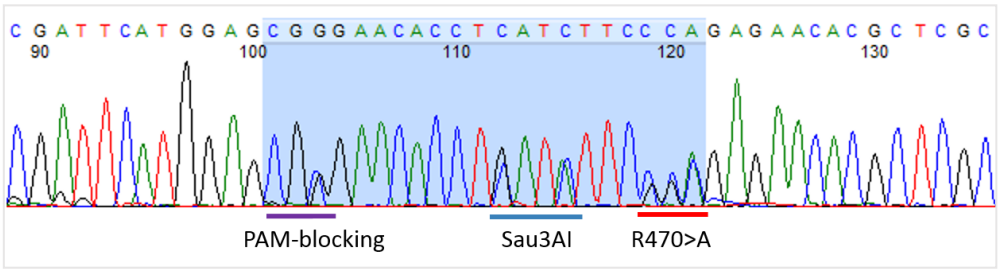

Figure 4.10 | Germline transmission of R470A mutation.

A. PCR genotyping of F1 mice. F1 agouti pups were genotyped by restriction enzyme, and the presence of a 277 bp cleavage product was considered as a potential germline transmission. Note smaller cleavage bands (113 bp and 23 bp) were not visible.

B. DNA chromatogram of the heterozygous mouse. The target site is highlighted, and the mutation loci are indicated. Note doubles peaks carry either WT or mutant nucleotide.

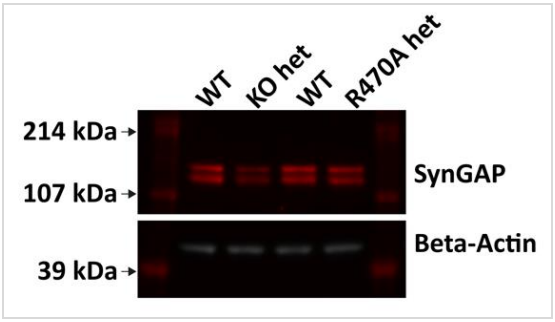

Figure 4.111 | Western blot of SynGAP1 mutant mice.

Representative blot (performed by Sarah Lempriere) of hippocampal homogenates from wildtype, heterozygous SynGAP1 knckout and heterozygous SynGAP1 R470A mutant mice. Red = Pan SynGAP1 antibody, Grescale = Beta-actin loading conrol.

Chapter 5 Conclusion

5.1 General methodological discussion

This study demonstrates the successful generation of novel mouse lines, SHANK3 knockout and SYNGAP1 R470A (GAP-deficiency) using ES cells modified by the CRISPR/Cas9 system. Our data suggest a high efficiency of CRISPR/Cas9-mediated gene deletion (62.5%) and point mutation (4.2%) in ES cells. The germline transmission rate was 9.6% for the SHANK3 knockout mutation and 2.66 % for SYNGAP1 R470A (**Table 5.1**). The combination of biallelic genome editing in ES cells and subsequent generation of chimeric animals offers a robust tool for efficient gene function analysis in animal models. There are several advantages for using ES cell-mediated approach over direct zygote injection. First, ES cells modified by the CRISPR/Cas9 system can be differentiated into post-mitotic neurons for cellular phenotypic analysis even before the generation of animal models. Secondly, while animals born without the desired mutations are culled after zygote injection, hundreds of ES cell lines can be screened to obtain the precise modification without having to sacrifice animal lives. Moreover, mosaicism in the founder generation is highly prevalent in zygote injection obfuscating genotyping analysis (Yen et al. 2014; Oliver et al. 2015). On the other hand, ES cell-derived chimaeric animals require a straightforward PCR-based analysis for genotyping. Mosaic animals obtained by zygote injection are crossed to generate the heterozygous F1 generation, and further breeding is necessary to produce the homozygous F2 generation. Therefore, the amount of time for mouse line generation is similar to the ES cell mediated approach (about 2-3 months for each generation) (Oji et al. 2016).

Mouse line	F1 het/ Total F1 mice	Germline transmission rate
SHANK3-KO	12/125	9.60%
SYNGAP1-R470A	2/75	2.66%

Table 5.1 | Germline transmission rate of ES cell lines modified by CRISPR/Cas9.

5.2 Applications of CRISPR-based technologies

Recent development of CRISPR-based technologies has extended its application to base editing, genome-scale screening, and clinical therapy (Doench et al. 2014; Zhang et al. 2018a).

Base editing: Compared to end joining, the HDR-dependent genome editing occurs at a low frequency, making CRISPR/Cas9-mediated precise modifications less efficient. To make point mutations without using the HDR pathway, researchers have developed CRISPR base editors that allow the direct alteration of target DNA bases without double-stranded DNA breaks or a donor DNA (Komor et al. 2017; Gaudelli et al. 2017; Nishida et al. 2016). The base editors are composed of catalytically dead Cas9 (dCas9) fused with a cytidine deaminase, and are directed to a target region by a guide RNA. The base editors can switch cytosine to uracil near the PAM site, without introducing a DNA cleavage (Komor et al. 2016). Uracil is then changed to thymine by DNA replication or repair facilitating C to T conversion or G to A on the opposite strand. The base editing results in a higher editing efficiency than HDR and fewer off-target effects than Cas9-mediated approach (Kim et al. 2017; Rees et al. 2017). Novel adenine base editors can now allow previously unavailable A to G (or T to C) conversion (Gaudelli et al. 2017). The ability to introduce or remove a single-nucleotide variation (SNV) in target genes indicates the potential of the CRISPR base editing in therapeutic applications. Targeting flexibility and specificity of the CRISPR base editing continues to be improved and assessed.

Genome-wide screening: The CRISPR technology has been repurposed to enable a large-scale genetic screening to identify specific genetic elements influencing a phenotype of interest. Traditionally, genetic screening approaches have relied on DNA mutagenesis (by chemical mutagen, radiation, or insertion of mobile genetic element) or RNAi for manipulation of transcript levels. However, screening using DNA mutagenesis requires laborious mapping of the

mutation sites (Sanjana 2017). RNAi-mediated screening is also limited by incomplete knockdown and high off-target effects (Jackson & Linsley 2010; Jackson et al. 2003). Recently, the CRISPR system has been adapted for genome-wide screening by combining Cas9 with pooled guide RNA libraries and next-generation sequencing. The pooled CRISPR screen has been used in loss-of-function assays to identify cancer drug targets (Shi et al. 2015), bacterial toxin resistance (Koike-Yusa et al. 2014), mitochondrial metabolism (Birsoy et al. 2015), and gene regulatory networks in immune cells (Parnas et al. 2015; Schmid-Burgk et al. 2016). In addition, dCas9-based screening has facilitated both genome-wide gain-of-function and loss-of-function screenings using arrays of transcriptional activator or repressor domains in combination with guide RNA libraries targeting gene promoters (Klann et al. 2017). Further developments in CRISPR-based RNA editing (Cox et al. 2017) and base editing (Gaudelli et al. 2017) will broaden the applicability of the CRISPR screen. Given the rapid pace of CRISPR-based technology development, the CRISPR pooled screening will deepen our understanding of genomic and epigenomic elements in both health and disease.

Clinical therapy: The CRISPR-based technology has shown potential in clinical therapy mainly involving immune cells and stem cells. The development of CRISPR technologies has enabled various *ex vivo* genetic engineering in human T cells to improve safety and efficiency of T cell-based immunotherapy (Zhang et al. 2017). Apart from T cells, genetic modification of induced pluripotent stem cells (iPSCs) has made progress in the field of neurodegenerative diseases including Alzheimer's disease (Pires et al. 2016) and Parkinson's disease (Heman-Ackah et al. 2017). The safety and efficiency of the iPSCs transplant as cell therapy remain to be validated. Although still in its infancy, CRISPR-based clinical therapy will likely offer the opportunity to develop novel cell therapies as further research will continue in order to augment gene targeting accuracy and efficiency.

Limitations: Given that off-target effects of the CRISPR system can be largely avoidable (see Chapter 1), the main technical challenge of CRISPR-based technologies may be Cas9 delivery. Initially, the CRISPR system relied on delivering plasmid or viral vectors encoding sgRNA and Cas9. However, this method suffers from limitations regarding plasmid transfection toxicity or immunity against viral vectors respectively (Kay 2011). More recently, the delivery of CRISPR components in a format of Cas9/sgRNA ribonucleoprotein complex has been shown to have several advantages because of lower off-target effects and higher nuclease activity compared to plasmid transfection (Kouranova et al. 2016; Kim et al. 2014; Staahl et al. 2017). The *in vivo* delivery, however, has to overcome several challenges including RNA-sensing innate immune responses leading to cytotoxicity (Kim et al. 2018), and inability for global delivery to the target cells, tissues or organs (Zhang et al. 2018b). For the efficient *in vivo* genome editing, further studies on delivery methods, such as nanoparticles (Lee et al. 2017) are necessary.

5.3 SHANK3 knockout mouse model

We created a novel SHANK3 knockout mouse line using the CRISPR/Cas9 technology leveraging the premature termination pathway. This is different from the existing mouse models of SHANK3 deficiency which have been generated from traditional gene targeting methods relying on homologous recombination (Bozdagi et al. 2010; Peça et al. 2011; Wang et al. 2011; Jaramillo et al. 2016). Although each of the existing lines targeted different exons (see

Figure 3.18**6**), all of these mutations disrupt the expression of the full-length SHANK3 (isoform 1), similar to the novel SHANK3 line; therefore the novel line is expected to have the similar phenotypes.

SHANK3 knockout mice display autism-related behaviours to different degrees (Bozdagi et al. 2010; Peça et al. 2011; Wang et al. 2011; Jaramillo et al. 2016). It

is worth testing, therefore, whether (and to what extent) our SHANK3 mice recapitulate core autism traits (i.e. social interaction deficits and repetitive behaviours). Autism-like phenotypes can be measured by a number of behavioural tests, for example, the three-chamber sociality test, ultrasonic vocalisation to examine communication patterns, and self-grooming for measuring repetitive behaviours (Wang *et al.*, 2011). A next question is how to rescue the autism-associated behavioural deficits. Several lines of evidence suggest pharmacological interventions can reverse the deficits in animals by targeting actin regulators (Duffney et al. 2015), mGluR5 (Vicidomini et al. 2016) or histone deacetylase (HDAC) (Qin et al. 2018). Future studies will determine whether these pharmacological experiments would be reproducible and clinically applicable.

The behavioural abnormalities observed in SHANK3 deficiency mice have been attributed to the dysfunction of glutamatergic synapses (Bozdagi et al. 2010; Peça et al. 2011; Wang et al. 2011; Jaramillo et al. 2016). In particular, the dysregulation of NMDARs is strongly related to social interaction deficits (Duffney et al. 2015; Qin et al. 2018). Previous studies show NMDAR hypofunction induced by SHANK3 deficiency is caused by the loss of synaptic trafficking of NMDARs (Duffney et al. 2015; Duffney et al. 2013). One critical issue is the molecular mechanism behind the loss of synaptic delivery of NMDARs.

MAGUKs, such as PSD95 and SAP102, are scaffolding proteins that anchor and traffic NMDARs to the synapse (Ryan & Grant 2009; Zhu et al. 2016), and physically interact with SHANK3 (Naisbitt et al. 1999; O'Connor et al. 2014). We therefore hypothesise the alteration in synaptic distributions of MAGUKs would be observed in mice lacking SHANK3. To test this hypothesis, an additional SHANK3 knockout mouse line was generated which expresses florescent tags in endogenous PSD95 and SAP102, as described in Chapter 3. PSD95- and SAP102-positive synapses will be directly visualised by high-resolution microscopy to investigate the morphology, density, intensity and size of MAGUK puncta in various brain regions. Supporting the hypothesis, loss of SHANK3 in mouse

models reduces spine density (Peça et al. 2011; Wang et al. 2011), and expression levels of multiple synaptic proteins (Peça et al. 2011; Wang et al. 2011; Bozdagi et al. 2010; Yang et al. 2012). Thus it is likely that changes in brain-wide synaptic maps will be observed from our SHANK3 knockout mouse line. Examining the effect of SHANK3 deficiency in the MAGUK synapse maps will provide crucial information on the molecular architecture of PSD proteins, and give an insight into the pathophysiology of the monogenic cause of autism.

5.4 SYNGAP1 GAP-deficient mouse model

We introduced the SYNGAP1-R470A point mutation into the mouse genome for the first time to investigate the role of GAP function in the pathophysiology of SYNGAP1 haploinsufficiency. A planned experiment is to characterise heterozygous SYNGAP1 GAP-deficient mice using a number of approaches for phenotypic analyses including behavioural tests, electrophysiology, and biochemistry. The phenotypes of the GAP-deficiency will be compared with the existing SYNGAP1 heterozygous null mutation mice to see whether the GAP-deficiency mirrors SYNGAP1 loss-of-function. If that is the case, this indicates human endophenotypes such as learning impairments and social deficits are largely caused by loss of GAP function, and can be rescued by a pharmacological therapy. The effective therapeutic can be developed by a simple compound library screening to identify a compound which enhances the GAP activity. Such pharmacological investigations will not only explore the therapeutic potentials of GAP enhancers but also provide a new insight into molecular mechanisms of PSD protein interactions involving SYNGAP1.

Alternatively, it is also possible that the phenotypic profile of the GAP-deficiency is significantly different from the knockout phenotypes. For example, if the GAP-deficiency has a significantly larger effect size than the knockout for the phenotype, this may be due to the dominant negative effect of the SYNGAP1 point mutation. In other words, the R470A mutant protein adversely affects the

normal functions of the wild-type protein. On the other hand, in case the GAP-deficiency has a less severe phenotype, this may indicate the other functions such as scaffolding play an important role in the pathophysiology of SYNGAP1 haploinsufficiency. Further experiment on mutations in protein-protein binding domains of SYNGAP1, such as the PDZ ligand domain (See **Figure 1.6**), will determine whether the scaffolding function is as crucial as the GAP function. Another possibility is that the phenotypes of the GAP-deficient mice are not significantly different from those of the wild-type mice. This may suggest that the GAP activity of SYNGAP1 is functionally redundant, and other GAP proteins or mechanisms that do not involve SYNGAP1 protein can regulate the appropriate levels of GTPase activation in cells. Taken together, further understanding of structural and functional roles of SYNGAP1 will deepen our understanding of the molecular organisation of NMDAR complexes and its associated pathways.

5.5 A common pathway of SHANK3 and SYNGAP1

Although many NMDAR-interacting proteins have been found in NMDAR complexes (Fan et al. 2014; Grant & O'Dell 2001), protein-protein interactions have not been investigated in detail. The current study has laid the foundations of a robust and efficient *in vivo* investigation of such protein interactions in NMDAR complexes. In particular, we focused our attention on two NMDAR-interacting proteins SHANK3 and SYNGAP1. Because of the commonalities between the two proteins as described previously, we hypothesised these two proteins would be identified in NMDAR complexes, and they are involved in a common molecular pathway. Analyses of the novel mutant mice will not only validate these protein interactions *in vivo*, but also determine whether SYNGAP1 and SHANK3 act as a direct downstream effector of the NMDA receptor signalling, and if these proteins regulate the same downstream signalling pathway which may be targeted therapeutically. As molecular mechanisms,

cellular events, and alterations in brain connectivity are conserved among mice and humans (Nithianantharajah et al. 2013), further research on this topic may open new avenues for diagnosis and therapeutic discoveries.

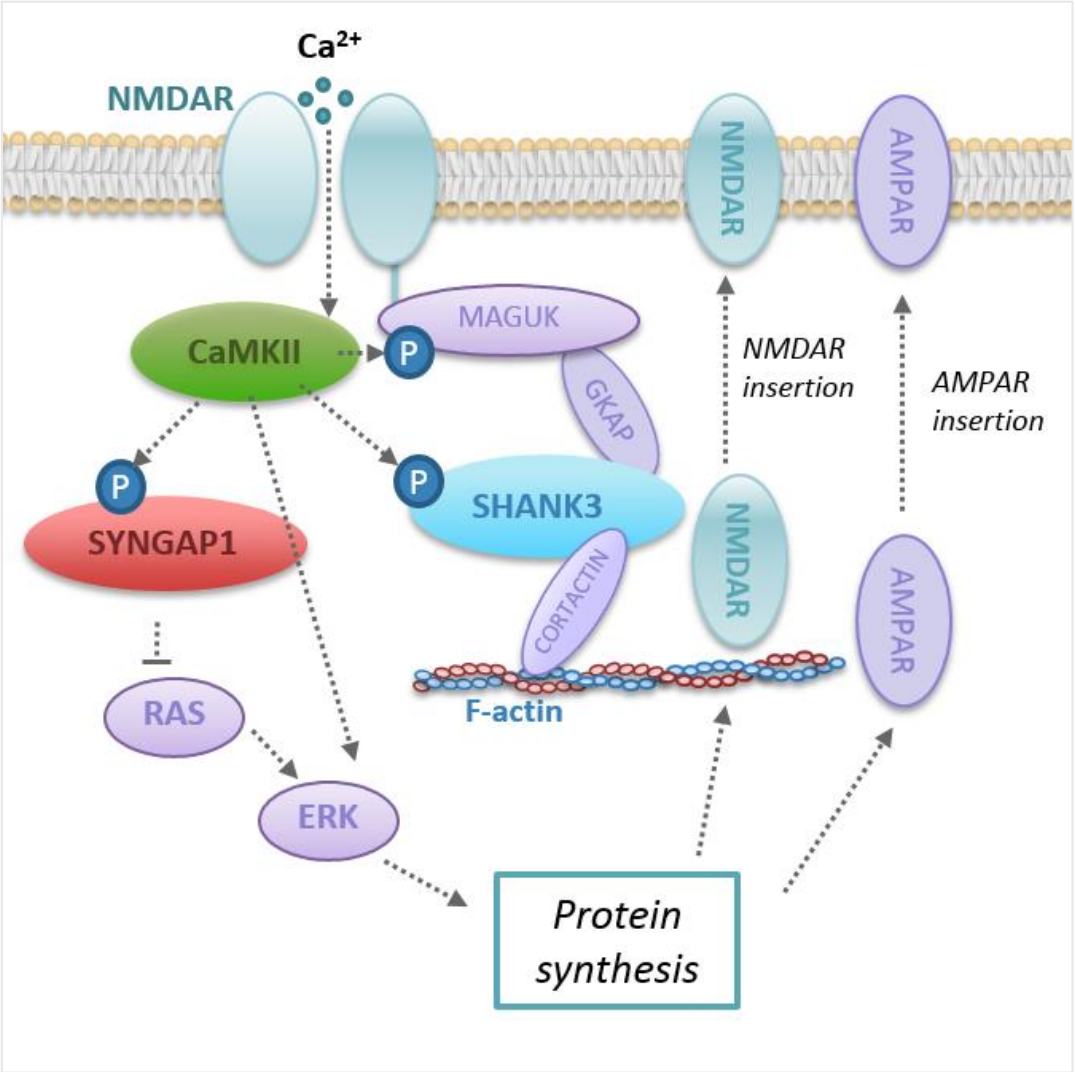

Figure 5.1 | Molecular pathway involving SHANK3 and SYNGAP1.

Diagram illustrating Ras-ERK dependent protein synthesis as a common molecular pathway of SHANK3 and SYNGAP1. NMDAR activation allows Ca^{2+} influx which enables CaMKII to phosphorylate many postsynaptic proteins including SYNGAP1, SHANK3 and MAGUKs. Phosphorylated SYNGAP1 inhibits Ras, thereby downregulating ERK-dependent protein synthesis. CaMKII may also directly influence ERK. Altered protein synthesis will have an impact on trafficking of receptor proteins such as NMDARs and AMPARs.

One potential common pathway of SHANK3 and SYNGAP1 is the Ras-ERK signal transduction cascade (**Figure 5.1**). Upon activation of NMDARs, Ca^{2+} flows through the receptors activating CaMKII (Kennedy 2016). The active CaMKII phosphorylates SYNGAP1 which, in turn, decreases the activity of Rap and Ras, leading to a rapid reduction in AMPAR endocytosis via the regulation of the Ras-ERK pathway (Walkup et al. 2016). SHANK3 is also phosphorylated by CaMKII, and is an abundant component of CaMKII multiprotein complexes at the PSD (Baucum et al. 2015). Supporting the potential involvement of CaMKII in the physiological regulation of SYNGAP1 and SHANK3, CaMKII mutations were identified in ASDs (Chiocchetti et al. 2018; Iossifov et al. 2014). Thus, it is possible that CaMKII, SHANK3 and SYNGAP1 converge on the Ras-ERK signalling. Consistent with this hypothesis, pathway and network analyses of ASD-related genes show calcium signalling and the Ras-ERK pathway are the most enriched pathways indicating the process involving calcium-Ras-ERK is a major contributor to the pathophysiology of ASDs (Wen et al. 2016). Given perturbed proteostasis has been associated with ASDs (Louros & Osterweil 2016), it is conceivable that a disrupted Ras-ERK pathway is linked to an imbalance in protein homeostasis in synapses. Further examination of the interplay of SHANK3 and SYNGAP1 in the Ras-ERK pathway will facilitate the discovery of novel drug targets for ASDs and other NMDAR complexes-related brain disorders.

Bibliography

Aceti, M., Creson, T. K., Vaissiere, T., Rojas, C., Huang, W.-C., Wang, Y.-X., Petralia, R. S., Page, D. T., Miller, C. A. and Rumbaugh, G. (2015) 'Syngap1 haploinsufficiency damages a postnatal critical period of pyramidal cell structural maturation linked to cortical circuit assembly.', *Biological psychiatry*. NIH Public Access, 77(9), pp. 805–15. doi: 10.1016/j.biopsych.2014.08.001.

Ahmadian, M. R., Stege, P., Scheffzek, K. and Wittinghofer, A. (1997) 'Confirmation of the arginine-finger hypothesis for the GAP-stimulated GTP-hydrolysis reaction of Ras', *Nature Structural Biology*. Nature Publishing Group, 4(9), pp. 686–689. doi: 10.1038/nsb0997-686.

Aida, T., Chiyo, K., Usami, T., Ishikubo, H., Imahashi, R., Wada, Y., Tanaka, K. F., Sakuma, T., Yamamoto, T. and Tanaka, K. (2015) 'Cloning-free CRISPR/Cas system facilitates functional cassette knock-in in mice', *Genome Biology*, 16(1), p. 87. doi: 10.1186/s13059-015-0653-x.

Akashi, K., Kakizaki, T., Kamiya, H., Fukaya, M., Yamasaki, M., Abe, M., Natsume, R., Watanabe, M. and Sakimura, K. (2009) 'NMDA receptor GluN2B (GluR epsilon 2/NR2B) subunit is crucial for channel function, postsynaptic macromolecular organization, and actin cytoskeleton at hippocampal CA3 synapses.', *The Journal of neuroscience : the official journal of the Society for Neuroscience*, 29(35), pp. 10869–82. doi: 10.1523/JNEUROSCI.5531-08.2009.

Alic, N., Hoddinott, M. P., Foley, A., Slack, C., Piper, M. D. W. and Partridge, L. (2012) 'Detrimental Effects of RNAi: A Cautionary Note on Its Use in Drosophila Ageing Studies', *PLoS ONE*. Edited by S. Cotterill. Public Library of Science, 7(9), p. e45367. doi: 10.1371/journal.pone.0045367.

Araki, Y., Zeng, M., Zhang, M. and Huganir, R. L. (2015) 'Rapid Dispersion of SynGAP from Synaptic Spines Triggers AMPA Receptor Insertion and Spine Enlargement during LTP', *Neuron*. Elsevier Inc., 85(1), pp. 173–190. doi: 10.1016/j.neuron.2014.12.023.

Bae, S., Park, J. and Kim, J.-S. (2014) 'Cas-OFFinder: a fast and versatile algorithm that searches for potential off-target sites of Cas9 RNA-guided endonucleases', *Bioinformatics*. Oxford University Press, 30(10), pp. 1473–1475. doi: 10.1093/bioinformatics/btu048.

Baucum, A. J., Shonesy, B. C., Rose, K. L. and Colbran, R. J. (2015) 'Quantitative Proteomics Analysis of CaMKII Phosphorylation and the CaMKII Interactome in the Mouse Forebrain', *ACS Chemical Neuroscience*, 6(4), pp. 615–631. doi: 10.1021/cn500337u.

Berryer, M. H., Hamdan, F. F., Klitten, L. L., Møller, R. S., Carmant, L., Schwartzentruber, J., Patry, L., Dobrzeniecka, S., Rochefort, D., Neugnot-Cerioli, M., Lacaille, J.-C., Niu, Z., Eng, C. M., Yang, Y.,

Palardy, S., Belhumeur, C., Rouleau, G. A., Tommerup, N., Immken, L., Beauchamp, M. H., Patel, G. S., Majewski, J., Tarnopolsky, M. A., Scheffzek, K., Hjalgrim, H., Michaud, J. L. and Di Cristo, G. (2013) 'Mutations in *SYNGAP1* Cause Intellectual Disability, Autism, and a Specific Form of Epilepsy by Inducing Haploinsufficiency', *Human Mutation*, 34(2), pp. 385–394. doi: 10.1002/humu.22248.

Birsoy, K., Wang, T., Chen, W. W., Freinkman, E., Abu-Remaileh, M. and Sabatini, D. M. (2015) 'An Essential Role of the Mitochondrial Electron Transport Chain in Cell Proliferation Is to Enable Aspartate Synthesis', *Cell*. Cell Press, 162(3), pp. 540–551. doi: 10.1016/J.CELL.2015.07.016.

Boccuto, L., Lauri, M., Sarasua, S. M., Skinner, C. D., Buccella, D., Dwivedi, A., Orteschi, D., Collins, J. S., Zollino, M., Visconti, P., DuPont, B., Tiziano, D., Schroer, R. J., Neri, G., Stevenson, R. E., Gurrieri, F. and Schwartz, C. E. (2013) 'Prevalence of SHANK3 variants in patients with different subtypes of autism spectrum disorders', *European Journal of Human Genetics*, 21(3), pp. 310–316. doi: 10.1038/ejhg.2012.175.

Boeckers, T. M., Kreutz, M. R., Winter, C., Zuschratter, W., Smalla, K. H., Sanmarti-Vila, L., Wex, H., Langnaese, K., Bockmann, J., Garner, C. C. and Gundelfinger, E. D. (1999) 'Proline-rich synapse-associated protein-1/cortactin binding protein 1 (ProSAP1/CortBP1) is a PDZ-domain protein highly enriched in the postsynaptic density.', *The Journal of neuroscience : the official journal of the Society for Neuroscience*, 19(15), pp. 6506–18. Available at: http://www.ncbi.nlm.nih.gov/pubmed/10414979 (Accessed: 29 September 2015).

Boeckers, T. M., Liedtke, T., Spilker, C., Dresbach, T., Bockmann, J., Kreutz, M. R. and Gundelfinger, E. D. (2005) 'C-terminal synaptic targeting elements for postsynaptic density proteins ProSAP1/Shank2 and ProSAP2/Shank3', *Journal of Neurochemistry*. Blackwell Science Ltd, 92(3), pp. 519–524. doi: 10.1111/j.1471-4159.2004.02910.x.

Bonaglia, M. C., Giorda, R., Borgatti, R., Felisari, G., Gagliardi, C., Selicorni, A. and Zuffardi, O. (2001) 'Disruption of the ProSAP2 gene in a t(12;22)(q24.1;q13.3) is associated with the 22q13.3 deletion syndrome.', *American journal of human genetics*. Elsevier, 69(2), pp. 261–8. doi: 10.1086/321293.

Bonetti, B., Fu, L., Moon, J. and Bedwell, D. M. (1995) 'The Efficiency of Translation Termination is Determined by a Synergistic Interplay Between Upstream and Downstream Sequences inSaccharomyces cerevisiae', *Journal of Molecular Biology*, 251(3), pp. 334–345. doi: 10.1006/jmbi.1995.0438.

Bortesi, L. and Fischer, R. (2015) 'The CRISPR/Cas9 system for plant genome editing and beyond', *Biotechnology Advances*, 33(1), pp. 41–52. doi: 10.1016/j.biotechadv.2014.12.006.

Bos, J. L., Rehmann, H. and Wittinghofer, A. (2007) 'GEFs and GAPs: Critical Elements in the Control of Small G Proteins', *Cell*. Cell Press, 129(5), pp. 865–877. doi: 10.1016/J.CELL.2007.05.018.

Bozdagi, O., Sakurai, T., Papapetrou, D., Wang, X., Dickstein, D. L., Takahashi, N., Kajiwara, Y., Yang, M., Katz, A. M., Scattoni, M. L., Harris, M. J., Saxena, R., Silverman, J. L., Crawley, J. N., Zhou, Q., Hof, P. R. and Buxbaum, J. D. (2010) 'Haploinsufficiency of the autism-associated Shank3 gene leads to deficits in synaptic function, social interaction, and social communication.', *Molecular autism*, 1(1), p. 15. doi: 10.1186/2040-2392-1-15.

Brogna, S. and Wen, J. (2009) 'Nonsense-mediated mRNA decay (NMD) mechanisms', *Nature Structural & Molecular Biology*. Nature Publishing Group, 16(2), pp. 107–113. doi: 10.1038/nsmb.1550.

Capecchi, M. R. (2005) 'Gene targeting in mice: functional analysis of the mammalian genome for the twenty-first century.', *Nature reviews. Genetics*, 6(6), pp. 507–12. doi: 10.1038/nrg1619.

Carlisle, H. J., Manzerra, P., Marcora, E. and Kennedy, M. B. (2008) 'SynGAP regulates steady-state and activity-dependent phosphorylation of cofilin', *J Neurosci*, 28(50), pp. 13673–13683. doi: 10.1523/JNEUROSCI.4695-08.2008.

Cassan, M. and Rousset, J. P. (2001) 'UAG readthrough in mammalian cells: effect of upstream and downstream stop codon contexts reveal different signals.', *BMC molecular biology*, 2, p. 3. Available at: http://www.ncbi.nlm.nih.gov/pubmed/11242562 (Accessed: 12 February 2018).

Chen, F., Pruett-Miller, S. M., Huang, Y., Gjoka, M., Duda, K., Taunton, J., Collingwood, T. N., Frodin, M. and Davis, G. D. (2011) 'High-frequency genome editing using ssDNA oligonucleotides with zinc-finger nucleases.', *Nature methods*. NIH Public Access, 8(9), pp. 753–5. doi: 10.1038/nmeth.1653.

Chen, H.-J., Rojas-Soto, M., Oguni, A. and Kennedy, M. B. (1998) 'A Synaptic Ras-GTPase Activating Protein (p135 SynGAP) Inhibited by CaM Kinase II', *Neuron*. Cell Press, 20(5), pp. 895–904. doi: 10.1016/S0896-6273(00)80471-7.

Cheng, D., Hoogenraad, C. C., Rush, J., Ramm, E., Schlager, M. A., Duong, D. M., Xu, P., Wijayawardana, S. R., Hanfelt, J., Nakagawa, T., Sheng, M. and Peng, J. (2006) 'Relative and absolute quantification of postsynaptic density proteome isolated from rat forebrain and cerebellum.', *Molecular & cellular proteomics : MCP*. American Society for Biochemistry and Molecular Biology, 5(6), pp. 1158–70. doi: 10.1074/mcp.D500009-MCP200.

Chiocchetti, A. G., Yousaf, A., Bour, H. S., Haslinger, D., Waltes, R., Duketis, E., Jarczok, T., Sachse, M., Biscaldi, M., Degenhardt, F., Herms, S., Cichon, S., Ackermann, J., Koch, I., Klauck, S. M. and Freitag,

C. M. (2018) ‘Common functional variants of the glutamatergic system in Autism spectrum disorder with high and low intellectual abilities’, *Journal of Neural Transmission*, 125(2), pp. 259–271. doi: 10.1007/s00702-017-1813-9.

Cho, S. W., Kim, S., Kim, Y., Kweon, J., Kim, H. S., Bae, S. and Kim, J.-S. (2014) ‘Analysis of off-target effects of CRISPR/Cas-derived RNA-guided endonucleases and nickases’, *Genome Research*, 24(1), pp. 132–141. doi: 10.1101/gr.162339.113.

Clement, J. P., Ozkan, E. D., Aceti, M., Miller, C. A. and Rumbaugh, G. (2013) ‘SYNGAP1 Links the Maturation Rate of Excitatory Synapses to the Duration of Critical-Period Synaptic Plasticity’, *Journal of Neuroscience*, 33(25), pp. 10447–10452. doi: 10.1523/JNEUROSCI.0765-13.2013.

Clement, J. P. P., Aceti, M., Creson, T. K. K., Ozkan, E. D. D., Shi, Y., Reish, N. J. J., Almonte, A. G. G., Miller, B. H. H., Wiltgen, B. J. J., Miller, C. A. A., Xu, X. and Rumbaugh, G. (2012) ‘Pathogenic SYNGAP1 mutations impair cognitive development by disrupting maturation of dendritic spine synapses.’, *Cell*, 151(4), pp. 709–23. doi: 10.1016/j.cell.2012.08.045.

Clements, J. D. and Westbrook, G. L. (1991) ‘Activation kinetics reveal the number of glutamate and glycine binding sites on the N-methyl-D-aspartate receptor.’, *Neuron*, 7(4), pp. 605–13. Available at: http://www.ncbi.nlm.nih.gov/pubmed/1681832 (Accessed: 28 March 2018).

Cohen, G. B., Ren, R. and Baltimore, D. (1995) ‘Modular binding domains in signal transduction proteins.’, *Cell*, 80(2), pp. 237–48. Available at: http://www.ncbi.nlm.nih.gov/pubmed/7834743 (Accessed: 15 February 2018).

Collingridge, G. L., Olsen, R. W., Peters, J. and Spedding, M. (2009) ‘A nomenclature for ligand-gated ion channels’, *Neuropharmacology*, 56(1), pp. 2–5. doi: 10.1016/j.neuropharm.2008.06.063.

Cong, L., Ran, F. A., Cox, D., Lin, S., Barretto, R., Habib, N., Hsu, P. D., Wu, X., Jiang, W., Marraffini, L. A. and Zhang, F. (2013) ‘Multiplex genome engineering using CRISPR/Cas systems.’, *Science (New York, N.Y.)*, 339(6121), pp. 819–23. doi: 10.1126/science.1231143.

Cox, D. B. T., Gootenberg, J. S., Abudayyeh, O. O., Franklin, B., Kellner, M. J., Joung, J. and Zhang, F. (2017) ‘RNA editing with CRISPR-Cas13’, *Science*, 358(6366), pp. 1019–1027. doi: 10.1126/science.aaq0180.

Deciphering Developmental Disorders Study (2017) ‘Prevalence and architecture of de novo mutations in developmental disorders’, *Nature*, 542(7642), pp. 433–438. doi: 10.1038/nature21062.

Dickinson, D. J. and Goldstein, B. (2016) ‘CRISPR-Based Methods for Caenorhabditis elegans Genome

Engineering.', *Genetics*. Genetics, 202(3), pp. 885–901. doi: 10.1534/genetics.115.182162.

Doench, J. G., Hartenian, E., Graham, D. B., Tothova, Z., Hegde, M., Smith, I., Sullender, M., Ebert, B. L., Xavier, R. J. and Root, D. E. (2014) 'Rational design of highly active sgRNAs for CRISPR-Cas9–mediated gene inactivation', *Nature Biotechnology*. doi: 10.1038/nbt.3026.

Dominguez, A. A., Lim, W. A. and Qi, L. S. (2016) 'Beyond editing: repurposing CRISPR-Cas9 for precision genome regulation and interrogation.', *Nature reviews. Molecular cell biology*. NIH Public Access, 17(1), pp. 5–15. doi: 10.1038/nrm.2015.2.

Duan, J., Lu, G., Xie, Z., Lou, M., Luo, J., Guo, L. and Zhang, Y. (2014) 'Genome-wide identification of CRISPR/Cas9 off-targets in human genome', *Cell Research*. Nature Publishing Group, 24(8), pp. 1009–1012. doi: 10.1038/cr.2014.87.

Duffney, L. J., Wei, J., Cheng, J., Liu, W., Smith, K. R., Kittler, J. T. and Yan, Z. (2013) 'Shank3 deficiency induces NMDA receptor hypofunction via an actin-dependent mechanism.', *The Journal of neuroscience : the official journal of the Society for Neuroscience*, 33(40), pp. 15767–78. doi: 10.1523/JNEUROSCI.1175-13.2013.

Duffney, L. J., Zhong, P., Wei, J., Matas, E., Cheng, J., Qin, L., Ma, K., Dietz, D. M., Kajiwara, Y., Buxbaum, J. D. and Yan, Z. (2015) 'Autism-like Deficits in Shank3-Deficient Mice Are Rescued by Targeting Actin Regulators', *Cell Reports*. The Authors, 11(9), pp. 1400–1413. doi: 10.1016/j.celrep.2015.04.064.

Durand, C. M., Betancur, C., Boeckers, T. M., Bockmann, J., Chaste, P., Fauchereau, F., Nygren, G., Rastam, M., Gillberg, C. C., Anckarsäter, H., Sponheim, E., Goubran-Botros, H., Delorme, R., Chabane, N., Mouren-Simeoni, M.-C., de Mas, P., Bieth, E., Rogé, B., Héron, D., Burglen, L., Gillberg, C. C., Leboyer, M., Bourgeron, T., Gillberg, I. C., Anckarsäter, H., Sponheim, E., Goubran-Botros, H., Delorme, R., Chabane, N., Mouren-Simeoni, M.-C., de Mas, P., Bieth, E., Rogé, B., Héron, D., Burglen, L., Gillberg, C. C., Leboyer, M. and Bourgeron, T. (2007) 'Mutations in the gene encoding the synaptic scaffolding protein SHANK3 are associated with autism spectrum disorders.', *Nature genetics*, 39(1), pp. 25–7. doi: 10.1038/ng1933.

Durand, C. M., Perroy, J., Loll, F., Perrais, D., Fagni, L., Bourgeron, T., Montcouquiol, M. and Sans, N. (2011) 'SHANK3 mutations identified in autism lead to modification of dendritic spine morphology via an actin-dependent mechanism', *Molecular Psychiatry*, 17(1), pp. 71–84. doi: 10.1038/mp.2011.57.

Durfee, T., Nelson, R., Baldwin, S., Plunkett, G., Burland, V., Mau, B., Petrosino, J. F., Qin, X., Muzny,

D. M., Ayele, M., Gibbs, R. A., Csörgo, B., Pósfai, G., Weinstock, G. M., Blattner, F. R. and Blattner, F. R. (2008) 'The complete genome sequence of Escherichia coli DH10B: insights into the biology of a laboratory workhorse.', *Journal of bacteriology*. American Society for Microbiology (ASM), 190(7), pp. 2597–606. doi: 10.1128/JB.01695-07.

Elbashir, S. M., Harborth, J., Lendeckel, W., Yalcin, A., Weber, K. and Tuschl, T. (2001) 'Duplexes of 21-nucleotide RNAs mediate RNA interference in cultured mammalian cells.', *Nature*, 411(6836), pp. 494–498. doi: 10.1038/35078107.

Fan, X., Jin, W. Y. and Wang, Y. T. (2014) 'The NMDA receptor complex: a multifunctional machine at the glutamatergic synapse.', *Frontiers in cellular neuroscience*, 8, p. 160. doi: 10.3389/fncel.2014.00160.

Fernández, E., Collins, M. O., Uren, R. T., Kopanitsa, M. V, Komiyama, N. H., Croning, M. D. R., Zografos, L., Armstrong, J. D., Choudhary, J. S. and Grant, S. G. N. (2009) 'Targeted tandem affinity purification of PSD-95 recovers core postsynaptic complexes and schizophrenia susceptibility proteins.', *Molecular systems biology*. European Molecular Biology Organization, 5, p. 269. doi: 10.1038/msb.2009.27.

Feyder, M., Karlsson, R.-M., Mathur, P., Lyman, M., Bock, R., Momenan, R., Munasinghe, J., Scattoni, M. L., Ihne, J., Camp, M., Graybeal, C., Strathdee, D., Begg, A., Alvarez, V. A., Kirsch, P., Rietschel, M., Cichon, S., Walter, H., Meyer-Lindenberg, A., Grant, S. G. N. and Holmes, A. (2010) 'Association of mouse Dlg4 (PSD-95) gene deletion and human DLG4 gene variation with phenotypes relevant to autism spectrum disorders and Williams' syndrome.', *The American journal of psychiatry*. NIH Public Access, 167(12), pp. 1508–17. doi: 10.1176/appi.ajp.2010.10040484.

Frank, R. A. W., Komiyama, N. H., Ryan, T. J., Zhu, F., O'Dell, T. J. and Grant, S. G. N. (2016) 'NMDA receptors are selectively partitioned into complexes and supercomplexes during synapse maturation', *Nature Communications*, 7, p. 11264. doi: 10.1038/ncomms11264.

Furukawa, H., Singh, S. K., Mancusso, R. and Gouaux, E. (2005) 'Subunit arrangement and function in NMDA receptors', *Nature*. Nature Publishing Group, 438(7065), pp. 185–192. doi: 10.1038/nature04089.

Garneau, J. E., Dupuis, M.-È., Villion, M., Romero, D. A., Barrangou, R., Boyaval, P., Fremaux, C., Horvath, P., Magadán, A. H. and Moineau, S. (2010) 'The CRISPR/Cas bacterial immune system cleaves bacteriophage and plasmid DNA', *Nature*. Nature Publishing Group, 468(7320), pp. 67–71. doi: 10.1038/nature09523.

Gaudelli, N. M., Komor, A. C., Rees, H. A., Packer, M. S., Badran, A. H., Bryson, D. I. and Liu, D. R. (2017) 'Programmable base editing of A•T to G•C in genomic DNA without DNA cleavage', *Nature*. Nature Publishing Group, 551(7681), pp. 464–471. doi: 10.1038/nature24644.

Gauthier, J., Champagne, N., Lafrenière, R. G., Xiong, L., Spiegelman, D., Brustein, E., Lapointe, M., Peng, H., Côté, M., Noreau, A., Hamdan, F. F., Addington, A. M., Rapoport, J. L., DeLisi, L. E., Krebs, M.-O., Joober, R., Fathalli, F., Mouaffak, F., Haghighi, A. P., Néri, C., Dubé, M.-P., Samuels, M. E., Marineau, C., Stone, E. A., Awadalla, P., Barker, P. A., Carbonetto, S., Drapeau, P. and Rouleau, G. A. (2010) 'De novo mutations in the gene encoding the synaptic scaffolding protein *SHANK3* in patients ascertained for schizophrenia', *Proceedings of the National Academy of Sciences*, 107(17), pp. 7863–7868. doi: 10.1073/pnas.0906232107.

Gauthier, J., Spiegelman, D., Piton, A., Lafrenière, R. G., Laurent, S., St-Onge, J., Lapointe, L., Hamdan, F. F., Cossette, P., Mottron, L., Fombonne, É., Joober, R., Marineau, C., Drapeau, P. and Rouleau, G. A. (2009) 'Novel de novo SHANK3 mutation in autistic patients', *American Journal of Medical Genetics Part B: Neuropsychiatric Genetics*. Wiley Subscription Services, Inc., A Wiley Company, 150B(3), pp. 421–424. doi: 10.1002/ajmg.b.30822.

Gilbert, L. A., Larson, M. H., Morsut, L., Liu, Z., Brar, G. A., Torres, S. E., Stern-Ginossar, N., Brandman, O., Whitehead, E. H., Doudna, J. A., Lim, W. A., Weissman, J. S. and Qi, L. S. (2013) 'CRISPR-Mediated Modular RNA-Guided Regulation of Transcription in Eukaryotes', *Cell*, 154(2), pp. 442–451. doi: 10.1016/j.cell.2013.06.044.

Grant, S. G. . and O'Dell, T. J. (2001) 'Multiprotein complex signaling and the plasticity problem', *Current Opinion in Neurobiology*, 11(3), pp. 363–368. doi: 10.1016/S0959-4388(00)00220-8.

Grant, S. G., Jessee, J., Bloom, F. R. and Hanahan, D. (1990) 'Differential plasmid rescue from transgenic mouse DNAs into Escherichia coli methylation-restriction mutants.', *Proceedings of the National Academy of Sciences of the United States of America*. National Academy of Sciences, 87(12), pp. 4645–9. Available at: http://www.ncbi.nlm.nih.gov/pubmed/2162051 (Accessed: 27 August 2017).

Guo, X., Hamilton, P. J., Reish, N. J., Sweatt, J. D., Miller, C. A. and Rumbaugh, G. (2009) 'Reduced expression of the NMDA receptor-interacting protein SynGAP causes behavioral abnormalities that model symptoms of Schizophrenia.', *Neuropsychopharmacology : official publication of the American College of Neuropsychopharmacology*. Nature Publishing Group, 34(7), pp. 1659–72. doi: 10.1038/npp.2008.223.

Hamdan, F. F., Gauthier, J., Araki, Y., Lin, D. T., Yoshizawa, Y., Higashi, K., Park, A. R., Spiegelman, D.,

Dobrzeniecka, S., Piton, A., Tomitori, H., Daoud, H., Massicotte, C., Henrion, E., Diallo, O., Shekarabi, M., Marineau, C., Shevell, M., Maranda, B., Mitchell, G., Nadeau, A., D'Anjou, G., Vanasse, M., Srour, M., Lafrenière, R. G., Drapeau, P., Lacaille, J. C., Kim, E., Lee, J. R., Igarashi, K., Huganir, R. L., Rouleau, G. A. and Michaud, J. L. (2011) 'Excess of de novo deleterious mutations in genes associated with glutamatergic systems in nonsyndromic intellectual disability', *American Journal of Human Genetics*, 88(3), pp. 306–316. doi: 10.1016/j.ajhg.2011.02.001.

Hamdan, F. F., Gauthier, J., Spiegelman, D., Noreau, A., Yang, Y., Pellerin, S., Dobrzeniecka, S., Côté, M., Perreau-Linck, E., Carmant, L., D'Anjou, G., Fombonne, É., Addington, A. M., Rapoport, J. L., Delisi, L. E., Krebs, M.-O., Mouaffak, F., Joober, R., Mottron, L., Drapeau, P., Marineau, C., Lafrenière, R. G., Lacaille, J. C., Rouleau, G. A. and Michaud, J. L. (2009) 'Mutations in SYNGAP1 in Autosomal Nonsyndromic Mental Retardation', *New England Journal of Medicine*, 360(6), pp. 599–605. doi: 10.1056/NEJMoa0805392.

Harding, P., Fall, A., Honeyman, K., Fletcher, S. and Wilton, S. (2007) 'The Influence of Antisense Oligonucleotide Length on Dystrophin Exon Skipping', *Molecular Therapy*, 15, pp. 157–166. doi: 10.1038/sj.mt.6300006.

Heman-Ackah, S. M., Manzano, R., Hoozemans, J. J., Scheper, W., Flynn, R., Haerty, W., Cowley, S. A., Bassett, A. R. and Wood, M. J. (2017) 'Alpha-synuclein induces the unfolded protein response in Parkinson's disease SNCA triplication iPSC-derived neurons', *Human Molecular Genetics*, 26(22), pp. 4441–4450. doi: 10.1093/hmg/ddx331.

Hilton, I. B., D'Ippolito, A. M., Vockley, C. M., Thakore, P. I., Crawford, G. E., Reddy, T. E. and Gersbach, C. A. (2015) 'Epigenome editing by a CRISPR-Cas9-based acetyltransferase activates genes from promoters and enhancers', *Nature Biotechnology*, 33(5), pp. 510–517. doi: 10.1038/nbt.3199.

Husi, H., Ward, M. A., Choudhary, J. S., Blackstock, W. P. and Grant, S. G. N. (2000) 'Proteomic analysis of NMDA receptor–adhesion protein signaling complexes', *Nature Neuroscience*. Nature Publishing Group, 3(7), pp. 661–669. doi: 10.1038/76615.

Inui, M., Miyado, M., Igarashi, M., Tamano, M., Kubo, A., Yamashita, S., Asahara, H., Fukami, M. and Takada, S. (2014) 'Rapid generation of mouse models with defined point mutations by the CRISPR/Cas9 system', *Scientific Reports*. Nature Publishing Group, 4, p. 5396. doi: 10.1038/SREP05396.

Iossifov, I., O'Roak, B. J., Sanders, S. J., Ronemus, M., Krumm, N., Levy, D., Stessman, H. A., Witherspoon, K. T., Vives, L., Patterson, K. E., Smith, J. D., Paeper, B., Nickerson, D. A., Dea, J., Dong, S., Gonzalez, L. E., Mandell, J. D., Mane, S. M., Murtha, M. T., Sullivan, C. A., Walker, M. F., Waqar, Z.,

Wei, L., Willsey, A. J., Yamrom, B., Lee, Y., Grabowska, E., Dalkic, E., Wang, Z., Marks, S., Andrews, P., Leotta, A., Kendall, J., Hakker, I., Rosenbaum, J., Ma, B., Rodgers, L., Troge, J., Narzisi, G., Yoon, S., Schatz, M. C., Ye, K., McCombie, W. R., Shendure, J., Eichler, E. E., State, M. W. and Wigler, M. (2014) 'The contribution of de novo coding mutations to autism spectrum disorder', *Nature*, 515(7526), pp. 216–221. doi: 10.1038/nature13908.

Jackson, A. L., Bartz, S. R., Schelter, J., Kobayashi, S. V, Burchard, J., Mao, M., Li, B., Cavet, G. and Linsley, P. S. (2003) 'Expression profiling reveals off-target gene regulation by RNAi', *Nature Biotechnology*, 21(6), pp. 635–637. doi: 10.1038/nbt831.

Jackson, A. L. and Linsley, P. S. (2010) 'Recognizing and avoiding siRNA off-target effects for target identification and therapeutic application', *Nature Reviews Drug Discovery*, 9(1), pp. 57–67. doi: 10.1038/nrd3010.

Jaramillo, T. C., Speed, H. E., Xuan, Z., Reimers, J. M., Liu, S. and Powell, C. M. (2016) 'Altered Striatal Synaptic Function and Abnormal Behaviour in Shank3 Exon4-9 Deletion Mouse Model of Autism.', *Autism research : official journal of the International Society for Autism Research*. NIH Public Access, 9(3), pp. 350–75. doi: 10.1002/aur.1529.

Jeyabalan, N. and Clement, J. P. (2016) 'SYNGAP1: Mind the Gap', *Frontiers in Cellular Neuroscience*. Frontiers Media SA, 10, p. 32. doi: 10.3389/fncel.2016.00032.

Jinek, M., Chylinski, K., Fonfara, I., Hauer, M., Doudna, J. A. and Charpentier, E. (2012) 'A Programmable Dual-RNA-Guided DNA Endonuclease in Adaptive Bacterial Immunity', *Science*, 337(6096), pp. 816–821. doi: 10.1126/science.1225829.

Kay, M. A. (2011) 'State-of-the-art gene-based therapies: the road ahead', *Nature Reviews Genetics*, 12(5), pp. 316–328. doi: 10.1038/nrg2971.

Keeling, K. M., Wang, D., Conard, S. E. and Bedwell, D. M. (2012) 'Suppression of Premature Termination Codons as a Therapeutic Approach', *Critical reviews in biochemistry and molecular biology*. NIH Public Access, 47(5), p. 444. doi: 10.3109/10409238.2012.694846.

Kelleher III, R. J., Geigenmüller, U., Hovhannisyan, H., Trautman, E., Pinard, R., Rathmell, B., Carpenter, R. and Margulies, D. (2012) 'High-Throughput Sequencing of mGluR Signaling Pathway Genes Reveals Enrichment of Rare Variants in Autism', *PLoS ONE*. Edited by F. J. Esteban, 7(4), p. e35003. doi: 10.1371/journal.pone.0035003.

Kennedy, M. B. (2016) 'Synaptic Signaling in Learning and Memory', *Cold Spring Harbor Perspectives in Biology*, 8(2), p. a016824. doi: 10.1101/cshperspect.a016824.

Kim, D., Lim, K., Kim, S.-T., Yoon, S., Kim, K., Ryu, S.-M. and Kim, J.-S. (2017) 'Genome-wide target specificities of CRISPR RNA-guided programmable deaminases', *Nature Biotechnology*, 35(5), pp. 475–480. doi: 10.1038/nbt.3852.

Kim, J. H., Lee, H.-K., Takamiya, K. and Huganir, R. L. (2003) 'The role of synaptic GTPase-activating protein in neuronal development and synaptic plasticity.', *The Journal of neuroscience : the official journal of the Society for Neuroscience*, 23(4), pp. 1119–1124. doi: 23/4/1119 [pii].

Kim, J. H., Liao, D., Lau, L.-F. and Huganir, R. L. (1998) 'SynGAP: a Synaptic RasGAP that Associates with the PSD-95/SAP90 Protein Family', *Neuron*. Cell Press, 20(4), pp. 683–691. doi: 10.1016/S0896-6273(00)81008-9.

Kim, M. J., Dunah, A. W., Wang, Y. T. and Sheng, M. (2005) 'Differential roles of NR2A- and NR2B-containing NMDA receptors in Ras-ERK signaling and AMPA receptor trafficking.', *Neuron*, 46(5), pp. 745–60. doi: 10.1016/j.neuron.2005.04.031.

Kim, S., Kim, D., Cho, S. W., Kim, J. and Kim, J.-S. (2014) 'Highly efficient RNA-guided genome editing in human cells via delivery of purified Cas9 ribonucleoproteins.', *Genome research*. Cold Spring Harbor Laboratory Press, 24(6), pp. 1012–9. doi: 10.1101/gr.171322.113.

Kim, S., Koo, T., Jee, H.-G., Cho, H.-Y., Lee, G., Lim, D.-G., Shin, H. S. and Kim, J.-S. (2018) 'CRISPR RNAs trigger innate immune responses in human cells', *Genome Research*, 28(3), pp. 367–373. doi: 10.1101/gr.231936.117.

Kimura, Y., Akahira-Azuma, M., Harada, N., Enomoto, Y., Tsurusaki, Y. and Kurosawa, K. (2018) 'Novel SYNGAP1 variant in a patient with intellectual disability and distinctive dysmorphisms', *Congenital Anomalies*. John Wiley & Sons Australia, Ltd. doi: 10.1111/cga.12273.

Klann, T. S., Black, J. B., Chellappan, M., Safi, A., Song, L., Hilton, I. B., Crawford, G. E., Reddy, T. E. and Gersbach, C. A. (2017) 'CRISPR–Cas9 epigenome editing enables high-throughput screening for functional regulatory elements in the human genome', *Nature Biotechnology*, 35(6), pp. 561–568. doi: 10.1038/nbt.3853.

Koike-Yusa, H., Li, Y., Tan, E.-P., Velasco-Herrera, M. D. C. and Yusa, K. (2014) 'Genome-wide recessive genetic screening in mammalian cells with a lentiviral CRISPR-guide RNA library', *Nature Biotechnology*. Nature Publishing Group, 32(3), pp. 267–273. doi: 10.1038/nbt.2800.

Komiyama, N. H., Watabe, A. M., Carlisle, H. J., Porter, K., Charlesworth, P., Monti, J., Strathdee, D. J. C., O'Carroll, C. M., Martin, S. J., Morris, R. G. M., O'Dell, T. J. and Grant, S. G. N. (2002) 'SynGAP regulates ERK/MAPK signaling, synaptic plasticity, and learning in the complex with postsynaptic

density 95 and NMDA receptor.', *The Journal of neuroscience : the official journal of the Society for Neuroscience*, 22(22), pp. 9721–32. Available at: http://www.ncbi.nlm.nih.gov/pubmed/12427827 (Accessed: 12 January 2015).

Komor, A. C., Kim, Y. B., Packer, M. S., Zuris, J. A. and Liu, D. R. (2016) 'Programmable editing of a target base in genomic DNA without double-stranded DNA cleavage', *Nature*, 533(7603), pp. 420–424. doi: 10.1038/nature17946.

Komor, A. C., Zhao, K. T., Packer, M. S., Gaudelli, N. M., Waterbury, A. L., Koblan, L. W., Kim, Y. B., Badran, A. H. and Liu, D. R. (2017) 'Improved base excision repair inhibition and bacteriophage Mu Gam protein yields C:G-to-T:A base editors with higher efficiency and product purity', *Science Advances*, 3(8), p. eaao4774. doi: 10.1126/sciadv.aao4774.

Kouranova, E., Forbes, K., Zhao, G., Warren, J., Bartels, A., Wu, Y. and Cui, X. (2016) 'CRISPRs for Optimal Targeting: Delivery of CRISPR Components as DNA, RNA, and Protein into Cultured Cells and Single-Cell Embryos', *Human Gene Therapy*, 27(6), pp. 464–475. doi: 10.1089/hum.2016.009.

Kouser, M., Speed, H. E., Dewey, C. M., Reimers, J. M., Widman, A. J., Gupta, N., Liu, S., Jaramillo, T. C., Bangash, M., Xiao, B., Worley, P. F. and Powell, C. M. (2013) 'Loss of predominant Shank3 isoforms results in hippocampus-dependent impairments in behavior and synaptic transmission.', *The Journal of neuroscience : the official journal of the Society for Neuroscience*. Society for Neuroscience, 33(47), pp. 18448–68. doi: 10.1523/JNEUROSCI.3017-13.2013.

Kozol, R. A., Cukier, H. N., Zou, B., Mayo, V., De Rubeis, S., Cai, G., Griswold, A. J., Whitehead, P. L., Haines, J. L., Gilbert, J. R., Cuccaro, M. L., Martin, E. R., Baker, J. D., Buxbaum, J. D., Pericak-Vance, M. A. and Dallman, J. E. (2015) 'Two knockdown models of the autism genes SYNGAP1 and SHANK3 in zebrafish produce similar behavioral phenotypes associated with embryonic disruptions of brain morphogenesis', *Human Molecular Genetics*, 24(14), pp. 4006–4023. doi: 10.1093/hmg/ddv138.

Krab, L. C., Goorden, S. M. I. and Elgersma, Y. (2008) 'Oncogenes on my mind: ERK and MTOR signaling in cognitive diseases', *Trends in Genetics*, 24(10), pp. 498–510. doi: 10.1016/j.tig.2008.07.005.

Krapivinsky, G., Medina, I., Krapivinsky, L., Gapon, S. and Clapham, D. E. (2004) 'SynGAP-MUPP1-CaMKII Synaptic Complexes Regulate p38 MAP Kinase Activity and NMDA Receptor- Dependent Synaptic AMPA Receptor Potentiation', *Neuron*, 43(4), pp. 563–574. doi: 10.1016/j.neuron.2004.08.003.

Leblond, C. S., Heinrich, J., Delorme, R., Proepper, C., Betancur, C., Huguet, G., Konyukh, M., Chaste,

P., Ey, E., Rastam, M., Anckarsäter, H., Nygren, G., Gillberg, I. C., Melke, J., Toro, R., Regnault, B., Fauchereau, F., Mercati, O., Lemière, N., Skuse, D., Poot, M., Holt, R., Monaco, A. P., Järvelä, I., Kantojärvi, K., Vanhala, R., Curran, S., Collier, D. A., Bolton, P., Chiocchetti, A., Klauck, S. M., Poustka, F., Freitag, C. M., Waltes, R., Kopp, M., Duketis, E., Bacchelli, E., Minopoli, F., Ruta, L., Battaglia, A., Mazzone, L., Maestrini, E., Sequeira, A. F., Oliveira, B., Vicente, A., Oliveira, G., Pinto, D., Scherer, S. W., Zelenika, D., Delepine, M., Lathrop, M., Bonneau, D., Guinchat, V., Devillard, F., Assouline, B., Mouren, M.-C., Leboyer, M., Gillberg, C., Boeckers, T. M. and Bourgeron, T. (2012) 'Genetic and Functional Analyses of SHANK2 Mutations Suggest a Multiple Hit Model of Autism Spectrum Disorders', *PLoS Genetics*. Edited by M. State, 8(2), p. e1002521. doi: 10.1371/journal.pgen.1002521.

Leblond, C. S., Nava, C., Polge, A., Gauthier, J., Huguet, G., Lumbroso, S., Giuliano, F., Stordeur, C., Depienne, C., Mouzat, K., Pinto, D., Howe, J., Lemière, N., Durand, C. M., Guibert, J., Ey, E., Toro, R., Peyre, H., Mathieu, A., Amsellem, F., Rastam, M., Gillberg, I. C., Rappold, G. A., Holt, R., Monaco, A. P., Maestrini, E., Galan, P., Heron, D., Jacquette, A., Afenjar, A., Rastetter, A., Brice, A., Devillard, F., Assouline, B., Laffargue, F., Lespinasse, J., Chiesa, J., Rivier, F., Bonneau, D., Regnault, B., Zelenika, D., Delepine, M., Lathrop, M., Sanlaville, D., Schluth-Bolard, C., Edery, P., Perrin, L., Tabet, A. C., Schmeisser, M. J., Boeckers, T. M., Coleman, M., Sato, D., Szatmari, P., Scherer, S. W., Rouleau, G. A., Betancur, C., Leboyer, M., Gillberg, C., Delorme, R. and Bourgeron, T. (2014) 'Meta-analysis of SHANK Mutations in Autism Spectrum Disorders: A Gradient of Severity in Cognitive Impairments', *PLoS Genetics*. Edited by G. S. Barsh. Public Library of Science, 10(9), p. e1004580. doi: 10.1371/journal.pgen.1004580.

Lee, J., Chung, C., Ha, S., Lee, D., Kim, D.-Y., Kim, H. and Kim, E. (2015) 'Shank3-mutant mice lacking exon 9 show altered excitation/inhibition balance, enhanced rearing, and spatial memory deficit.', *Frontiers in cellular neuroscience*, 9, p. 94. doi: 10.3389/fncel.2015.00094.

Lee, K., Conboy, M., Park, H. M., Jiang, F., Kim, H. J., Dewitt, M. A., Mackley, V. A., Chang, K., Rao, A., Skinner, C., Shobha, T., Mehdipour, M., Liu, H., Huang, W., Lan, F., Bray, N. L., Li, S., Corn, J. E., Kataoka, K., Doudna, J. A., Conboy, I. and Murthy, N. (2017) 'Nanoparticle delivery of Cas9 ribonucleoprotein and donor DNA in vivo induces homology-directed DNA repair', *Nature Biomedical Engineering*. Nature Publishing Group, 1(11), pp. 889–901. doi: 10.1038/s41551-017-0137-2.

Lemmon, M. A. (2004) 'Pleckstrin homology domains: not just for phosphoinositides: Figure 1', *Biochemical Society Transactions*, 32(5), pp. 707–711. doi: 10.1042/BST0320707.

Li, J., Shi, M., Ma, Z., Zhao, S., Euskirchen, G., Ziskin, J., Urban, A., Hallmayer, J. and Snyder, M. (2014) 'Integrated systems analysis reveals a molecular network underlying autism spectrum disorders.', *Molecular systems biology*. EMBO Press, 10(12), p. 774. doi: 10.15252/MSB.20145487.

Li, W., Okano, A., Tian, Q. B., Nakayama, K., Furihata, T., Nawa, H. and Suzuki, T. (2001) 'Characterization of a Novel synGAP Isoform, synGAP-β', *Journal of Biological Chemistry*, 276(24), pp. 21417–21424. doi: 10.1074/jbc.M010744200.

Liu, T. and Huang, J. (2016) 'DNA End Resection: Facts and Mechanisms.', *Genomics, proteomics & bioinformatics*. Elsevier, 14(3), pp. 126–130. doi: 10.1016/j.gpb.2016.05.002.

Liu, X. S., Wu, H., Ji, X., Stelzer, Y., Wu, X., Czauderna, S., Shu, J., Dadon, D., Young, R. A. and Jaenisch, R. (2016) 'Editing DNA Methylation in the Mammalian Genome', *Cell*, 167(1), p. 233–247.e17. doi: 10.1016/j.cell.2016.08.056.

Louros, S. R. and Osterweil, E. K. (2016) 'Perturbed proteostasis in autism spectrum disorders', *Journal of Neurochemistry*, 139(6), pp. 1081–1092. doi: 10.1111/jnc.13723.

Makarova, K. S., Haft, D. H., Barrangou, R., Brouns, S. J. J., Charpentier, E., Horvath, P., Moineau, S., Mojica, F. J. M., Wolf, Y. I., Yakunin, A. F., van der Oost, J. and Koonin, E. V. (2011) 'Evolution and classification of the CRISPR–Cas systems', *Nature Reviews Microbiology*. Nature Publishing Group, 9(6), pp. 467–477. doi: 10.1038/nrmicro2577.

Mali, P., Aach, J., Stranges, P. B., Esvelt, K. M., Moosburner, M., Kosuri, S., Yang, L. and Church, G. M. (2013) 'CAS9 transcriptional activators for target specificity screening and paired nickases for cooperative genome engineering.', *Nature biotechnology*. Nature Publishing Group, a division of Macmillan Publishers Limited. All Rights Reserved., 31(9), pp. 833–8. doi: 10.1038/nbt.2675.

Mashiko, D., Fujihara, Y., Satouh, Y., Miyata, H., Isotani, A. and Ikawa, M. (2013) 'Generation of mutant mice by pronuclear injection of circular plasmid expressing Cas9 and single guided RNA', *Scientific Reports*, 3. doi: 10.1038/srep03355.

McMahon, A. C., Barnett, M. W., O'Leary, T. S., Stoney, P. N., Collins, M. O., Papadia, S., Choudhary, J. S., Komiyama, N. H., Grant, S. G. N., Hardingham, G. E., Wyllie, D. J. A. and Kind, P. C. (2012) 'SynGAP isoforms exert opposing effects on synaptic strength.', *Nature communications*. Nature Publishing Group, a division of Macmillan Publishers Limited. All Rights Reserved., 3, p. 900. doi: 10.1038/ncomms1900.

Mei, Y., Monteiro, P., Zhou, Y., Kim, J.-A., Gao, X., Fu, Z. and Feng, G. (2016) 'Adult restoration of Shank3 expression rescues selective autistic-like phenotypes', *Nature*. Nature Publishing Group, 530(7591), pp. 481–4. doi: 10.1038/nature16971.

Mignot, C., von Stülpnagel, C., Nava, C., Ville, D., Sanlaville, D., Lesca, G., Rastetter, A., Gachet, B., Marie, Y., Korenke, G. C., Borggraefe, I., Hoffmann-Zacharska, D., Szczepanik, E., Rudzka-Dybała, M.,

Yiş, U., Çağlayan, H., Isapof, A., Marey, I., Panagiotakaki, E., Korff, C., Rossier, E., Riess, A., Beck-Woedl, S., Rauch, A., Zweier, C., Hoyer, J., Reis, A., Mironov, M., Bobylova, M., Mukhin, K., Hernandez-Hernandez, L., Maher, B., Sisodiya, S., Kuhn, M., Glaeser, D., Weckhuysen, S., Myers, C. T., Mefford, H. C., Hörtnagel, K., Biskup, S., EuroEPINOMICS-RES MAE working group, E.-R. M. working, Lemke, J. R., Héron, D., Kluger, G. and Depienne, C. (2016) 'Genetic and neurodevelopmental spectrum of SYNGAP1-associated intellectual disability and epilepsy.', *Journal of medical genetics*. BMJ Publishing Group Ltd, 53(8), pp. 511–22. doi: 10.1136/jmedgenet-2015-103451.

Miller, J. C., Tan, S., Qiao, G., Barlow, K. A., Wang, J., Xia, D. F., Meng, X., Paschon, D. E., Leung, E., Hinkley, S. J., Dulay, G. P., Hua, K. L., Ankoudinova, I., Cost, G. J., Urnov, F. D., Zhang, H. S., Holmes, M. C., Zhang, L., Gregory, P. D. and Rebar, E. J. (2011) 'A TALE nuclease architecture for efficient genome editing', *Nature Biotechnology*, 29(2), pp. 143–148. doi: 10.1038/nbt.1755.

Moessner, R., Marshall, C. R., Sutcliffe, J. S., Skaug, J., Pinto, D., Vincent, J., Zwaigenbaum, L., Fernandez, B., Roberts, W., Szatmari, P. and Scherer, S. W. (2007) 'Contribution of SHANK3 mutations to autism spectrum disorder.', *American journal of human genetics*. Elsevier, 81(6), pp. 1289–97. doi: 10.1086/522590.

Monteiro, P. and Feng, G. (2017) 'SHANK proteins: roles at the synapse and in autism spectrum disorder', *Nature Reviews Neuroscience*. Nature Publishing Group. doi: 10.1038/nrn.2016.183.

Muhia, M., Willadt, S., Yee, B. K., Feldon, J., Paterna, J.-C., Schwendener, S., Vogt, K., Kennedy, M. B. and Knuesel, I. (2012) 'Molecular and behavioral changes associated with adult hippocampus-specific SynGAP1 knockout', *Learning & Memory*, 19(7), pp. 268–281. doi: 10.1101/lm.026351.112.

Muhia, M., Yee, B. K., Feldon, J., Markopoulos, F. and Knuesel, I. (2010) 'Disruption of hippocampus-regulated behavioural and cognitive processes by heterozygous constitutive deletion of SynGAP', *European Journal of Neuroscience*, 31(3), pp. 529–543. doi: 10.1111/j.1460-9568.2010.07079.x.

Naisbitt, S., Kim, E., Tu, J. C., Xiao, B., Sala, C., Valtschanoff, J., Weinberg, R. J., Worley, P. F. and Sheng, M. (1999) 'Shank, a Novel Family of Postsynaptic Density Proteins that Binds to the NMDA Receptor/PSD-95/GKAP Complex and Cortactin', *Neuron*, 23(3), pp. 569–582. doi: 10.1016/S0896-6273(00)80809-0.

Naito, Y., Hino, K., Bono, H. and Ui-Tei, K. (2015) 'CRISPRdirect: software for designing CRISPR/Cas guide RNA with reduced off-target sites.', *Bioinformatics (Oxford, England)*. Oxford University Press, 31(7), pp. 1120–3. doi: 10.1093/bioinformatics/btu743.

Nishida, K., Arazoe, T., Yachie, N., Banno, S., Kakimoto, M., Tabata, M., Mochizuki, M., Miyabe, A.,

Araki, M., Hara, K. Y., Shimatani, Z. and Kondo, A. (2016) 'Targeted nucleotide editing using hybrid prokaryotic and vertebrate adaptive immune systems.', *Science (New York, N.Y.)*. American Association for the Advancement of Science, 353(6305), p. aaf8729. doi: 10.1126/science.aaf8729.

Nithianantharajah, J., Komiyama, N. H., McKechanie, A., Johnstone, M., Blackwood, D. H., Clair, D. S., Emes, R. D., van de Lagemaat, L. N., Saksida, L. M., Bussey, T. J., Grant, S. G. N., St Clair, D., Emes, R. D., van de Lagemaat, L. N., Saksida, L. M., Bussey, T. J. and Grant, S. G. N. (2013) 'Synaptic scaffold evolution generated components of vertebrate cognitive complexity.', *Nature neuroscience*. Nature Publishing Group, a division of Macmillan Publishers Limited. All Rights Reserved., 16(1), pp. 16–24. doi: 10.1038/nn.3276.

O'Connor, E. C., Bariselli, S. and Bellone, C. (2014) 'Synaptic basis of social dysfunction: a focus on postsynaptic proteins linking group-I mGluRs with AMPARs and NMDARs.', *The European journal of neuroscience*, 39(7), pp. 1114–29. doi: 10.1111/ejn.12510.

O'Roak, B. J., Vives, L., Girirajan, S., Karakoc, E., Krumm, N., Coe, B. P., Levy, R., Ko, A., Lee, C., Smith, J. D., Turner, E. H., Stanaway, I. B., Vernot, B., Malig, M., Baker, C., Reilly, B., Akey, J. M., Borenstein, E., Rieder, M. J., Nickerson, D. A., Bernier, R., Shendure, J. and Eichler, E. E. (2012) 'Sporadic autism exomes reveal a highly interconnected protein network of de novo mutations.', *Nature*. Nature Publishing Group, a division of Macmillan Publishers Limited. All Rights Reserved., 485(7397), pp. 246–50. doi: 10.1038/nature10989.

Oji, A., Noda, T., Fujihara, Y., Miyata, H., Kim, Y. J., Muto, M., Nozawa, K., Matsumura, T., Isotani, A. and Ikawa, M. (2016) 'CRISPR/Cas9 mediated genome editing in ES cells and its application for chimeric analysis in mice', *Scientific Reports*. Nature Publishing Group, 6(1), p. 31666. doi: 10.1038/srep31666.

Oliver, D., Yuan, S., McSwiggin, H. and Yan, W. (2015) 'Pervasive Genotypic Mosaicism in Founder Mice Derived from Genome Editing through Pronuclear Injection', *PLOS ONE*. Edited by H. Fujii, 10(6), p. e0129457. doi: 10.1371/journal.pone.0129457.

Ozkan, E. D., Creson, T. K., Kramár, E. A., Rojas, C., Seese, R. R., Babyan, A. H., Shi, Y., Lucero, R., Xu, X., Noebels, J. L., Miller, C. A., Lynch, G. and Rumbaugh, G. (2014) 'Reduced cognition in Syngap1 mutants is caused by isolated damage within developing forebrain excitatory neurons.', *Neuron*, 82(6), pp. 1317–33. doi: 10.1016/j.neuron.2014.05.015.

Paquet, D., Kwart, D., Chen, A., Sproul, A., Jacob, S., Teo, S., Olsen, K. M., Gregg, A., Noggle, S. and Tessier-Lavigne, M. (2016) 'Efficient introduction of specific homozygous and heterozygous mutations using CRISPR/Cas9', *Nature*. Nature Research, 533(7601), pp. 125–129. doi:

10.1038/nature17664.

Parker, J. (1989) 'Errors and alternatives in reading the universal genetic code.', *Microbiological reviews*, 53(3), pp. 273–98. Available at: http://www.ncbi.nlm.nih.gov/pubmed/2677635 (Accessed: 12 February 2018).

Parnas, O., Jovanovic, M., Eisenhaure, T. M., Herbst, R. H., Dixit, A., Ye, C. J., Przybylski, D., Platt, R. J., Tirosh, I., Sanjana, N. E., Shalem, O., Satija, R., Raychowdhury, R., Mertins, P., Carr, S. A., Zhang, F., Hacohen, N. and Regev, A. (2015) 'A Genome-wide CRISPR Screen in Primary Immune Cells to Dissect Regulatory Networks', *Cell*. Cell Press, 162(3), pp. 675–686. doi: 10.1016/J.CELL.2015.06.059.

Peça, J., Feliciano, C., Ting, J. T., Wang, W., Wells, M. F., Venkatraman, T. N., Lascola, C. D., Fu, Z. and Feng, G. (2011) 'Shank3 mutant mice display autistic-like behaviours and striatal dysfunction.', *Nature*. Nature Publishing Group, a division of Macmillan Publishers Limited. All Rights Reserved., 472(7344), pp. 437–42. doi: 10.1038/nature09965.

Pena, V., Hothorn, M., Eberth, A., Kaschau, N., Parret, A., Gremer, L., Bonneau, F., Ahmadian, M. R. and Scheffzek, K. (2008) 'The C2 domain of SynGAP is essential for stimulation of the Rap GTPase reaction.', *EMBO reports*, 9(4), pp. 350–5. doi: 10.1038/embor.2008.20.

Phelan, K. and McDermid, H. E. (2012) 'The 22q13.3 Deletion Syndrome (Phelan-McDermid Syndrome).', *Molecular syndromology*. Karger Publishers, 2(3–5), pp. 186–201. doi: 000334260.

Pires, C., Schmid, B., Petræus, C., Poon, A., Nimsanor, N., Nielsen, T. T., Waldemar, G., Hjermind, L. E., Nielsen, J. E., Hyttel, P. and Freude, K. K. (2016) 'Generation of a gene-corrected isogenic control cell line from an Alzheimer's disease patient iPSC line carrying a A79V mutation in PSEN1', *Stem Cell Research*, 17(2), pp. 285–288. doi: 10.1016/j.scr.2016.08.002.

Prasad, C., Prasad, A. N., Chodirker, B. N., Lee, C., Dawson, A. K., Jocelyn, L. J. and Chudley, A. E. (2001) 'Genetic evaluation of pervasive developmental disorders: the terminal 22q13 deletion syndrome may represent a recognizable phenotype', *Clinical Genetics*. Munksgaard International Publishers, 57(2), pp. 103–109. doi: 10.1034/j.1399-0004.2000.570203.x.

Purcell, S. M., Moran, J. L., Fromer, M., Ruderfer, D., Solovieff, N., Roussos, P., O'Dushlaine, C., Chambert, K., Bergen, S. E., Kähler, A., Duncan, L., Stahl, E., Genovese, G., Fernández, E., Collins, M. O., Komiyama, N. H., Choudhary, J. S., Magnusson, P. K. E., Banks, E., Shakir, K., Garimella, K., Fennell, T., DePristo, M., Grant, S. G. N., Haggarty, S. J., Gabriel, S., Scolnick, E. M., Lander, E. S., Hultman, C. M., Sullivan, P. F., McCarroll, S. A. and Sklar, P. (2014) 'A polygenic burden of rare disruptive mutations in schizophrenia.', *Nature*, 506(7487), pp. 185–90. doi: 10.1038/nature12975.

Qi, L. S., Larson, M. H., Gilbert, L. A., Doudna, J. A., Weissman, J. S., Arkin, A. P. and Lim, W. A. (2013) 'Repurposing CRISPR as an RNA-Guided Platform for Sequence-Specific Control of Gene Expression', *Cell*, 152(5), pp. 1173–1183. doi: 10.1016/j.cell.2013.02.022.

Qin, L., Ma, K., Wang, Z.-J., Hu, Z., Matas, E., Wei, J. and Yan, Z. (2018) 'Social deficits in Shank3-deficient mouse models of autism are rescued by histone deacetylase (HDAC) inhibition', *Nature Neuroscience*. Nature Publishing Group, p. 1. doi: 10.1038/s41593-018-0110-8.

Ran, F. A., Hsu, P. D., Wright, J., Agarwala, V., Scott, D. A. and Zhang, F. (2013) 'Genome engineering using the CRISPR-Cas9 system.', *Nature protocols*. Nature Publishing Group, a division of Macmillan Publishers Limited. All Rights Reserved., 8(11), pp. 2281–308. doi: 10.1038/nprot.2013.143.

Rauch, A., Wieczorek, D., Graf, E., Wieland, T., Endele, S., Schwarzmayr, T., Albrecht, B., Bartholdi, D., Beygo, J., Di Donato, N., Dufke, A., Cremer, K., Hempel, M., Horn, D., Hoyer, J., Joset, P., Röpke, A., Moog, U., Riess, A., Thiel, C. T., Tzschach, A., Wiesener, A., Wohlleber, E., Zweier, C., Ekici, A. B., Zink, A. M., Rump, A., Meisinger, C., Grallert, H., Sticht, H., Schenck, A., Engels, H., Rappold, G., Schröck, E., Wieacker, P., Riess, O., Meitinger, T., Reis, A. and Strom, T. M. (2012) 'Range of genetic mutations associated with severe non-syndromic sporadic intellectual disability: an exome sequencing study.', *Lancet (London, England)*. Elsevier, 380(9854), pp. 1674–82. doi: 10.1016/S0140-6736(12)61480-9.

Rees, H. A., Komor, A. C., Yeh, W.-H., Caetano-Lopes, J., Warman, M., Edge, A. S. B. and Liu, D. R. (2017) 'Improving the DNA specificity and applicability of base editing through protein engineering and protein delivery', *Nature Communications*, 8, p. 15790. doi: 10.1038/ncomms15790.

Rehmann, H. and Bos, J. L. (2004) 'Signal transduction: Thumbs up for inactivation', *Nature*. Nature Publishing Group, 429(6988), pp. 138–139. doi: 10.1038/429138a.

De Rubeis, S., He, X., Goldberg, A. P., Poultney, C. S., Samocha, K., Ercument Cicek, A., Kou, Y., Liu, L., Fromer, M., Walker, S., Singh, T., Klei, L., Kosmicki, J., Fu, S.-C., Aleksic, B., Biscaldi, M., Bolton, P. F., Brownfeld, J. M., Cai, J., Campbell, N. G., Carracedo, A., Chahrour, M. H., Chiocchetti, A. G., Coon, H., Crawford, E. L., Crooks, L., Curran, S. R., Dawson, G., Duketis, E., Fernandez, B. A., Gallagher, L., Geller, E., Guter, S. J., Sean Hill, R., Ionita-Laza, I., Jimenez Gonzalez, P., Kilpinen, H., Klauck, S. M., Kolevzon, A., Lee, I., Lei, J., Lehtimäki, T., Lin, C.-F., Ma'ayan, A., Marshall, C. R., McInnes, A. L., Neale, B., Owen, M. J., Ozaki, N., Parellada, M., Parr, J. R., Purcell, S., Puura, K., Rajagopalan, D., Rehnström, K., Reichenberg, A., Sabo, A., Sachse, M., Sanders, S. J., Schafer, C., Schulte-Rüther, M., Skuse, D., Stevens, C., Szatmari, P., Tammimies, K., Valladares, O., Voran, A., Wang, L.-S., Weiss, L. A., Jeremy Willsey, A., Yu, T. W., Yuen, R. K. C., Cook, E. H., Freitag, C. M., Gill, M., Hultman, C. M., Lehner, T., Palotie, A., Schellenberg, G. D., Sklar, P., State, M. W., Sutcliffe, J. S., Walsh, C. A., Scherer, S. W., Zwick, M. E., Barrett, J. C., Cutler, D. J., Roeder, K., Devlin, B., Daly, M. J. and Buxbaum, J. D. (2014)

'Synaptic, transcriptional and chromatin genes disrupted in autism', *Nature*. Nature Publishing Group, a division of Macmillan Publishers Limited. All Rights Reserved., 515(7526), pp. 209–215. doi: 10.1038/nature13772.

Rumbaugh, G., Adams, J. P., Kim, J. H. and Huganir, R. L. (2006) 'SynGAP regulates synaptic strength and mitogen-activated protein kinases in cultured neurons.', *Proceedings of the National Academy of Sciences of the United States of America*, 103(12), pp. 4344–51. doi: 10.1073/pnas.0600084103.

Ryan, T. J., Emes, R. D., Grant, S. G. and Komiyama, N. H. (2008) 'Evolution of NMDA receptor cytoplasmic interaction domains: implications for organisation of synaptic signalling complexes.', *BMC neuroscience*, 9, p. 6. doi: 10.1186/1471-2202-9-6.

Ryan, T. J. and Grant, S. G. N. (2009) 'The origin and evolution of synapses', *Nature Reviews Neuroscience*. Nature Publishing Group, 10(10), pp. 701–712. doi: 10.1038/nrn2717.

Sakai, Y., Shaw, C. A., Dawson, B. C., Dugas, D. V., Al-Mohtaseb, Z., Hill, D. E. and Zoghbi, H. Y. (2011) 'Protein Interactome Reveals Converging Molecular Pathways Among Autism Disorders', *Science Translational Medicine*, 3(86), p. 86ra49-86ra49. doi: 10.1126/scitranslmed.3002166.

Sakuma, T., Nishikawa, A., Kume, S., Chayama, K. and Yamamoto, T. (2015) 'Multiplex genome engineering in human cells using all-in-one CRISPR/Cas9 vector system', *Scientific Reports*, 4(1), p. 5400. doi: 10.1038/srep05400.

Sala, C., Vicidomini, C., Bigi, I., Mossa, A. and Verpelli, C. (2015) 'Shank synaptic scaffold proteins: keys to understanding the pathogenesis of autism and other synaptic disorders', *Journal of Neurochemistry*, 135(5), pp. 849–858. doi: 10.1111/jnc.13232.

Sanjana, N. E. (2017) 'Genome-scale CRISPR pooled screens', *Analytical Biochemistry*. Academic Press, 532, pp. 95–99. doi: 10.1016/J.AB.2016.05.014.

Sapranauskas, R., Gasiunas, G., Fremaux, C., Barrangou, R., Horvath, P. and Siksnys, V. (2011) 'The Streptococcus thermophilus CRISPR/Cas system provides immunity in Escherichia coli', *Nucleic Acids Research*, 39(21), pp. 9275–9282. doi: 10.1093/nar/gkr606.

Scheffzek, K., Ahmadian, M. R., Kabsch, W., Wiesmüller, L., Lautwein, A., Schmitz, F. and Wittinghofer, A. (1997) 'The Ras-RasGAP complex: structural basis for GTPase activation and its loss in oncogenic Ras mutants.', *Science (New York, N.Y.)*, 277(5324), pp. 333–8. Available at: http://www.ncbi.nlm.nih.gov/pubmed/9219684 (Accessed: 15 February 2018).

van Schendel, R., Roerink, S. F., Portegijs, V., van den Heuvel, S. and Tijsterman, M. (2015)

'Polymerase Θ is a key driver of genome evolution and of CRISPR/Cas9-mediated mutagenesis', *Nature Communications*, 6(1), p. 7394. doi: 10.1038/ncomms8394.

Schmeisser, M. J., Ey, E., Wegener, S., Bockmann, J., Stempel, a V., Kuebler, A., Janssen, A.-L., Udvardi, P. T., Shiban, E., Spilker, C., Balschun, D., Skryabin, B. V, Dieck, S. T., Smalla, K.-H., Montag, D., Leblond, C. S., Faure, P., Torquet, N., Le Sourd, A.-M., Toro, R., Grabrucker, A. M., Shoichet, S. a, Schmitz, D., Kreutz, M. R., Bourgeron, T., Gundelfinger, E. D. and Boeckers, T. M. (2012) 'Autistic-like behaviours and hyperactivity in mice lacking ProSAP1/Shank2.', *Nature*. Nature Publishing Group, 486(7402), pp. 256–60. doi: 10.1038/nature11015.

Schmid-Burgk, J. L., Chauhan, D., Schmidt, T., Ebert, T. S., Reinhardt, J., Endl, E. and Hornung, V. (2016) 'A Genome-wide CRISPR (Clustered Regularly Interspaced Short Palindromic Repeats) Screen Identifies NEK7 as an Essential Component of NLRP3 Inflammasome Activation.', *The Journal of biological chemistry*. American Society for Biochemistry and Molecular Biology, 291(1), pp. 103–9. doi: 10.1074/jbc.C115.700492.

Shi, J., Wang, E., Milazzo, J. P., Wang, Z., Kinney, J. B. and Vakoc, C. R. (2015) 'Discovery of cancer drug targets by CRISPR-Cas9 screening of protein domains', *Nature Biotechnology*, 33(6), pp. 661–667. doi: 10.1038/nbt.3235.

Singh, P., Schimenti, J. C. and Bolcun-Filas, E. (2014) 'A Mouse Geneticist's Practical Guide to CRISPR Applications.', *Genetics*, p. genetics.114.169771-. doi: 10.1534/genetics.114.169771.

Speed, H. E., Kouser, M., Xuan, Z., Reimers, J. M., Ochoa, C. F., Gupta, N., Liu, S. and Powell, C. M. (2015) 'Autism-Associated Insertion Mutation (InsG) of Shank3 Exon 21 Causes Impaired Synaptic Transmission and Behavioral Deficits', *Journal of Neuroscience*, 35(26), pp. 9648–9665. doi: 10.1523/JNEUROSCI.3125-14.2015.

Staahl, B. T., Benekareddy, M., Coulon-Bainier, C., Banfal, A. A., Floor, S. N., Sabo, J. K., Urnes, C., Munares, G. A., Ghosh, A. and Doudna, J. A. (2017) 'Efficient genome editing in the mouse brain by local delivery of engineered Cas9 ribonucleoprotein complexes', *Nature Biotechnology*, 35(5), pp. 431–434. doi: 10.1038/nbt.3806.

Steinberg, J. and Webber, C. (2013) 'The Roles of FMRP-Regulated Genes in Autism Spectrum Disorder: Single- and Multiple-Hit Genetic Etiologies', *The American Journal of Human Genetics*. Cell Press, 93(5), pp. 825–839. doi: 10.1016/J.AJHG.2013.09.013.

Stemmer, M., Thumberger, T., del Sol Keyer, M., Wittbrodt, J. and Mateo, J. L. (2015) 'CCTop: An Intuitive, Flexible and Reliable CRISPR/Cas9 Target Prediction Tool', *PLOS ONE*. Edited by S. Maas.

Public Library of Science, 10(4), p. e0124633. doi: 10.1371/journal.pone.0124633.

von Stülpnagel, C., Funke, C., Haberl, C., Hörtnagel, K., Jüngling, J., Weber, Y., Staudt, M. and Kluger, G. (2015) 'SYNGAP1 Mutation in Focal and Generalized Epilepsy: A Literature Overview and A Case Report with Special Aspects of the EEG', *Neuropediatrics*. Georg Thieme Verlag KG, 46(04), pp. 287–291. doi: 10.1055/s-0035-1554098.

Südhof, T. C. and Rizo, J. (1996) 'Synaptotagmins: C2-Domain Proteins That Regulate Membrane Traffic', *Neuron*. Cell Press, 17(3), pp. 379–388. doi: 10.1016/S0896-6273(00)80171-3.

Ulbrich, M. H. and Isacoff, E. Y. (2008) 'Rules of engagement for NMDA receptor subunits.', *Proceedings of the National Academy of Sciences of the United States of America*, 105(37), pp. 14163–8. doi: 10.1073/pnas.0802075105.

Urnov, F. D., Rebar, E. J., Holmes, M. C., Zhang, H. S. and Gregory, P. D. (2010) 'Genome editing with engineered zinc finger nucleases.', *Nature reviews. Genetics*, 11(9), pp. 636–46. doi: 10.1038/nrg2842.

Vadodaria, K. C. and Jessberger, S. (2013) 'Maturation and integration of adult born hippocampal neurons: signal convergence onto small Rho GTPases', *Frontiers in Synaptic Neuroscience*. Frontiers, 5, p. 4. doi: 10.3389/fnsyn.2013.00004.

Vazquez, L. E., Chen, H.-J., Sokolova, I., Knuesel, I. and Kennedy, M. B. (2004) 'SynGAP Regulates Spine Formation', *Journal of Neuroscience*, 24(40), pp. 8862–8872. doi: 10.1523/JNEUROSCI.3213-04.2004.

Veres, A., Gosis, B. S., Ding, Q., Collins, R., Ragavendran, A., Brand, H., Erdin, S., Cowan, C. A., Talkowski, M. E. and Musunuru, K. (2014) 'Low incidence of off-target mutations in individual CRISPR-Cas9 and TALEN targeted human stem cell clones detected by whole-genome sequencing.', *Cell stem cell*. NIH Public Access, 15(1), pp. 27–30. doi: 10.1016/j.stem.2014.04.020.

Vicente-Crespo, M. and Palacios, I. M. (2010) 'Nonsense-mediated mRNA decay and development: shoot the messenger to survive?', *Biochemical Society transactions*. Europe PMC Funders, 38(6), pp. 1500–5. doi: 10.1042/BST0381500.

Vicidomini, C., Ponzoni, L., Lim, D., Schmeisser, M. J., Reim, D., Morello, N., Orellana, D., Tozzi, a, Durante, V., Scalmani, P., Mantegazza, M., Genazzani, a a, Giustetto, M., Sala, M., Calabresi, P., Boeckers, T. M., Sala, C. and Verpelli, C. (2016) 'Pharmacological enhancement of mGlu5 receptors rescues behavioral deficits in SHANK3 knock-out mice', *Molecular Psychiatry*. Nature Publishing Group, (August 2015), pp. 1–14. doi: 10.1038/mp.2016.30.

Walkup, W. G., Mastro, T. L., Schenker, L. T., Vielmetter, J., Hu, R., Iancu, A., Reghunathan, M., Bannon, B. D. and Kennedy, M. B. (2016) 'A model for regulation by SynGAP-α1 of binding of synaptic proteins to PDZ-domain "Slots" in the postsynaptic density.', *eLife*. eLife Sciences Publications Limited, 5, p. e16813. doi: 10.7554/eLife.16813.

Wang, C.-C., Held, R. G. and Hall, B. J. (2013) 'SynGAP regulates protein synthesis and homeostatic synaptic plasticity in developing cortical networks.', *PloS one*. Edited by L. Groc. Public Library of Science, 8(12), p. e83941. doi: 10.1371/journal.pone.0083941.

Wang, H., Yang, H., Shivalila, C. S., Dawlaty, M. M., Cheng, A. W., Zhang, F. and Jaenisch, R. (2013) 'One-step generation of mice carrying mutations in multiple genes by CRISPR/cas-mediated genome engineering', *Cell*. doi: 10.1016/j.cell.2013.04.025.

Wang, X., Bey, A. L., Katz, B. M., Badea, A., Kim, N., David, L. K., Duffney, L. J., Kumar, S., Mague, S. D., Hulbert, S. W., Dutta, N., Hayrapetyan, V., Yu, C., Gaidis, E., Zhao, S., Ding, J.-D., Xu, Q., Chung, L., Rodriguiz, R. M., Wang, F., Weinberg, R. J., Wetsel, W. C., Dzirasa, K., Yin, H. and Jiang, Y.-H. (2016) 'Altered mGluR5-Homer scaffolds and corticostriatal connectivity in a Shank3 complete knockout model of autism.', *Nature communications*. Nature Publishing Group, 7, p. 11459. doi: 10.1038/ncomms11459.

Wang, X., McCoy, P. A., Rodriguiz, R. M., Pan, Y., Je, H. S., Roberts, A. C., Kim, C. J., Berrios, J., Colvin, J. S., Bousquet-Moore, D., Lorenzo, I., Wu, G., Weinberg, R. J., Ehlers, M. D., Philpot, B. D., Beaudet, A. L., Wetsel, W. C. and Jiang, Y.-H. (2011) 'Synaptic dysfunction and abnormal behaviors in mice lacking major isoforms of Shank3.', *Human molecular genetics*, 20(15), pp. 3093–108. doi: 10.1093/hmg/ddr212.

Wang, X., Xu, Q., Bey, A. L., Lee, Y. and Jiang, Y.-H. (2014) 'Transcriptional and functional complexity of Shank3 provides a molecular framework to understand the phenotypic heterogeneity of SHANK3 causing autism and Shank3 mutant mice.', *Molecular autism*, 5(1), p. 30. doi: 10.1186/2040-2392-5-30.

Welch, J. M., Lu, J., Rodriguiz, R. M., Trotta, N. C., Peca, J., Ding, J. D., Feliciano, C., Chen, M., Adams, J. P., Luo, J., Dudek, S. M., Weinberg, R. J., Calakos, N., Wetsel, W. C. and Feng, G. (2007) 'Cortico-striatal synaptic defects and OCD-like behaviours in Sapap3-mutant mice', *Nature*, 448(7156), pp. 894–900. doi: 10.1038/nature06104.

Wen, Y., Alshikho, M. J. and Herbert, M. R. (2016) 'Pathway Network Analyses for Autism Reveal Multisystem Involvement, Major Overlaps with Other Diseases and Convergence upon MAPK and Calcium Signaling', *PLOS ONE*. Edited by V. W. Hu. Public Library of Science, 11(4), p. e0153329. doi:

10.1371/journal.pone.0153329.

Wu, X., Scott, D. A., Kriz, A. J., Chiu, A. C., Hsu, P. D., Dadon, D. B., Cheng, A. W., Trevino, A. E., Konermann, S., Chen, S., Jaenisch, R., Zhang, F. and Sharp, P. A. (2014) 'Genome-wide binding of the CRISPR endonuclease Cas9 in mammalian cells', *Nature Biotechnology*, 32(7), pp. 670–676. doi: 10.1038/nbt.2889.

Yang, H., Wang, H., Shivalila, C. S., Cheng, A. W., Shi, L. and Jaenisch, R. (2013) 'One-step generation of mice carrying reporter and conditional alleles by CRISPR/cas-mediated genome engineering', *Cell*. Elsevier Inc., 154(6), pp. 1370–1379. doi: 10.1016/j.cell.2013.08.022.

Yang, M., Bozdagi, O., Scattoni, M. L., Wohr, M., Roullet, F. I., Katz, A. M., Abrams, D. N., Kalikhman, D., Simon, H., Woldeyohannes, L., Zhang, J. Y., Harris, M. J., Saxena, R., Silverman, J. L., Buxbaum, J. D. and Crawley, J. N. (2012) 'Reduced Excitatory Neurotransmission and Mild Autism-Relevant Phenotypes in Adolescent Shank3 Null Mutant Mice', *Journal of Neuroscience*, 32(19), pp. 6525–6541. doi: 10.1523/JNEUROSCI.6107-11.2012.

Yen, S.-T., Zhang, M., Deng, J. M., Usman, S. J., Smith, C. N., Parker-Thornburg, J., Swinton, P. G., Martin, J. F. and Behringer, R. R. (2014) 'Somatic mosaicism and allele complexity induced by CRISPR/Cas9 RNA injections in mouse zygotes', *Developmental Biology*, 393(1), pp. 3–9. doi: 10.1016/j.ydbio.2014.06.017.

Yu, C., Zhang, Y., Yao, S. and Wei, Y. (2014) 'A PCR Based Protocol for Detecting Indel Mutations Induced by TALENs and CRISPR/Cas9 in Zebrafish', *PLoS ONE*. Edited by B. Jennings. Public Library of Science, 9(6), p. e98282. doi: 10.1371/journal.pone.0098282.

Zeng, M., Shang, Y., Araki, Y., Guo, T., Huganir, R. L. L. and Zhang, M. (2016) 'Phase Transition in Postsynaptic Densities Underlies Formation of Synaptic Complexes and Synaptic Plasticity', *Cell*. Elsevier Inc., 166(5), p. 1163–1175.e12. doi: 10.1016/j.cell.2016.07.008.

Zhang, C., Quan, R. and Wang, J. (2018a) 'Development and application of CRISPR/Cas9 technologies in genomic editing', *Human Molecular Genetics*. doi: 10.1093/hmg/ddy120.

Zhang, C., Quan, R. and Wang, J. (2018b) 'Development and application of CRISPR/Cas9 technologies in genomic editing', *Human Molecular Genetics*. doi: 10.1093/hmg/ddy120.

Zhang, X.-H., Tee, L. Y., Wang, X.-G., Huang, Q.-S. and Yang, S.-H. (2015) 'Off-target Effects in CRISPR/Cas9-mediated Genome Engineering.', *Molecular therapy. Nucleic acids*. Elsevier, 4, p. e264. doi: 10.1038/mtna.2015.37.

Zhang, Y., Mu, W. and Wang, H. (2017) 'Gene editing in T cell therapy', *Journal of Genetics and Genomics*. Elsevier, 44(9), pp. 415–422. doi: 10.1016/J.JGG.2017.09.002.

Zhou, Y., Kaiser, T., Monteiro, P., Zhang, X., Van der Goes, M. S., Wang, D., Barak, B., Zeng, M., Li, C., Lu, C., Wells, M., Amaya, A., Nguyen, S., Lewis, M., Sanjana, N., Zhou, Y., Zhang, M., Zhang, F., Fu, Z. and Feng, G. (2016) 'Mice with Shank3 Mutations Associated with ASD and Schizophrenia Display Both Shared and Distinct Defects.', *Neuron*. NIH Public Access, 89(1), pp. 147–62. doi: 10.1016/j.neuron.2015.11.023.

Zhu, J., Shang, Y. and Zhang, M. (2016) 'Mechanistic basis of MAGUK-organized complexes in synaptic development and signalling', *Nature Reviews Neuroscience*. Nature Publishing Group, 17(4), pp. 209–223. doi: 10.1038/nrn.2016.18.

Zhu, L., Wang, X., Li, X.-L., Towers, A., Cao, X., Wang, P., Bowman, R., Yang, H., Goldstein, J., Li, Y.-J. and Jiang, Y.-H. (2014) 'Epigenetic dysregulation of SHANK3 in brain tissues from individuals with autism spectrum disorders.', *Human molecular genetics*. Oxford University Press, 23(6), pp. 1563–78. doi: 10.1093/hmg/ddt547.